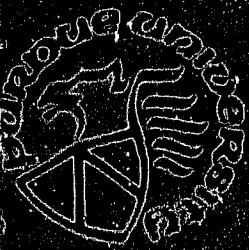


General Disclaimer

One or more of the Following Statements may affect this Document

- This document has been reproduced from the best copy furnished by the organizational source. It is being released in the interest of making available as much information as possible.
- This document may contain data, which exceeds the sheet parameters. It was furnished in this condition by the organizational source and is the best copy available.
- This document may contain tone-on-tone or color graphs, charts and/or pictures, which have been reproduced in black and white.
- This document is paginated as submitted by the original source.
- Portions of this document are not fully legible due to the historical nature of some of the material. However, it is the best reproduction available from the original submission.



(NASA-CR-168057) WAVE PROPAGATION IN
GRAPHITE/EPOXY LAMINATES DUE TO IMPACT
Interim Report (Purdue Univ.) 171 p
HC A08/MF A01

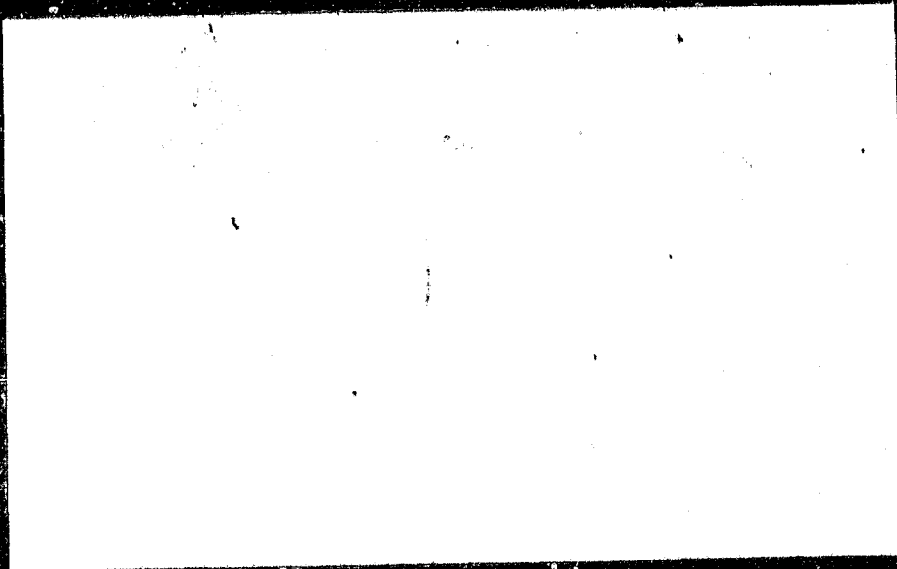
N83-22325

CSCCL IID

Unclas

G3/24

03376



COMPOSITE
MATERIALS
LABORATORY



PURDUE UNIVERSITY
School of Aeronautics and Astronautics
West Lafayette, Indiana 47907

CML 82-5

NASA CR 168057

WAVE PROPAGATION IN GRAPHITE/EPOXY
LAMINATES DUE TO IMPACT

by

T.M. Tan and C.T. Sun

December, 1982

1. Report No. NASA CR-168057		2. Government Accession No.		3. Recipient's Catalog No.	
4. Title and Subtitle WAVE PROPAGATION IN GRAPHITE/EPOXY LAMINATES DUE TO IMPACT				5. Report Date December 1982	
				6. Performing Organization Code	
7. Author(s) T. M. Tan and C. T. Sun				8. Performing Organization Report No.	
9. Performing Organization Name and Address Purdue University School of Aeronautics and Astronautics West Lafayette, IN 47907				10. Work Unit No.	
				11. Contract or Grant No. NSG 3185	
12. Sponsoring Agency Name and Address National Aeronautics & Space Administration Washington, DC 20546				13. Type of Report and Period Covered Interim Report	
				14. Sponsoring Agency Code	
15. Supplementary Notes Project Monitor: C. C. Chamis, Structures & Mechanical Technologies Div. NASA Lewis Research Center, M.S. 49-6 21000 Brookpark Road Cleveland, OH 44135					
16. Abstract The low velocity impact response of graphite/epoxy laminates is investigated theoretically and experimentally. A 9-node isoparametric finite element in conjunction with an empirical contact law was used for the theoretical investigation. Flat laminates subjected to pendulum impact were used for the experimental investigation. Theoretical results are in good agreement with strain gage experimental data. The collective results of the investigation indicate that the theoretical procedure describes the impact response of the laminate up to about 150 in/sec. impact velocity.					
ORIGINAL PAGE IS OF POOR QUALITY					
17. Key Words (Suggested by Author(s)) Impact fiber composites, laminates contact law, finite element, stress waves			18. Distribution Statement Unclassified, Unlimited		
19. Security Classif. (of this report) Unclassified		20. Security Classif. (of this page) Unlimited		21. No. of Pages 130	22. Price*

* For sale by the National Technical Information Service, Springfield, Virginia 22161

ORIGINAL PAGE IS
OF POOR QUALITY

TABLE OF CONTENTS

	Page
TABLE OF CONTENTS	iii
LIST OF TABLES	v
LIST OF FIGURES	vi
LIST OF SYMBOLS	ix
CHAPTER 1 - INTRODUCTION	1
CHAPTER 2 - STRESS WAVE IN A LAMINATED PLATE	5
2.1 Laminate Theory with Transverse shear effects	6
2.1.1 Lamina Constitutive Equations	6
2.1.2 Plate Strain-Displacement Relations	9
2.1.3 Stress-Resultants and Laminate Constitutive Equations	12
2.1.4 Plate Equations of Motion	16
2.2 Propagation of Harmonic Waves	18
2.3 Propagation of Wave Front	23
2.3.1 Kinematic Conditions of Compatibility on the Wave Front	25
2.3.2 Dynamical Conditions on the Wave Front	27
2.3.3 Propagation Velocity of the Wave Front	32
2.3.4 Wave Surface and Ray	35
CHAPTER 3 - STATICAL INDENTATION LAWS	48
3.1 Specimens and Experimental Procedure	52
3.2 Experimental Results	53
3.2.1 Loading Curves	53
3.2.2 Unloading Curves	57
3.2.3 Reloading Curves	71

3.3 Discussion	71
CHAPTER 4 - IMPACT EXPERIMENTS	80
4.1 Experimental Procedure	81
4.2 Calibration of Impact-Force Transducer	84
4.3 Finite Element Analysis	94
4.3.1 Plate Finite Element	94
4.3.2 Modeling of Projectile	97
44 Results and Discussion	100
CHAPTER 5 - SUMMARY AND CONCLUSION	113
LIST OF REFERENCES	116
APPENDIX: COMPUTER PROGRAM AND USER INSTRUCTIONS	119

LIST OF TABLES

Table	Page
3.1 Contact coefficient k of loading law $F = k\alpha^{1.5}$	60
4.1 Specifications for Model 200A05 Impact-Force Transducer.....	85

LIST OF FIGURES

Figure	Page
2.1 Lamina reference axes and laminate reference axes.....	8
2.2 Laminate displacement components for a cross-section perpendicular to the y-axis.....	10
2.3 Stress-resultants and geometry of a typical N-layer laminate.....	14
2.4 Dispersion curves for plane harmonic waves propagating in the 0°- 45°- and 90°- directions.....	22
2.5 Frequency curves for flexural waves propagating in the 0°- 45°- and 90°- directions.....	24
2.6 A deformed volume V divided by a travelling surface Ω	29
2.7 Normal velocities of in-plane wave fronts.....	36
2.8 Normal velocities of flexural wave fronts.....	37
2.9 Wave front positions at different times and rays for in-plane extensional mode.....	43
2.10 Wave front positions at different times and rays for in-plane shear mode.....	44
2.11 Wave front positions at different times and rays for bending mode.....	45
2.12 Wave front positions at different times and rays for twisting mode.....	46
3.1 Schematical diagram for the indentation test set-up.....	54
3.2 Loading curve of $[0^\circ/45^\circ/0^\circ/-45^\circ/0^\circ]_{2s}$ specimens with 0.5 inch indenter ($n=3/2$).....	55

3.3 Loading curve of $[90^{\circ}/45^{\circ}/90^{\circ}/-45^{\circ}/90^{\circ}]_{2s}$ specimens with 0.5 Inch Indenter ($n=3/2$).....	56
3.4 Loading curve of $[0^{\circ}/45^{\circ}/0^{\circ}/-45^{\circ}/0^{\circ}]_{2s}$ specimens with 0.75 Inch Indenter ($n=3/2$).....	58
3.5 Loading curve of $[90^{\circ}/45^{\circ}/90^{\circ}/-45^{\circ}/90^{\circ}]_{2s}$ specimens with 0.75 Inch Indenter ($n=3/2$).....	59
3.6 Relation between permanent indentation and maximum indentation.....	61
3.7 Unloading curves of $[0^{\circ}/45^{\circ}/0^{\circ}/-45^{\circ}/0^{\circ}]_{2s}$ specimens with 0.5 Inch Indenter ($q=2.2$).....	63
3.8 Unloading curves of $[90^{\circ}/45^{\circ}/90^{\circ}/-45^{\circ}/90^{\circ}]_{2s}$ specimens with 0.5 Inch Indenter ($q=2.2$).....	64
3.9 Unloading curves of $[0^{\circ}/45^{\circ}/0^{\circ}/-45^{\circ}/0^{\circ}]_{2s}$ specimens with 0.75 Inch Indenter ($q=1.8$).....	65
3.10 Unloading curves of $[90^{\circ}/45^{\circ}/90^{\circ}/-45^{\circ}/90^{\circ}]_{2s}$ specimens with 0.75 Inch Indenter ($q=1.8$).....	66
3.11 Unloading curves of $[0^{\circ}/45^{\circ}/0^{\circ}/-45^{\circ}/0^{\circ}]_{2s}$ specimens with 0.5 Inch Indenter ($q=2.5$).....	67
3.12 Unloading curves of $[90^{\circ}/45^{\circ}/90^{\circ}/-45^{\circ}/90^{\circ}]_{2s}$ specimens with 0.5 Inch Indenter ($q=2.5$).....	68
3.13 Unloading curves of $[0^{\circ}/45^{\circ}/0^{\circ}/-45^{\circ}/0^{\circ}]_{2s}$ specimens with 0.75 Inch Indenter ($q=2.0$).....	69
3.14 Unloading curves of $[90^{\circ}/45^{\circ}/90^{\circ}/-45^{\circ}/90^{\circ}]_{2s}$ specimens with 0.75 Inch Indenter ($q=2.0$).....	70
3.15 Reloading curve of $[0^{\circ}/45^{\circ}/0^{\circ}/-45^{\circ}/0^{\circ}]_{2s}$ specimen with 0.5 Inch Indenter ($p=1.5$).....	72
3.16 Reloading curve of $[90^{\circ}/45^{\circ}/90^{\circ}/-45^{\circ}/90^{\circ}]_{2s}$ specimen with 0.5 Inch Indenter ($p=1.5$).....	73
3.17 Reloading curve of $[0^{\circ}/45^{\circ}/0^{\circ}/-45^{\circ}/0^{\circ}]_{2s}$ specimen with 0.75 Inch Indenter ($p=1.5$).....	74
3.18 Reloading curve of $[90^{\circ}/45^{\circ}/90^{\circ}/-45^{\circ}/90^{\circ}]_{2s}$ specimen with 0.75 Inch Indenter ($p=1.5$).....	75
3.19 Unloading rigidity s as function of maximum indentation.....	78
4.1 Laminate dimension and strain gage locations.....	82

4.2	Graphical illustration of impact projectile.....	82
4.3	Schematic diagram for the impact experimental set-up.....	83
4.4	Experimental set-up for the calibration of impact-force transducer.....	86
4.5	Typical output voltages from transducer and accelerometer.....	88
4.6	Relation between V_F and V_B	88
4.7	Assumed exponential impulsive loading and the response history at the midpoint of the rod.....	90
4.8	Accelerations of rod for assumed exponential impulsive loading.....	92
4.9	Assumed sine-function impulsive loading and the response history at the midpoint of the rod.....	93
4.10	9-node isoparametric plate element.....	95
4.11	Finite element mesh for laminated plate and projectile.....	101
4.12	Strain response history at gage No.1.....	103
4.13	Strain response history at gage No.2.....	104
4.14	Strain response history at gage No.3.....	105
4.15	Strain response history at gage No.4.....	106
4.16	Strain response history at gage No.5.....	107
4.17	Strain response history at gage No.6.....	108
4.18	Transducer response and contact force histories from experimental and finite element results.....	109
4.19	Transducer response histories from experimental and finite element results up to 800 microseconds.....	111
4.20	Deformed configurations of laminated plate after impact.....	112

LIST OF SYMBOLS

A	Cross-sectional area of the projectile
A_{IJ}, B_{IJ}, D_{IJ}	Laminate stiffnesses
E_s	Young's modulus of the steel indenter
E_1	Young's modulus of lamina in the fiber direction
E_2	Young's modulus of lamina in the transverse direction
F	Contact force
F_m	Maximum contact force
G	Shear modulus
$[K_p], [K_r]$	Stiffness matrices
$[M_p], [M_r]$	Mass matrices
M	Stress couples of laminate
N	Stress resultants of laminate
$\{P_p\}, \{P_r\}$	Assembled global load vectors
Q	Transverse shear force of laminate
Q_{IJ}	Reduced stiffnesses
\bar{Q}_{IJ}	Transformed reduced stiffnesses
R_s	Radius of steel indenter
S_i	Shape functions of plate element
V_F	Output voltage of the force transducer
V_a	Output voltage of the accelerometer

a	Acceleration
c	Phase velocity
c_a	Sensitivity of the accelerometer
c_F	Sensitivity of the impact-force transducer
c_n	Normal velocity of wave front
f_i	Shape functions of rod element
$[f]$	Discontinuity of f across wave front surface
h	Laminate thickness
k	Wave number
k	Contact coefficient
k_1	Reloading rigidity
$[k_p], [k_r]$	Element stiffness matrices
$[m_p], [m_r]$	Element mass matrices
n	Power index of loading law
n_1	Unit normal on the wave front
p	Power index of reloading law
p_1	Slowness vector
$\{p_p\}_e, \{p_r\}_e$	Element load vectors
q	Power index of unloading law
$\{q_p\}, \{q_r\}$	Assembled global displacement vectors
$\{q_p\}_e, \{q_r\}_e$	Element displacement vectors
s	Unloading rigidity
t	Time
t^*	Non-dimensional time
u, v, w	Displacement components of laminate
u^0, v^0, w^0	Midplane displacement components

x, y, z	Laminate coordinate system
x_1, x_2, x_3	Laminar coordinate system
Ω	Wave front surface
α	Indentation depth
α_0	Permanent Indentation
α_m	Maximum Indentation
α_{cr}, α_p	Critical indentations
γ	Shearing strain
ϵ	Normal strain
$\kappa_x, \kappa_y, \kappa_{xy}$	Rotation gradients
λ	Wave length
ν	Poisson's ratio
ν_s	Poisson's ratio of the steel indenter
ξ, η	Normalized local coordinates of plate element
ρ	Mass density of laminate
σ	Normal stress
τ	Shearing stress
ϕ_x, ϕ_y	Rotations of cross-sections of laminate
ω	Frequency

ORIGINAL PAGE IS
OF POOR QUALITY

CHAPTER 1
INTRODUCTION

Advanced fiber-reinforced composite materials such as boron/epoxy and graphite/epoxy have been successfully employed as structural materials in aircrafts, missiles and space vehicles in recent years, and the performance of these composites has shown their superiority over metals in applications requiring high strength, high stiffness as well as low weight. The advantages of these composites, however, are overshadowed by their relatively poor resistance to the impact loadings, which has prevented the application of these materials to turbine fan bladings. Many other reports dealing with the responses of advanced composites to various types of impact have further increased the need for a better understanding of the problem so that the survivability of these composites can be improved.

It is obvious that impact produces damage and consequently reduces the strength of composite materials. The damage modes usually include local permanent deformations, breakage of fibers, delaminations, etc.. While the cause of these damages are still unknown and may not be simple in nature, in general, the impact of a soft object could give a longer contact duration, and the dynamic

ORIGINAL PAGE IS
OF POOR QUALITY

response of the whole structure is of importance. The hard object impact usually gives a short contact time and results in the initial transmission of impact energy into a local region of the structure. This initial energy will propagate into the rest of the structure in the form of stress waves. Far field damage away from the impact area could result from the reflection of stress waves. It is generally agreed that the cause of the sudden failure must be examined from the point of transient wave propagation phenomena.

Flexural waves induced by dynamic loads in laminated composites are more complicated than those in homogeneous and isotropic plates due to the anisotropic and nonhomogeneous properties in the laminate. Moreover, because of the low transverse shear modulus in fiber composites, the effect of transverse shear deformation becomes significant and should be considered in the formulation. In Chapter 2, the laminate theory which includes the transverse shear deformation effect is reviewed, and harmonic waves in a graphite/epoxy laminated plate are studied. The propagation of wave front which, for a given time after impact, bound the stressed region surrounding the impact point, is also investigated.

A survey of wave propagation and impact in composite materials has been given by Moon [1]. Many analytical [2-5], numerical [6-7] and experimental [8-10] methods have been employed to study the transient impact problems. The

response of a laminated plate can be analyzed using these methods provided the applied load history is prescribed. However if the dynamic load results from an impact of an object on the laminated plate, then the resulting contact force must be determined first. An accurate account of the contact behavior becomes the most important step in analyzing the impact response problems.

A classical contact law between two elastic spheres was derived by Hertz [11]. When letting the radius of one of the spheres go to infinity, one obtains the contact law between an elastic sphere and an elastic half-space. Many authors have used the Hertzian contact law for the study of impact on metals and composites. [12-13]. Recently, Yang and Sun [14] performed statical indentation tests on graphite/epoxy composite laminates using spherical steel indenters of different sizes and found that the Hertzian law of contact was not adequate. In particular, they found that significant permanent indentations existed and that the unloading paths were very different from the loading path. Noting that energy dissipation takes place during the process of impact, Yang and Sun [14] suggested that this energy is responsible for the local damage of the target materials. The unloading curves and permanent indentations obtained from the statical indentation tests may provide a useful information in estimating the amount of damage due to impact since this energy is simply the area enclosed by the

loading-unloading curves. In this study, similar statical indentation tests were conducted and the results are presented in Chapter 3.

Wang [15] has performed a number of impact tests on graphite/epoxy laminated beams and plates. It was shown that the strain responses calculated using finite element method and the statically determined contact laws from [14] agreed with the experimental measurements quite well. This indicates that the statical indentation law is reasonably adequate in the dynamical impact analysis. It was also suggested that the contact force should be measured experimentally to provide an additional basis for comparison with the finite element solution which could allow further evaluation the applicability of the contact laws in impact analysis. Chapter 4 describes an impact experiment on graphite/epoxy laminated plate using an impact-force transducer with a spherical steel cap as the impactor. The contact force history and strain responses at various points on the plate were measured by means of the transducer and surface strain gages, respectively, and were compared with the predictions of finite element analysis using the statically determined contact law.

Chapter 5 summarizes the results obtained in Chapter 2, 3 and 4.

ORIGINAL PAGE IS
OF POOR QUALITY

ORIGINAL PAGE IS
OF POOR QUALITY

CHAPTER 2

STRESS WAVE IN A LAMINATED PLATE

A laminated plate theory which includes the effects of transverse shear deformation and rotatory inertia was developed by Yang, Norris and Stavsky [16] in a way suggested by Mindlin [17] for homogeneous isotropic plates. It was shown that the frequency curves for the propagation of harmonic waves in an infinite two-layer isotropic plate in plane strain agreed with the predictions of the exact solution obtained from theory of elasticity very well. A similar laminated plate theory was developed by Whitney and Pagano [18] and was employed in the study of static bending and vibration for antisymmetric angle-ply composite plates with particular layer properties. It was found that the effect of shear deformation can be quite significant for composite plates with span-to-depth ratio as high as 20. Good agreement was also observed in numerical results for plate bending as comparing with exact solutions of elasticity. In this study, the laminate theory developed by Whitney and Pagano was used for its simplicity yet quite satisfactory in describing the harmonic wave propagation [19].

2.1 Laminate Theory with Transverse Shear Effects

2.1.1 Lamina Constitutive Equations

A laminated plate of constant thickness h consists of a number of thin laminae of unidirectionally fiber-reinforced composite perfectly bonded together. Each lamina, whose fiber may orient in any arbitrary direction, can be regarded as a homogeneous orthotropic solid. Consider a typical k -th lamina. A coordinate system (x_1, x_2, x_3) is chosen in such a way that the x_1 - x_2 plane coincides with the midplane of lamina, and x_1 and x_2 axes are parallel and perpendicular to the fiber direction, respectively. If a state of plane stress parallel to the x_1 - x_2 plane is assumed, then the in-plane stress-strain relations are given by

$$\begin{Bmatrix} \sigma_{11} \\ \sigma_{22} \\ \tau_{12} \end{Bmatrix}^k = \begin{bmatrix} Q_{11} & Q_{12} & 0 \\ Q_{12} & Q_{22} & 0 \\ 0 & 0 & Q_{66} \end{bmatrix} \begin{Bmatrix} \epsilon_{11} \\ \epsilon_{22} \\ \gamma_{12} \end{Bmatrix}^k \quad (2-1)$$

The transverse shear stress-strain relations are given by

$$\begin{Bmatrix} \tau_{23} \\ \tau_{13} \end{Bmatrix}^k = \begin{bmatrix} Q_{44} & 0 \\ 0 & Q_{55} \end{bmatrix} \begin{Bmatrix} \gamma_{23} \\ \gamma_{13} \end{Bmatrix}^k \quad (2-2)$$

In which

$$Q_{11} = E_1 / (1 - \nu_{12}\nu_{21})$$

ORIGINAL PAGE IS
OF POOR QUALITY

$$Q_{22} = E_2 / (1 - \nu_{12}\nu_{21})$$

$$Q_{12} = \nu_{12}E_2 / (1 - \nu_{12}\nu_{21}) = \nu_{21}E_1 / (1 - \nu_{12}\nu_{21})$$

$$Q_{66} = G_{12}$$

(2-3)

$$Q_{44} = G_{23}$$

$$Q_{55} = G_{13}$$

are the so-called reduced stiffnesses, where E , G and ν are Young's modulus, shear modulus and Poisson's ratio, respectively, and subscripts 1 and 2 denote the directions parallel to x_1 and x_2 axes, respectively.

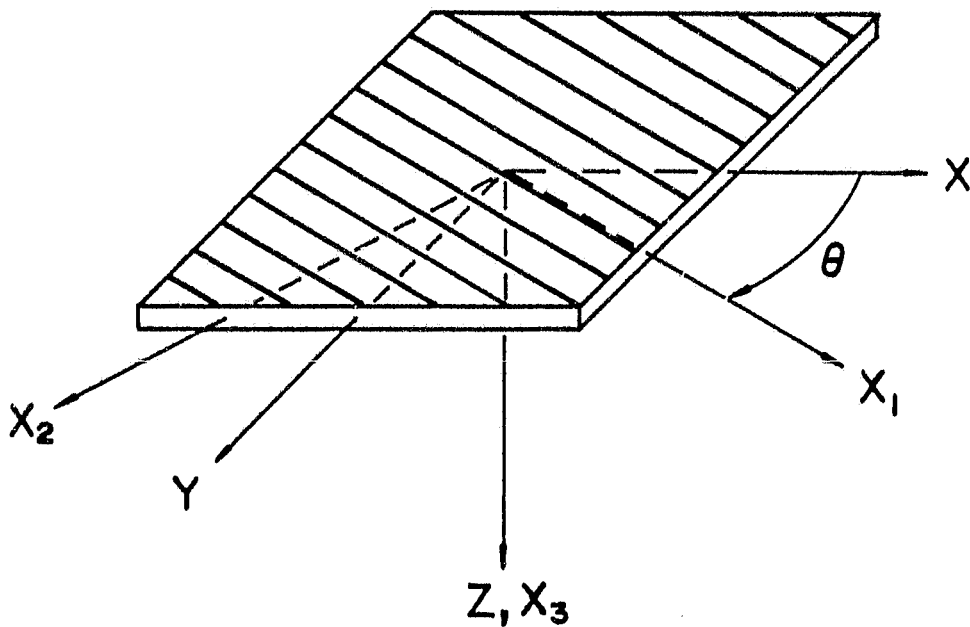
The coordinate system for an arbitrarily oriented lamina does not, in general, coincide with the reference axes (x, y, z) of laminated plate (see Figure 2.1). Using the coordinate transformation laws for stress and strain, we obtain the stress-strain relations in laminate reference system as

$$\begin{Bmatrix} \sigma_{xx} \\ \sigma_{yy} \\ \tau_{xy} \\ \tau_{yz} \\ \tau_{xz} \end{Bmatrix}^k = \begin{bmatrix} \bar{Q}_{11} & \bar{Q}_{12} & \bar{Q}_{16} & 0 & 0 \\ \bar{Q}_{12} & \bar{Q}_{22} & \bar{Q}_{26} & 0 & 0 \\ \bar{Q}_{16} & \bar{Q}_{26} & \bar{Q}_{66} & 0 & 0 \\ 0 & 0 & 0 & \bar{Q}_{44} & \bar{Q}_{45} \\ 0 & 0 & 0 & \bar{Q}_{45} & \bar{Q}_{55} \end{bmatrix} \begin{Bmatrix} \epsilon_{xx} \\ \epsilon_{yy} \\ \gamma_{xy} \\ \gamma_{yz} \\ \gamma_{xz} \end{Bmatrix}^k \quad (2-4)$$

In which \bar{Q}_{ij} are given by

$$\bar{Q}_{11} = Q_{11}m^4 + 2(Q_{12} + 2Q_{66})m^2n^2 + Q_{22}n^4$$

ORIGINAL PAGE IS
OF POOR QUALITY



(X_1, X_2, X_3) — Lamina Reference Axes

(X, Y, Z) — Laminate Reference Axes

Figure 2.1 Lamina reference axes and laminate reference axes

$$\begin{aligned}
 \bar{Q}_{22} &= Q_{11}n^4 + 2(Q_{12} + 2Q_{66})m^2n^2 + Q_{22}m^4 \\
 \bar{Q}_{12} &= (Q_{11} + Q_{22} - 4Q_{66})m^2n^2 + Q_{12}(m^4 + n^4) \\
 \bar{Q}_{16} &= (Q_{11} - Q_{12} - 2Q_{66})m^3n + (Q_{12} - Q_{22} + 2Q_{66})mn^3 \\
 \bar{Q}_{26} &= (Q_{11} - Q_{12} - 2Q_{66})mn^3 + (Q_{12} - Q_{22} + 2Q_{66})m^3n \\
 \bar{Q}_{66} &= (Q_{11} + Q_{22} - 2Q_{12} - 2Q_{66})m^2n^2 + Q_{66}(m^4 + n^4) \\
 \bar{Q}_{44} &= Q_{44}m^2 + Q_{55}n^2 \\
 \bar{Q}_{45} &= (Q_{44} - Q_{55})mn \\
 \bar{Q}_{55} &= Q_{44}n^2 + Q_{55}m^2
 \end{aligned} \tag{2-5}$$

where

$$m = \cos\theta \quad n = \sin\theta$$

and θ is the angle between x-axis and x_1 -axis measured from x to x_1 , counterclockwise as shown in Figure 2.1.

2.1.2 Plate Strain-Displacement Relations

The displacement components of the laminated plate are assumed to be of the form [16]

$$\begin{aligned}
 u(x,y,z) &= u^0(x,y) + z\phi_x(x,y) \\
 v(x,y,z) &= v^0(x,y) + z\phi_y(x,y) \\
 w(x,y,z) &= w^0(x,y) = w(x,y)
 \end{aligned} \tag{2-6}$$

where u^0 , v^0 and w^0 are the midplane displacement components in the x-, y- and z-directions, respectively, and ϕ_x and ϕ_y are rotations of cross-sections perpendicular to x- and y-axis, respectively (see Figure 2.2). In Equation (2.6) we

ORIGINAL PAGE IS
OF POOR QUALITY

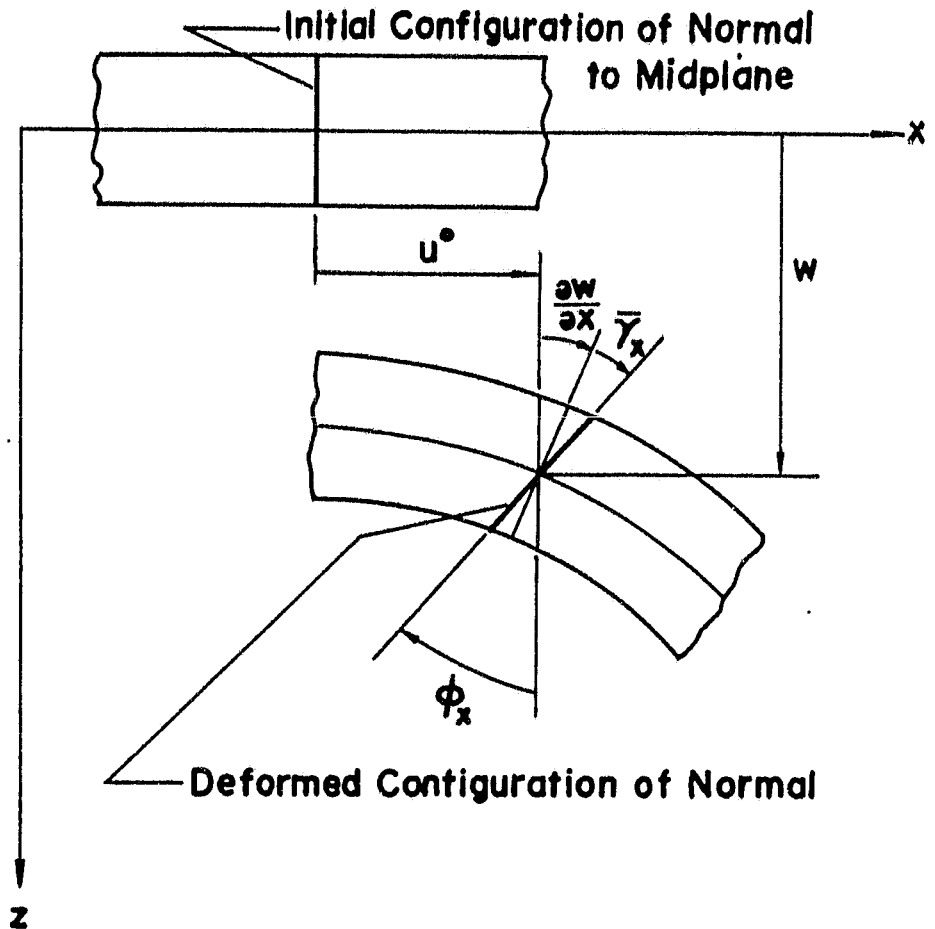


Figure 2.2 Laminate displacement components for a cross-section perpendicular to the y-axis

have assumed that u and v vary linearly in the thickness direction, while w is constant through the thickness.

The strain components for a point in k -th lamina of the laminated plate with a distance z from the midplane can be computed as

$$\begin{aligned}
 \epsilon_{xx}^k &= \epsilon_x^0 + z\kappa_x \\
 \epsilon_{yy}^k &= \epsilon_y^0 + z\kappa_y \\
 \gamma_{xy}^k &= \gamma_{xy}^0 + z\kappa_{xy} \\
 \gamma_{yz}^k &= \partial w/\partial y + \partial v/\partial z = \partial w/\partial y + \phi_y = \gamma_{yz}^0 \\
 \gamma_{xz}^k &= \partial w/\partial x + \partial u/\partial z = \partial w/\partial x + \phi_x = \gamma_{xz}^0
 \end{aligned}
 \tag{2-7}$$

where

$$\begin{aligned}
 \gamma_x^0 &= \partial u^0/\partial x \\
 \gamma_y^0 &= \partial v^0/\partial y \\
 \gamma_{xy}^0 &= \partial u^0/\partial y + \partial v^0/\partial x
 \end{aligned}
 \tag{2-8}$$

are the in-plane strain components of midplane, and

$$\begin{aligned}
 \kappa_x &= \partial \phi_x/\partial x \\
 \kappa_y &= \partial \phi_y/\partial x \\
 \kappa_{xy} &= \partial \phi_x/\partial y + \partial \phi_y/\partial x
 \end{aligned}
 \tag{2-9}$$

are the rotation gradients.

In Equation (2-7), since w , ϕ_x and ϕ_y are independent of z , it follows that the transverse shear strains are constant through the thickness of the plate.

Equation (2-7) can be written in concise matrix form as

$$\begin{Bmatrix} \epsilon \\ \gamma \end{Bmatrix}^k = \begin{Bmatrix} \epsilon_x \\ \epsilon_y \\ \gamma_{xy} \\ \gamma_{yz} \\ \gamma_{xz} \end{Bmatrix}^k = \begin{Bmatrix} \epsilon_x^0 \\ \epsilon_y^0 \\ \gamma_{xy}^0 \\ \gamma_{yz}^0 \\ \gamma_{xz}^0 \end{Bmatrix} + z \begin{Bmatrix} \kappa_x \\ \kappa_y \\ \kappa_{xy} \\ 0 \\ 0 \end{Bmatrix} = \begin{Bmatrix} \epsilon \\ \gamma \end{Bmatrix}^0 + z \begin{Bmatrix} \kappa \\ 0 \end{Bmatrix} \quad (2-10)$$

Thus, the strain components at any point in the plate can be determined from the extensional strain components of the midplane, the rotation gradients of the plate and the distance z from the midplane.

2.1.3 Stress-Resultants and Laminate Constitutive Equations

Substitution of Equation (2-10) in Equation (2-4) gives the stress components for a point in the k -th lamina as:

$$\begin{Bmatrix} \sigma_{xx} \\ \sigma_{yy} \\ \tau_{xy} \\ \tau_{yz} \\ \tau_{xz} \end{Bmatrix}^k = \begin{bmatrix} \bar{Q}_{11} & \bar{Q}_{12} & \bar{Q}_{16} & 0 & 0 \\ \bar{Q}_{12} & \bar{Q}_{22} & \bar{Q}_{26} & 0 & 0 \\ \bar{Q}_{16} & \bar{Q}_{26} & \bar{Q}_{66} & 0 & 0 \\ 0 & 0 & 0 & \bar{Q}_{44} & \bar{Q}_{45} \\ 0 & 0 & 0 & \bar{Q}_{45} & \bar{Q}_{55} \end{bmatrix} \begin{Bmatrix} \epsilon_x^0 \\ \epsilon_y^0 \\ \gamma_{xy}^0 \\ \gamma_{yz}^0 \\ \gamma_{xz}^0 \end{Bmatrix} + z \begin{Bmatrix} \kappa_x \\ \kappa_y \\ \kappa_{xy} \\ 0 \\ 0 \end{Bmatrix} \quad (2-11)$$

The stress-resultants acting on a laminate can be obtained by integration of the stresses in each lamina through the laminate thickness. Specifically, the in-plane

stress-resultants are given by

$$\begin{Bmatrix} N_x \\ N_y \\ N_{xy} \end{Bmatrix} = \int_{-h/2}^{h/2} \begin{Bmatrix} \sigma_{xx} \\ \sigma_{yy} \\ \gamma_{xy} \end{Bmatrix} dz = \sum_{k=1}^N \int_{h_{k-1}}^{h_k} \begin{Bmatrix} \sigma_{xx} \\ \sigma_{yy} \\ \tau_{xy} \end{Bmatrix}^k dz \quad (2-12)$$

the stress couples are given by

$$\begin{Bmatrix} M_x \\ M_y \\ M_{xy} \end{Bmatrix} = \int_{-h/2}^{h/2} \begin{Bmatrix} \sigma_{xx} \\ \sigma_{yy} \\ \gamma_{xy} \end{Bmatrix} z dz = \sum_{k=1}^N \int_{h_{k-1}}^{h_k} \begin{Bmatrix} \sigma_{xx} \\ \sigma_{yy} \\ \tau_{xy} \end{Bmatrix}^k z dz \quad (2-13)$$

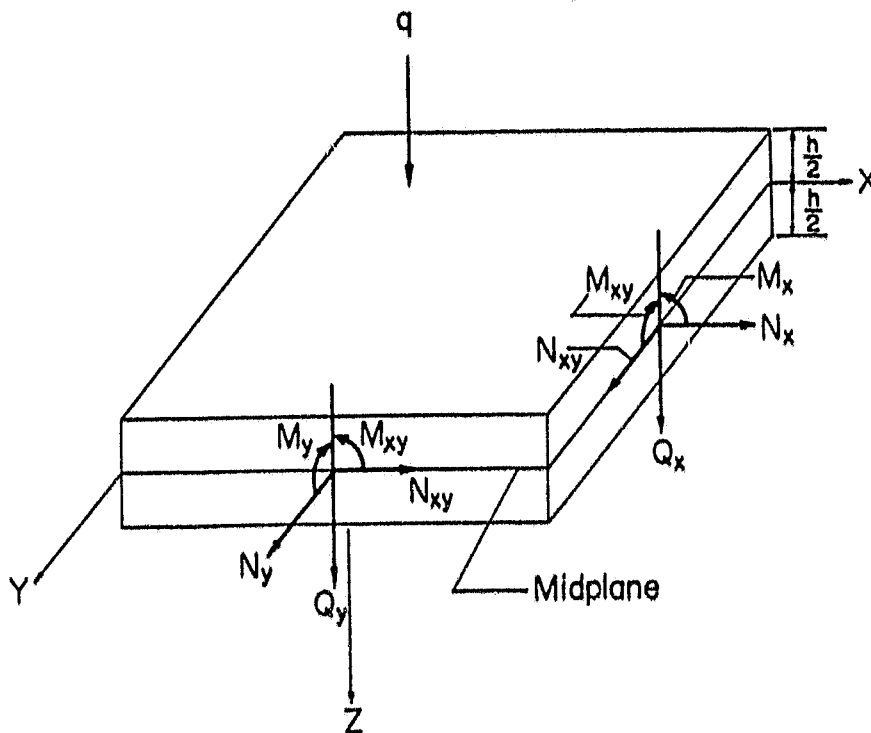
and the transverse shear forces are given by

$$\begin{Bmatrix} Q_y \\ Q_x \end{Bmatrix} = \int_{-h/2}^{h/2} \begin{Bmatrix} \tau_{yz} \\ \tau_{xz} \end{Bmatrix} dz = \sum_{k=1}^N \int_{h_{k-1}}^{h_k} \begin{Bmatrix} \tau_{yz} \\ \tau_{xz} \end{Bmatrix}^k dz \quad (2-14)$$

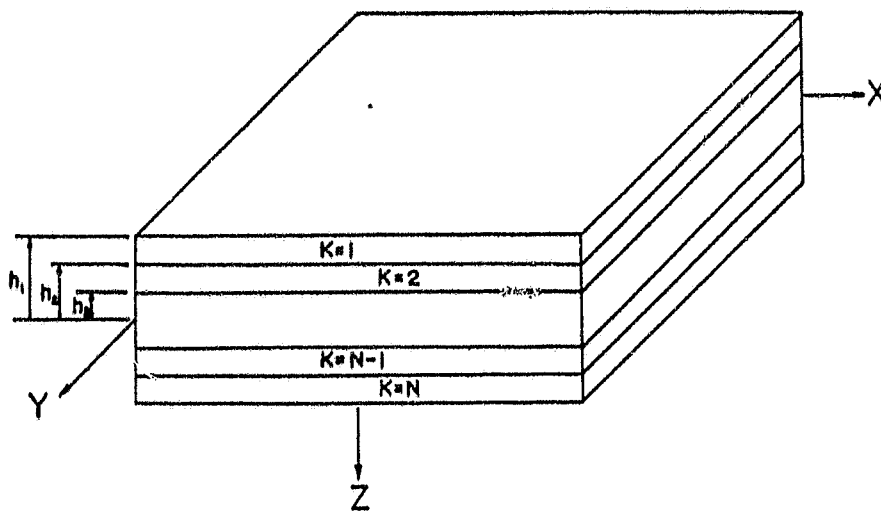
The sign convention for these stress-resultants along with the geometry of a typical N-layer laminated plate are shown in Figure 2.3.

Substituting Equation (2-11) into the right hand sides of the above three equations and performing the integrations, we obtain

ORIGINAL PAGE IS
OF POOR QUALITY



(a) STRESS RESULTANTS OF A LAMINATE



(b) GEOMETRY OF AN N -LAYER LAMINATE

Figure 2.3 Stress-resultants and geometry of a typical N -layer laminate

$$\begin{Bmatrix} N_x \\ N_y \\ N_{xy} \end{Bmatrix} = \begin{bmatrix} A_{11} & A_{12} & A_{16} \\ A_{12} & A_{22} & A_{26} \\ A_{16} & A_{26} & A_{66} \end{bmatrix} \begin{Bmatrix} \epsilon_x^0 \\ \epsilon_y^0 \\ \gamma_{xy}^0 \end{Bmatrix} + \begin{bmatrix} B_{11} & B_{12} & B_{16} \\ B_{12} & B_{22} & B_{26} \\ B_{16} & B_{26} & B_{66} \end{bmatrix} \begin{Bmatrix} \kappa_x \\ \kappa_y \\ \kappa_{xy} \end{Bmatrix} \quad (2-15)$$

$$\begin{Bmatrix} M_x \\ M_y \\ M_{xy} \end{Bmatrix} = \begin{bmatrix} B_{11} & B_{12} & B_{16} \\ B_{12} & B_{22} & B_{26} \\ B_{16} & B_{26} & B_{66} \end{bmatrix} \begin{Bmatrix} \epsilon_x^0 \\ \epsilon_y^0 \\ \gamma_{xy}^0 \end{Bmatrix} + \begin{bmatrix} D_{11} & D_{12} & D_{16} \\ D_{12} & D_{22} & D_{26} \\ D_{16} & D_{26} & D_{66} \end{bmatrix} \begin{Bmatrix} \kappa_x \\ \kappa_y \\ \kappa_{xy} \end{Bmatrix} \quad (2-16)$$

$$\begin{Bmatrix} Q_y \\ Q_x \end{Bmatrix} = \begin{bmatrix} A^*_{44} & A^*_{45} \\ A^*_{45} & A^*_{55} \end{bmatrix} \begin{Bmatrix} \gamma_{yz} \\ \gamma_{xz} \end{Bmatrix} \quad (2-17)$$

where

$$(A_{1j}, B_{1j}, D_{1j}) = \int_{-h/2}^{h/2} \bar{Q}_{1j}(1, z, z^2) dz \quad j = 1, 2, 6 \quad (2-18)$$

and

$$A^*_{ij} = \int_{-h/2}^{h/2} \bar{Q}_{ij} dz \quad i, j = 4, 5 \quad (2-19)$$

Equations (2-15) through (2-17) are usually written symbolically as

$$\begin{Bmatrix} N \\ M \\ Q \end{Bmatrix} = \begin{bmatrix} A & B & 0 \\ B & D & 0 \\ 0 & 0 & A^* \end{bmatrix} \begin{Bmatrix} \epsilon^0 \\ \kappa \\ \gamma \end{Bmatrix} \quad (2-20)$$

which is the laminate constitutive equation with transverse shear effect included.

2.1.4 Plate Equations of Motion

The stress-equations of motion for the k-th lamina are given by

$$\begin{aligned}\sigma_{xx,x} + \tau_{xy,y} + \tau_{xz,z} &= \rho \ddot{u} \\ \tau_{xy,x} + \sigma_{yy,y} + \tau_{yz,z} &= \rho \ddot{v} \\ \tau_{xz,x} + \tau_{yz,y} + \sigma_{zz,z} &= \rho \ddot{w}\end{aligned}\quad (2-21)$$

where ρ is the mass density. Integrating Equation (2-21) through the thickness of laminate and then substituting Equation (2-12), (2-14) and (2-6) in, we obtain

$$\begin{aligned}N_{x,x} + N_{xy,y} &= P\ddot{u}^0 + R\ddot{\phi}_x \\ N_{xy,x} + N_{y,y} &= P\ddot{v}^0 + R\ddot{\phi}_y \\ Q_{x,x} + Q_{y,y} + q &= P\ddot{w}\end{aligned}\quad (2-22)$$

where q is the normal traction on the plate. Multiplying the first two equations of Equation (2-21), integrating through the thickness of laminate and then substituting Equations (2-13), (2-14) and (2-5) in, we obtain

$$\begin{aligned}M_{x,x} + M_{xy,y} - Q_x &= R\ddot{u}^0 + I\ddot{\phi}_x \\ M_{xy,x} + M_{y,y} - Q_y &= R\ddot{v}^0 + I\ddot{\phi}_y\end{aligned}\quad (2-23)$$

In which P , R and I are defined as

$$(P, R, I) = \int_{-h/2}^{h/2} \rho(1, z, z^2) dz \quad (2-24)$$

Equations (2-22) and (2-23) are the plate equations of

motion. Substitution of Equation (2-20) and then the strain-displacement relations in these two equations yield the equations of motion in terms of midplane displacements and rotations of the plate.

A graphite/epoxy laminated plate provided by NASA Lewis Research Center was used throughout this study. This laminate is a $[0^\circ/45^\circ/0^\circ/-45^\circ/0^\circ]_{2s}$ graphite/epoxy composite with 0.0053 inch ply thickness and the following ply properties [15]:

$$\begin{aligned} E_1 &= 17.5 \times 10^6 \text{ psi.} \\ E_2 &= 1.15 \times 10^6 \text{ psi.} \\ G_{12} = G_{13} = G_{23} &= 0.8 \times 10^6 \text{ psi.} \\ \nu_{12} &= 0.30 \\ \rho &= 0.000148 \text{ lb-sec}^2/\text{in}^4 \end{aligned} \tag{2-25}$$

For symmetrically laminated composite plate, $B_{ij} = 0$ and $R = 0$. In addition, by choosing the x-axis of the laminate reference system to coincide with the 0° fiber direction, we obtain $A_{16} = A_{26} = 0$ and $D_{16} = D_{26}$. Further, in this study, we assume $G_{13} = G_{23} = G_{12}$, and consequently, $A^*_{45} = 0$ and $A^*_{44} = A^*_{55}$. For this particular laminate, the displacement-equations of motion are given by

$$\begin{aligned} A_{11} \partial^2 u^0 / \partial x^2 + A_{66} \partial^2 u^0 / \partial y^2 + (A_{12} + A_{66}) \partial^2 v^0 / \partial x \partial y &= P \ddot{u}^0 \\ (A_{12} + A_{66}) \partial^2 u^0 / \partial x \partial y + A_{66} \partial^2 v^0 / \partial x^2 + A_{22} \partial^2 v^0 / \partial y^2 &= P \ddot{v}^0 \end{aligned}$$

$$\begin{aligned}
 & D_{11} \partial^2 \phi_x / \partial x^2 + 2D_{16} \partial^2 \phi_x / \partial x \partial y + D_{66} \partial^2 \phi_x / \partial y^2 \\
 & + D_{16} (\partial^2 \phi_y / \partial x^2 + \partial^2 \phi_y / \partial y^2) + (D_{12} + D_{66}) \partial^2 \phi_y / \partial x \partial y \\
 & - A^*_{44} (\partial w / \partial x + \phi_x) = I \ddot{\phi}_x \quad (2-26)
 \end{aligned}$$

$$\begin{aligned}
 & D_{16} (\partial^2 \phi_x / \partial x^2 + \partial \phi_x / \partial y^2) + (D_{12} + D_{66}) \partial^2 \phi_x / \partial x \partial y \\
 & + D_{66} \partial^2 \phi_y / \partial x^2 + 2D_{16} \partial^2 \phi_y / \partial x \partial y + D_{22} \partial^2 \phi_y / \partial y^2 \\
 & - A^*_{44} (\partial w / \partial y + \phi_y) = I \ddot{\phi}_y
 \end{aligned}$$

$$A^*_{44} (\partial^2 w / \partial x^2 + \partial^2 w / \partial y^2 + \partial \phi_x / \partial x + \partial \phi_y / \partial y) + q = \rho \ddot{w}$$

In Equation (2-26), the first two equations govern the in-plane motion while the last three equations govern the flexural motion.

2.2 Propagation of Harmonic Waves

Consider a infinitely large laminated plate governed by the equations of motion (2-26). We assume plane harmonic waves in the form

$$\begin{aligned}
 u^0 &= U \exp[ik(\eta - ct)] \\
 v^0 &= V \exp[ik(\eta - ct)] \\
 w &= W \exp[ik(\eta - ct)] \\
 \phi_x &= \Phi_x \exp[ik(\eta - ct)] \\
 \phi_y &= \Phi_y \exp[ik(\eta - ct)]
 \end{aligned} \quad (2-27)$$

propagating over the plate, where U , V , W , Φ_x and Φ_y are constant amplitudes, k is the wave number, c is the phase

velocity and η is given by

$$\eta = x \cos\alpha + y \sin\alpha$$

ORIGINAL PAGE IS
OF POOR QUALITY

(2-28)

In which α is the angle between the direction of wave propagation and x-axis.

Substitution of Equation (2-27) into Equation (2-26) with $q = 0$ yields a system of five homogeneous equations for the five constant amplitudes. In order to have a nontrivial solution, the determinant of the coefficient matrix is set equal to zero. Since the equations are uncoupled into two groups, the determinantal equation can be separated into two equations as

$$|a_{ij}| = 0 \quad (2-29)$$

for the in-plane extensional and in-plane shear waves, and

$$|b_{ij}| = 0 \quad (2-30)$$

for the flexural waves. In Equations (2-29) and (2-30) the coefficients a_{ij} and b_{ij} are given by

$$\begin{aligned} a_{11} &= A_{11} \cos^2\alpha + A_{66} \sin^2\alpha - \rho c^2 \\ a_{12} &= a_{21} = (A_{12} + A_{66}) \sin\alpha \cos\alpha \\ a_{22} &= A_{66} \cos^2\alpha + A_{22} \sin^2\alpha - \rho c^2 \end{aligned} \quad (2-31)$$

and

$$\begin{aligned} b_{11} &= D_{11} k^2 \cos^2\alpha + 2D_{16} k^2 \sin\alpha \cos\alpha + D_{66} k^2 \sin^2\alpha \\ &\quad + A_{44}^* - I k^2 c^2 \end{aligned}$$

$$b_{12} = b_{21} = D_{16}k^2 \cos^2 \alpha + (D_{12} + D_{66})k^2 \sin \alpha \cos \alpha + D_{16}k^2 \sin^2 \alpha$$

$$b_{13} = b_{31} = 1A^*_{44}k \cos \alpha \quad (2-32)$$

$$b_{22} = D_{66}k^2 \cos^2 \alpha + 2D_{16}k^2 \sin \alpha \cos \alpha + D_{22}k^2 \sin^2 \alpha + A^*_{44} - Ik^2 c^2$$

$$b_{23} = b_{32} = 1A^*_{44}k \sin \alpha$$

$$b_{33} = -A^*_{44}k^2 + Pk^2 c^2$$

Expanding Equation (2-29) we obtain a quadratic equation in c^2 as

$$c^4 - d_1 c^2 + d_2 = 0 \quad (2-33)$$

where

$$d_1 = (A_{11} \cos^2 \alpha + A_{22} \sin^2 \alpha + A_{66})/P \quad (2-34)$$

$$d_2 = \begin{vmatrix} A_{11} \cos^2 \alpha + A_{66} \sin^2 \alpha & (A_{12} + A_{66}) \sin \alpha \cos \alpha \\ (A_{12} + A_{66}) \sin \alpha \cos \alpha & A_{66} \cos^2 \alpha + A_{22} \sin^2 \alpha \end{vmatrix}$$

It is noted that the phase velocity c does not depend on the wave number k , thus these waves are nondispersive. In studying of transverse impact problem where in-plane deformation is negligible, this nondispersive property has no significant effect. Should in-plane deformation become important, higher order approximation of displacement

components u and v must be assumed and the dispersive property of these in-plane waves could be included.

From Equation (2-34) it is evident that there exist two phase velocities corresponding to two modes of wave. Although these two waves involve both in-plane extensional deformation as well as in-plane shear, from the eigenvectors we are able to tell which one is dominant. Thus we label the two waves as in-plane extensional wave and in-plane shear wave accordingly.

The determinantal equation given by Equation (2-30) yields three positive roots in c^2 indicating that three flexural waves exist. These phase velocities are functions of the wave number k , thus they are dispersive. Among these three modes of wave, only the lowest one corresponding to the transverse shear wave has a finite velocity as $k \rightarrow 0$ or as the wave length becomes infinite. The dispersion curves for the waves of the lowest mode propagating in the directions of 0° , 45° and 90° respectively are plotted in Figure 2.4 with the non-dimensional phase velocity vs. the non-dimensional wavelength λ/h . It can be seen that they all approach the value of $\sqrt{G_{13}/\rho}$ as the wavelength becomes shorter. The phase velocities for the two higher modes, however, approach different values in different propagation directions when $\lambda \rightarrow 0$. For laminated composite which are anisotropic in general, the phase velocity varies from one direction to another. As a result the wave surface will

ORIGINAL PAGE IS
OF POOR QUALITY

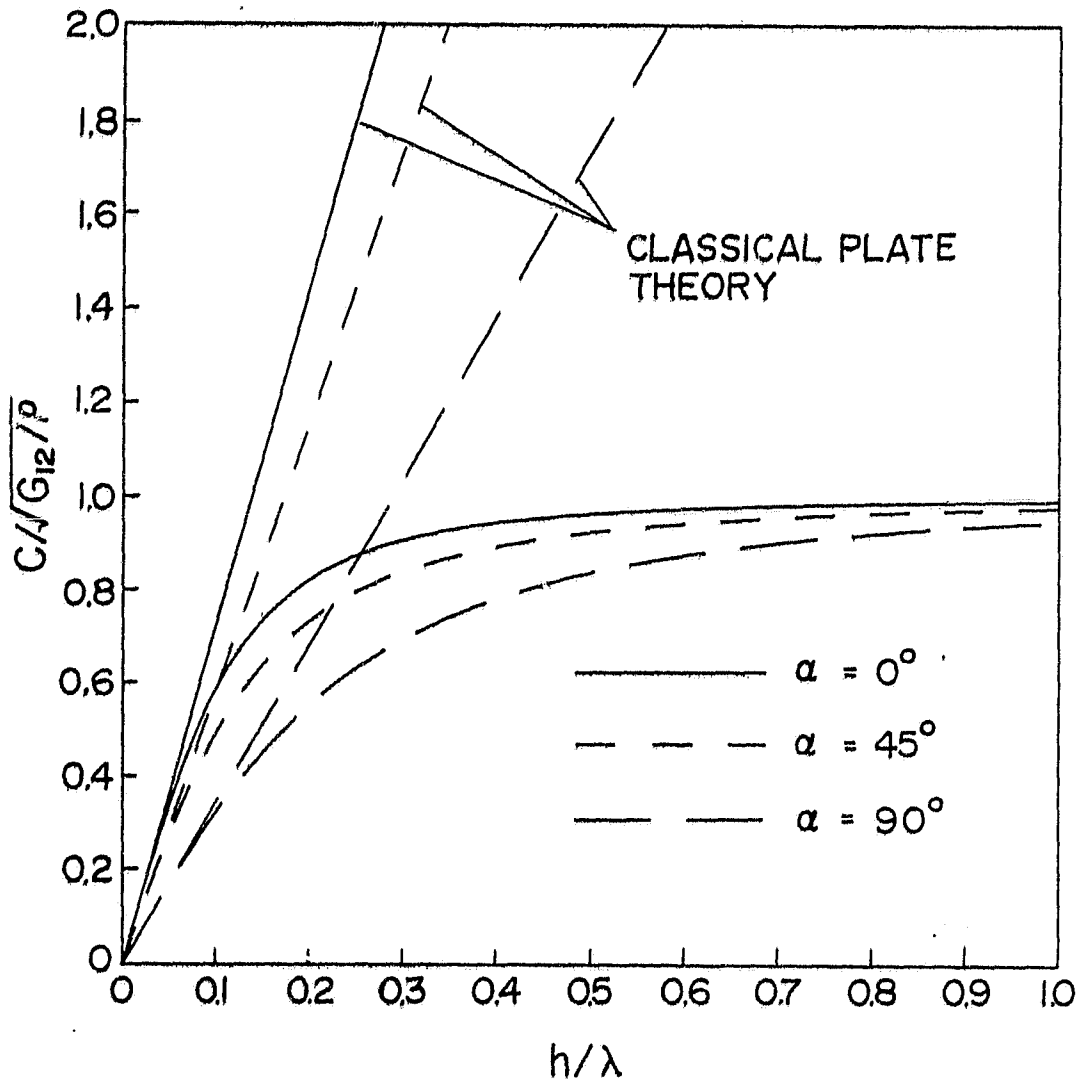


Figure 2.4 Dispersion curves for plane harmonic waves propagating in the 0° - 45° - and 90° - directions

become a rather complicated shape as it propagates. This will be discussed in the next section.

Substitution of $\omega = kc$ in Equation (2-32) yields a set of frequency equations for flexural waves. Figure 2.5 shows the frequency curves of these waves for $\alpha = 0^\circ, 45^\circ$ and 90° , respectively, with the non-dimensional frequency vs. the non-dimensional wavelength. The cutoff frequencies for the two higher modes have a value of $\sqrt{12G_{13}/\rho}/h$. Comparing with the exact cutoff frequency $(\pi/h)\sqrt{G_{13}/\rho}$, it can be seen that if the shear correction factor $\pi^2/12$ is introduced, this theory will predict the correct cutoff frequency.

2.3 Propagation of Wave Front

Impact of foreign objects on a laminated plate with a very short duration could generate weak shock waves which will propagate into the rest of the structure with finite velocities, and the positions of the wave fronts define the regions being disturbed at any instant after impact. Damages to the laminated plate may possibly occur as the first wave front hits the weakest part. It is hence important to investigate the propagation of these shocks in the plate. There have been works dealing with the propagation of wave front: in anisotropic elastic media [20-22]. Moon [23] presented an analysis of wave surfaces in a laminate by treating it as an equivalent homogeneous

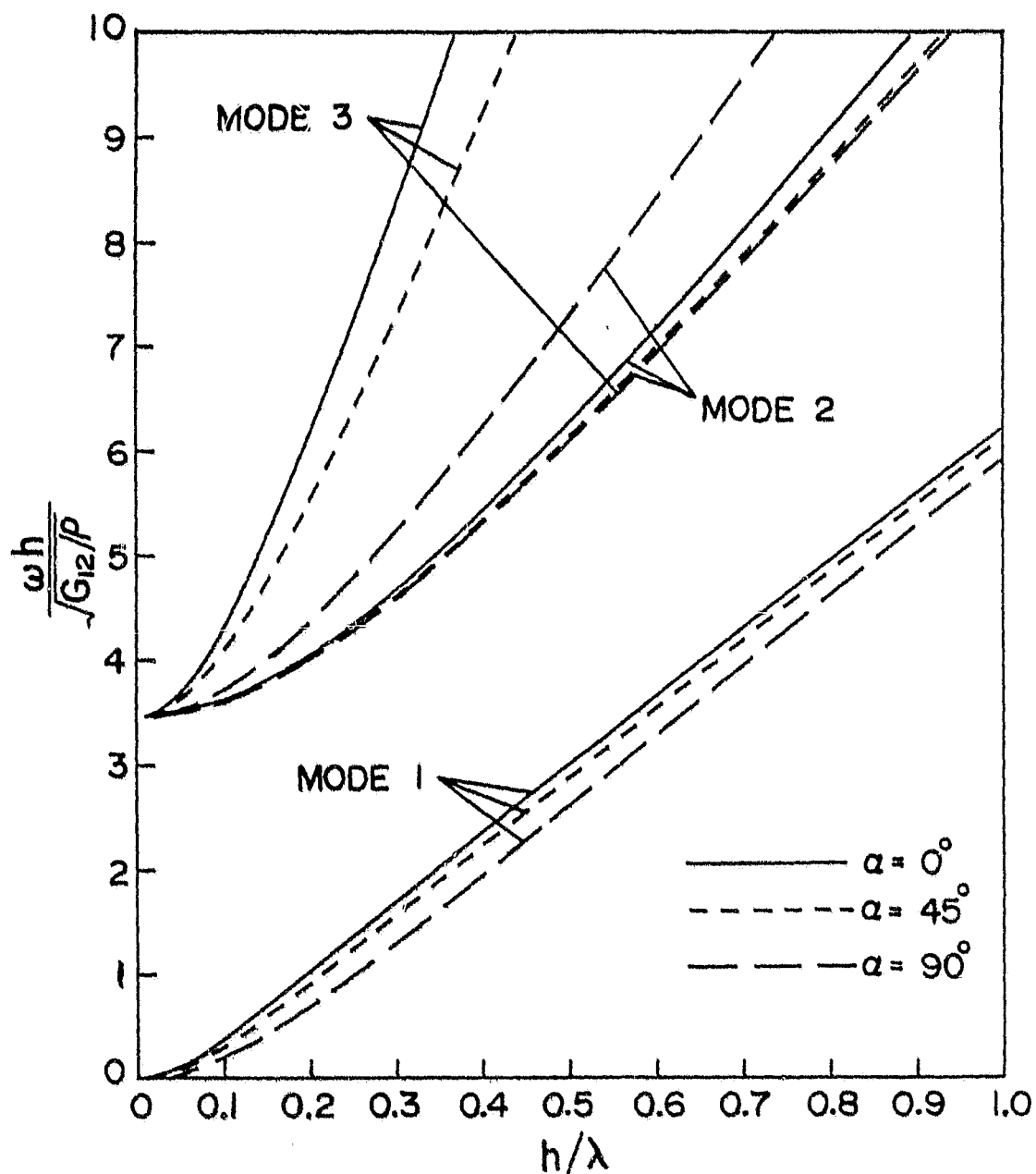
ORIGINAL PAGE IS
OF POOR QUALITY

Figure 2.5 Frequency curves for flexural waves propagating in the 0° - 45° - and 90° - directions

orthotropic plate. The acceleration waves and their wave fronts were investigated. The propagation of shock waves in more general laminates which exhibit the bending-extensional coupling were studied by Sun [2]. The ray theory was employed to construct the wave front surface. The growth and decay of the shock strength were also discussed. In this section, the analytical procedures developed by Sun [2] were applied on a $[0^\circ/45^\circ/0^\circ/-45^\circ/0^\circ]_{2s}$ graphite/epoxy laminated plate.

2.3.1. Kinematic Conditions of Compatibility on the Wave Front

A wave front, which will be denoted by Ω , is defined as a surface travelling over the plate as time varies continuously, and across which there may exist a discontinuity in the stress, particle velocity and their derivatives.

Consider a discontinuous surface Ω passing some observation point in a medium at a certain time t . Let f^- be the value of a field function $f(x_i, t)$ (e.g. stress, particle velocity, etc.) behind the surface Ω , and f^+ be the value of f in front of it, then the discontinuity of function f can be expressed as

$$[f] = f^+ - f^- \quad (2-35)$$

In which the right hand side is to be evaluated at the time and location on Ω passing the observation point, and the jump across the wave front is denoted by square bracket.

Surface Ω may be expressed mathematically by an equation of the form

$$\psi(x_1, t) = 0 \quad (2-36)$$

or, by making t explicit, as

$$\psi(x_1, t) = F(x_1) - t = 0 \quad (2-37)$$

which represents a family of surfaces in x_1 -space with t as a parameter. By evaluating f^+ and f^- at $t = F(x_1)$, the jump of f across the wave front becomes

$$[f(x_1)] = f^+(x_1, F(x_1)) - f^-(x_1, F(x_1)) \quad (2-38)$$

The rate of change of $[f]$ for an observer moving with Ω is given by

$$\begin{aligned} d[f]/dt &= (\partial f^+/\partial x_1 - \partial f^-/\partial x_1) dx_1/dt + (\partial f^+/\partial t - \partial f^-/\partial t) \\ &= c_1 [\partial f / \partial x_1] + [\partial f / \partial t] \end{aligned} \quad (2-39)$$

where $t = F(x_1)$ is substituted, and $c_1 = dx_1/dt$ are velocity components of wave front relative to the material.

If the laminate theory introduced in previous section is used, then the plate displacement components are u^0 , v^0 , w , ϕ_x and ϕ_y , while the spatial variables are $x_1 = x$ and $x_2 = y$. It is assumed that the integrity of the material is not

affected by the propagation of the stress wave front, then these displacement components will remain continuous. Consequently, we have

$$[u^0] = [v^0] = [w] = [\phi_x] = [\phi_y] = 0 \quad (2-40)$$

across the wave front. Applying the general condition of Equation (2-39) on u^0 , together with Equation (2-40), we obtain

$$[\partial u^0 / \partial x_j] c_j + [\dot{u}^0] = 0 \quad j = 1, 2 \quad (2-41)$$

Let c_n and n_j be the normal velocity and the unit normal on the wave front, respectively, it follows that

$$n_j c_j = c_n \quad (2-42)$$

and Equation (2-41) becomes

$$[\partial u^0 / \partial x_j] = -[\dot{u}^0] n_j / c_n \quad j = 1, 2 \quad (2-43)$$

Similar relations can be derived for the other displacement components v^0 , w , ϕ_x and ϕ_y . Together they specify the kinematic conditions of compatibility on the wave front.

2.3.2 Dynamical Conditions on the Wave Front

Consider a finite volume V of a material medium and denoted by S the boundary or surface of V . For a continuous and differentiable function $f(x_i, t)$ in V , it can be shown

[23] that

$$\frac{d}{dt} \int_V f(x_i, t) dV = \int_V f_{,t} dV + \int_S G f dS \quad (2-44)$$

under deformation of the medium, where G is the normal velocity of the surface S . In the case where the deformation of the volume V is determined solely by the motion of material particles, we have

$$G = \dot{u}_i n_i = \dot{u}_n \quad (2-45)$$

where u_i is the displacement components, n_i is the outward normal on S , and \dot{u}_n is the normal velocity of material particle on S . If there exists a discontinuity surface (or wave front) travelling with velocity c_i in the medium, by choosing this surface as the boundary of V , we have

$$G = c_i n_i = c_n \quad (2-46)$$

where c_n is the normal velocity of wave front.

Suppose that a volume V whose motion is determined by the deformation of the material medium, is divided by a travelling surface Ω into two volumes V^- and V^+ as shown in Figure 2.6. The surface S is also divided into two portions S^- and S^+ which form parts of the boundaries of V^- and V^+ , respectively. The remaining part of the boundary is formed by Ω_0 which is a segment of Ω . In Figure 2.6, n_i denotes the unit normal of Ω in the direction of travelling, and n_i^* denotes the unit outward normal of S .

ORIGINAL PAGE IS
OF POOR QUALITY

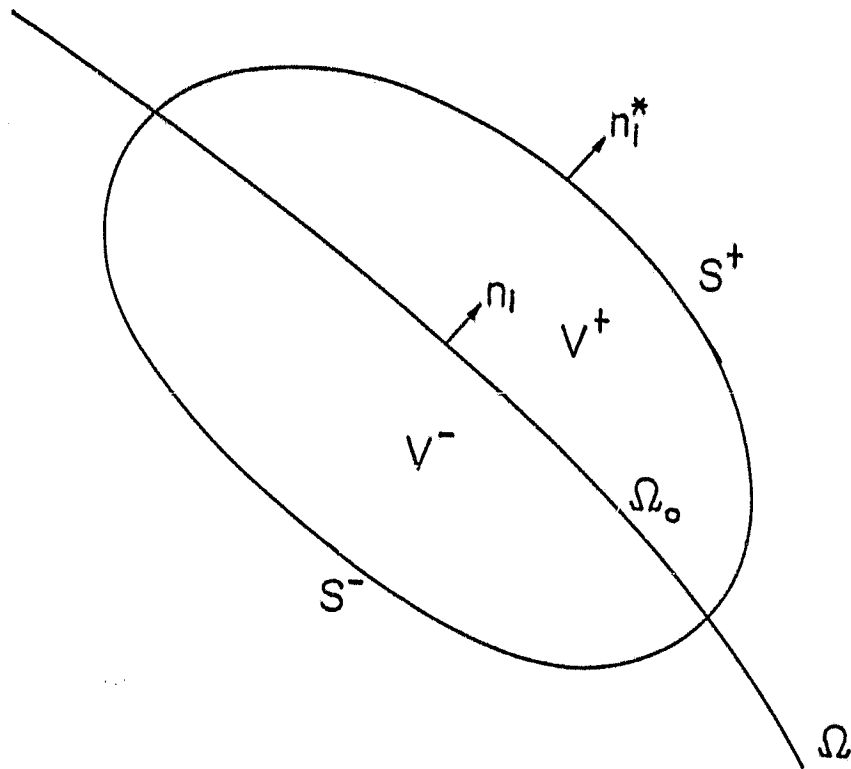


Figure 2.6 A deformed volume V divided by a travelling surface Ω

Taking $f = \rho \dot{u}_i$, in Equation (2-44) and using equation (2-45) and (2-46), we obtain

$$\frac{d}{dt} \int_{V^-} \rho \dot{u}_i dV = \int_{V^-} (\rho \dot{u}_i)_{,t} dV + \int_{S^-} \dot{u}_n^- \rho \dot{u}_i dS + \int_{\Omega_0} c_n \rho \dot{u}_i d\Omega \quad (2-47)$$

$$\frac{d}{dt} \int_{V^+} \rho \dot{u}_i dV = \int_{V^+} (\rho \dot{u}_i)_{,t} dV + \int_{S^+} \dot{u}_n^+ \rho \dot{u}_i dS - \int_{\Omega_0} c_n \rho \dot{u}_i d\Omega \quad (2-48)$$

where \dot{u}_i^- and \dot{u}_i^+ are the velocity components of material particle in V^- and V^+ , respectively. Combining the above two equations gives

$$\begin{aligned} \frac{d}{dt} \int_V \rho \dot{u}_i dV &= \int_V (\rho \dot{u}_i)_{,t} dV + \int_{S^-} \dot{u}_n^- \rho \dot{u}_i dS + \int_{S^+} \dot{u}_n^+ \rho \dot{u}_i dS \\ &\quad + \int_{\Omega_0} c_n \rho (\dot{u}_i^- - \dot{u}_i^+) d\Omega \end{aligned} \quad (2-49)$$

From theory of elasticity we have

$$\frac{d}{dt} \int_V \rho \dot{u}_i dV = \int_{\sigma} \sigma_{ij} n_j dS \quad (2-50)$$

If we let the volume V approach zero at a fixed time in such a way that it will pass into Ω_0 , then the volume integral in Equation (2-49) will evidently approach zero; however

$$\int_{S^+} \dot{u}_n^+ \rho \dot{u}_i dS = - \int_{\Omega_0} \dot{u}_n^+ \rho \dot{u}_i d\Omega \quad (2-51)$$

ORIGINAL PAGE IS
OF POOR QUALITY

$$\int_{\Omega_0} \dot{u}_n^- \rho \dot{u}_n^- dS = \int_{\Omega_0} \dot{u}_n^- \rho \dot{u}_n^- d\Omega \quad (2-52)$$

$$\int_{\Omega_0} \sigma_{IJ} n_J dS = \int_{\Omega_0} (\sigma_{IJ}^+ - \sigma_{IJ}^-) n_J d\Omega \quad (2-53)$$

where σ_{IJ}^- and σ_{IJ}^+ are the stress components on the sides of Ω_0 , respectively.

Substituting Equations (2-50) through (2-53) into Equation (2-49) gives

$$\int_{\Omega_0} (\sigma_{IJ}^+ - \sigma_{IJ}^-) n_J d\Omega = \int_{\Omega_0} \rho \dot{u}_n^- (c_n - \dot{u}_n^-) d\Omega - \int_{\Omega_0} \rho \dot{u}_n^+ (c_n - \dot{u}_n^+) d\Omega \quad (2-54)$$

Using $[\sigma_{IJ}]$ and $[\dot{u}_I]$ to represent the jumps of stress and particle velocity across the wave front, and utilizing the fact that $c_n \gg \dot{u}_n$, we obtain

$$\int_{\Omega_0} [\sigma_{IJ}] n_J d\Omega = - \int_{\Omega_0} \rho c_n [\dot{u}_I] d\Omega \quad (2-55)$$

Since this condition is independent of the extent of the surface integration Ω_0 , it follows that

$$[\sigma_{IJ}] n_J = - \rho c_n [\dot{u}_I] \quad (2-56)$$

In the case of laminated plate, $I = x, y, z$ and $J = x, y$.

Substitution of Equation (2-6) into Equation (2-56) yields

$$\begin{aligned}
 [\sigma_{1j}]n_j &= -\rho c_n \{ [\dot{u}^0] + z[\dot{\phi}_x] \} \\
 [\sigma_{2j}]n_j &= -\rho c_n \{ [\dot{v}^0] + z[\dot{\phi}_y] \} \\
 [\sigma_{3j}]n_j &= -\rho c_n [\dot{w}]
 \end{aligned}
 \tag{2-57}$$

ORIGINAL PAGE IS
OF POOR QUALITY

Integrating Equation (2-57) over the thickness of plate gives

$$\begin{aligned}
 [N_x]n_x + [N_{xy}]n_y &= -Pc_n[\dot{u}^0] - Rc_n[\dot{\phi}_x] \\
 [N_{xy}]n_x + [N_y]n_y &= -Pc_n[\dot{v}^0] - Rc_n[\dot{\phi}_y] \\
 [Q_x]n_x + [Q_y]n_y &= -Pc_n[\dot{w}]
 \end{aligned}
 \tag{2-58}$$

Multiplying the first two equations of Equation (2-57) by z and then integrating over the thickness, we obtain two more equations

$$\begin{aligned}
 [M_x]n_x + [M_{xy}]n_y &= -Rc_n[\dot{u}^0] - Ic_n[\dot{\phi}_x] \\
 [M_{xy}]n_x + [M_y]n_y &= -Rc_n[\dot{v}^0] - Ic_n[\dot{\phi}_y]
 \end{aligned}
 \tag{2-59}$$

where P , R and I have been defined in Equation (2-24)

The five equations given by Equations (2-58) and (2-59) are the dynamical conditions on the wave front for the laminated plate.

2.3.3 Propagation Velocity of the Wave Front

Across the wave front, the laminate constitutive relations given by Equation (2-20) can be written as

$$\begin{Bmatrix} [N] \\ [M] \\ [Q] \end{Bmatrix} = \begin{bmatrix} A & B & 0 \\ B & D & 0 \\ 0 & 0 & A^* \end{bmatrix} \begin{Bmatrix} [\epsilon] \\ [\kappa] \\ [\gamma] \end{Bmatrix} \quad \begin{array}{l} \text{ORIGINAL PAGE IS} \\ \text{OF POOR QUALITY} \end{array} \quad (2-60)$$

where

$$\begin{aligned} \{ [N] \}^T &= \{ [N_x], [N_y], [N_{xy}] \} \\ \{ [M] \}^T &= \{ [M_x], [M_y], [M_{xy}] \} \\ \{ [Q] \}^T &= \{ [Q_x], [Q_y] \} \end{aligned} \quad (2-61)$$

are the jumps of the stress resultants, and

$$\begin{aligned} \{ [\epsilon] \}^T &= \{ [\partial u^0 / \partial x], [\partial v^0 / \partial y], [\partial u^0 / \partial y] + [\partial v^0 / \partial x] \} \\ \{ [\kappa] \}^T &= \{ [\partial \phi_x / \partial x], [\partial \phi_y / \partial y], [\partial \phi_x / \partial y] + [\partial \phi_y / \partial x] \} \\ \{ [\gamma] \}^T &= \{ [\partial w / \partial y], [\partial w / \partial x] \} \end{aligned} \quad (2-62)$$

are the jumps of the strain components. In Equation (2-62), the conditions $[\phi_x] = [\phi_y] = 0$ are substituted.

Substituting of Equation (2-43) and the similar relations for other kinematic variables in Equation (2-60), we can express the jumps of the stress resultants in terms of the jumps of the time derivatives of the displacement components u^0 , v^0 , w , ϕ_x and ϕ_y . These relations are then substituted in Equations (2-58) and (2-59), which results in five homogeneous equations. For $[0^\circ/45^\circ/0^\circ/-45^\circ/0^\circ]_{2s}$ graphite/epoxy laminated plate which is symmetrical and balanced (i.e. $B_{1j} = 0$, $A_{16} = A_{26} = 0$, $R = 0$ and $D_{16} = D_{26}$), these five equations are uncoupled into three groups as

$$[a_{ij}] \begin{Bmatrix} [\dot{u}^0] \\ [\dot{v}^0] \end{Bmatrix} = 0 \quad \begin{array}{l} \text{ORIGINAL VELOCITY} \\ \text{OF POOR QUALITY} \end{array} \quad (2-63)$$

$$[b_{ij}] \begin{Bmatrix} [\phi_x] \\ [\phi_y] \end{Bmatrix} = 0 \quad (2-64)$$

$$(A^*_{44} - Pc_n^2) [w] = 0 \quad (2-65)$$

In which $[a_{ij}]$ and $[b_{ij}]$ are both two by two symmetric matrices, and their entries are given by

$$\begin{aligned} a_{11} &= n_x^2 A_{11} + n_y^2 A_{66} - Pc_n^2 \\ a_{12} &= a_{21} = n_x n_y (A_{12} + A_{66}) \\ a_{22} &= n_x^2 A_{66} + n_y^2 A_{22} - Pc_n^2 \end{aligned} \quad (2-66)$$

$$\begin{aligned} b_{11} &= n_x^2 D_{11} + 2n_x n_y D_{16} + n_y^2 D_{66} - Ic_n^2 \\ b_{12} &= b_{21} = D_{16} + n_x n_y (D_{12} + D_{66}) \\ b_{22} &= n_x^2 D_{66} + 2n_x n_y D_{16} + n_y^2 D_{22} - Ic_n^2 \end{aligned} \quad (2-67)$$

It can be seen that Equation (2-63) describes the in-plane extensional and the in-plane shear wave fronts, Equation (2-64) describes the bending moment and the twisting moment wave fronts and Equation (2-65) describes the transverse shear wave front.

From Equation (2-65), we obtain the normal velocity with which the transverse shear wave front propagates as

$$c_n^2 = A^*_{44}/P \quad (2-68)$$

It is noted that this velocity is independent of the direction of propagation, and is called directionally

Isotropic wave front.

Equations (2-63) and (2-64) yield non-trivial solutions only if the determinant of the coefficients matrices vanish, i.e.

$$|a_{ij}| = 0 \quad (2-69)$$

$$|b_{ij}| = 0 \quad (2-70)$$

Each of the above equations can be expanded into a quadratic equation of c_n^2 . For $[0^\circ/45^\circ/0^\circ/-45^\circ/0^\circ]_{2s}$ graphite/epoxy laminated plate, the normal velocities of wave fronts corresponding to the in-plane modes and flexural modes are plotted in Figure 2.7 and 2.8, respectively. It is noted that the normal velocities of the in-plane extensional and in-plane shear modes are symmetrical about x-axis and y-axis, while there is no such symmetry for the bending moment and twisting moment modes.

2.3.4 Wave Surface and Ray

From Figure 2.7 and 2.8, it can be seen that for laminated composites which are anisotropic in general, the in-plane and flexural wave fronts travel with different normal velocities in different directions. In other words, the initial shape of a wave surface will be distorted after it propagates. However, Equations (2-66) and (2-67) show

ORIGINAL PAGE IS
OF POOR QUALITY

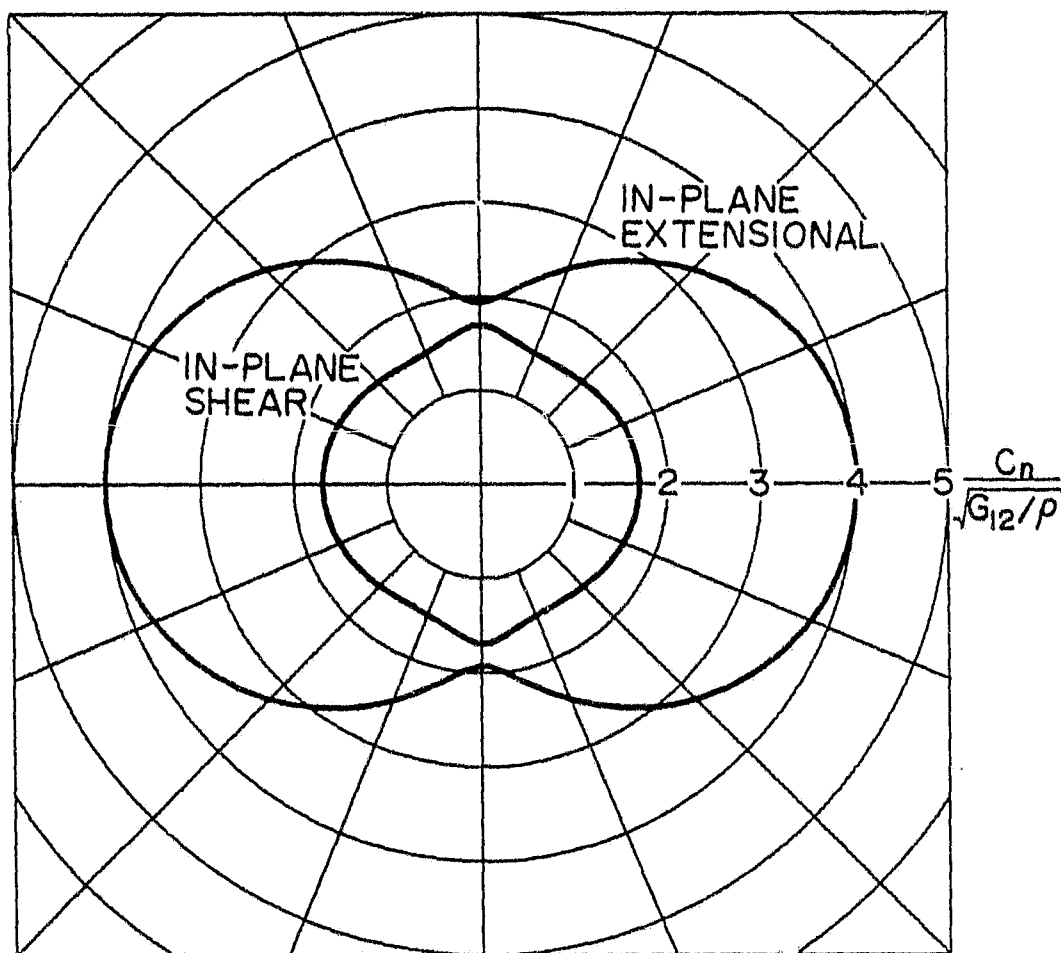


Figure 2.7 Normal velocities of in-plane wave fronts

ORIGINAL PAGE IS
OF POOR QUALITY

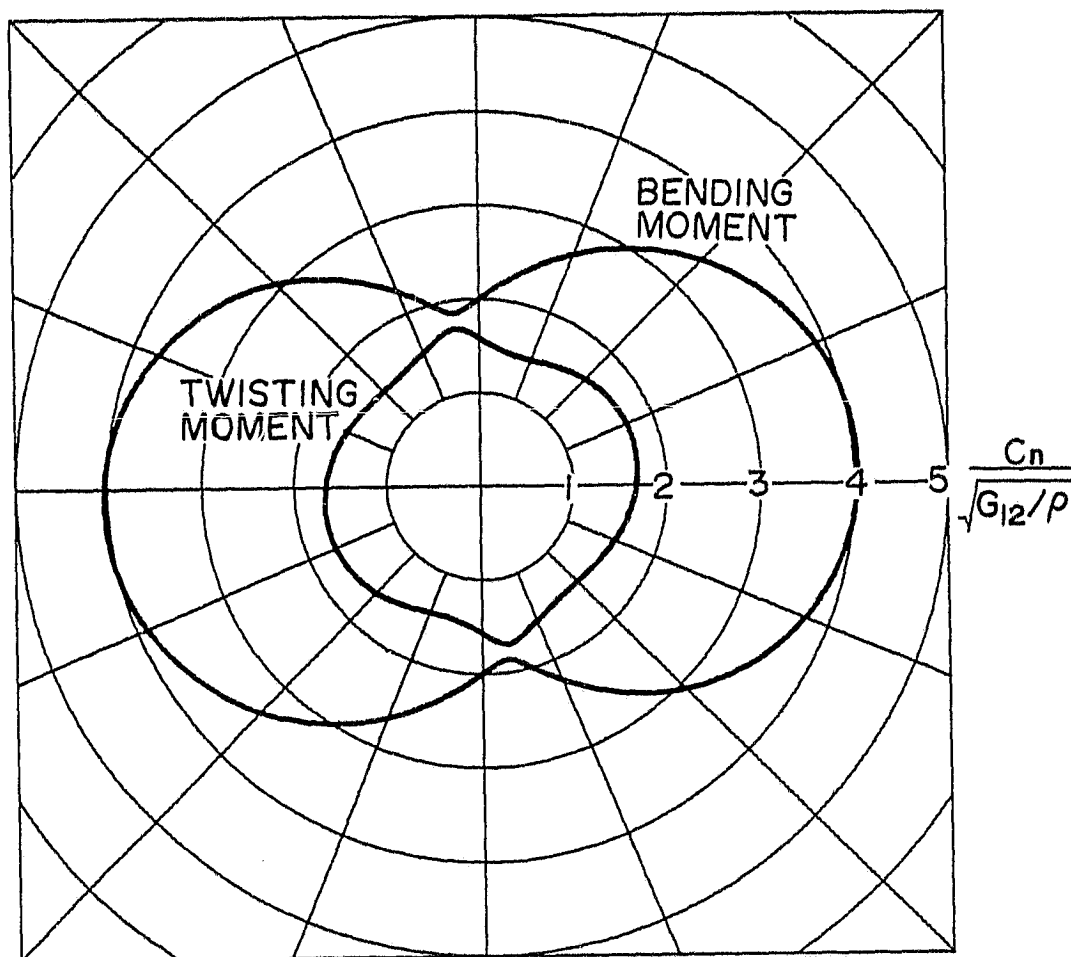


Figure 2.8 Normal velocities of flexural wave fronts

that for any fixed normal direction n_i , c_n is a constant. Connecting the points having the same unit normals to the travelling wave front surface, we obtain a family of lines which are called rays. Thus, along a ray, the normal velocity of wave front remains unchanged. By using the ray theory which has been well established in the field of geometrical optics, we are able to construct the wave front surface.

Recall Equation (2.37)

$$F(x_i) - t = 0 \quad i = 1, 2 \quad (2-37)$$

which represents a family of wave fronts propagating over the plate with t as a parameter. It follows that

$$dF/dt = (\partial F/\partial x_i)(dx_i/dt) = (\partial F/\partial x_i)c_i = 1 \quad (2-71)$$

By putting

$$p_i = \partial F/\partial x_i = \nabla F \quad (2-72)$$

Equation (2-71) becomes

$$p_i c_i = 1 \quad (2-73)$$

Since p_i is normal to the surface F , it can be written as

$$p_i = |p_i| n_i \quad (2-74)$$

where $|p_i|$ denotes the length of p_i . Combining (2-73) and (2-74), we obtain

$$|p_i|n_i/c_i = |p_i|c_n = 1 \quad (2-75)$$

from which we obtain

$$p_i = n_i/c_n \quad (2-76)$$

In Equation (2-76), p_i is called the slowness vector which has the direction normal to the wave front with the magnitude being equal to the inverse of normal velocity c_n .

Substituting Equation (2-76) in Equation (2-69) and (2-70), we obtain two equations in terms of p_i

$$\begin{vmatrix} p_x^2 A_{11} + p_y^2 A_{55} - P & p_x p_y (A_{12} + A_{56}) \\ p_x p_y (A_{12} + A_{56}) & p_x^2 A_{66} + p_y^2 A_{22} - P \end{vmatrix} = 0$$

$$\begin{vmatrix} p_x^2 D_{11} + 2p_x p_y D_{15} + p_y^2 D_{55} - I & D_{15} + p_x p_y (D_{12} + D_{56}) \\ D_{15} + p_x p_y (D_{12} + D_{56}) & p_x^2 D_{66} + 2p_x p_y D_{15} + p_y^2 D_{22} - I \end{vmatrix} = 0$$

which can be written in a general form as

$$g(p_i) = 0 \quad i = 1, 2 \quad (2-77)$$

In view of Equation (2-72), we recognize that Equation (2-77) may be regarded as a set of first-order partial differential equation for F . A standard method of solving first-order partial differential equation is by means of characteristics [24], which reduces the equation to a system of first-order ordinary differential equations. In our case, Equation (2-77) then is equivalent to the following

$$dx/ds = \partial g/\partial p_x \quad dy/ds = \partial g/\partial p_y \quad (2-78)$$

$$dp_x/ds = -\partial g/\partial x \quad dp_y/ds = -\partial g/\partial y \quad (2-79)$$

where s is a parameter. These equations, together with Equation (2-77) describe the ray geometry and the normal direction of the wave front propagating along the ray.

From Equation (2-78), we have

$$dy/dx = (\partial g/\partial p_y)/(\partial g/\partial p_x) \quad (2-80)$$

Since the normal direction of wave front along a ray is constant, it can be seen from Equation (2-76) that p_i is also constant along a ray. For laminated composite which is assumed to have homogeneous material properties, Equation (2-77) shows that $g(p_i)$ does not depend on x_i , consequently, $\partial g/\partial p_x$ and $\partial g/\partial p_y$ are all constants along a ray. Thus, the solution of Equation (2-80) is then given by

$$y = \zeta(x - x_0) + y_0 \quad (2-81)$$

where x_0 and y_0 are the initial values of x and y at $t = 0$, and $\zeta = (\partial g/\partial p_y)/(\partial g/\partial p_x)$. This equation shows that the rays in a homogeneous solid are straight lines.

From Equations (2-73) and (2-77), we have

$$c_i dp_i = 0 \quad (2-82)$$

$$dg = (\partial g/\partial p_i) dp_i = 0 \quad (2-83)$$

Eliminating dp_i from these equations yields

$$dx_i/dt = c_i = (\partial g/\partial p_i)/(\rho_j \partial g/\partial p_j) \quad (2-84)$$

where summation over j is understood.

Equation (2-84) can be solved to obtain the position of wave front at time t . Again, since $\partial g/\partial p_i$ and p_i are all constant along a ray, we obtain the solution of Equation (2-84) as

$$x = (\partial g/\partial p_x)t/(\rho_j \partial g/\partial p_j) + x_0 \quad (2-85)$$

$$y = (\partial g/\partial p_y)t/(\rho_j \partial g/\partial p_j) + y_0 \quad (2-86)$$

where x_0 and y_0 denote the initial wave position at $t = 0$.

Consider at $t = 0$, a wave front forms a circle given by

$$\begin{aligned} x_0 &= h \cos \alpha \\ y_0 &= h \sin \alpha \end{aligned} \quad (2-87)$$

At this instant, the normal directions to the wave front coincide with the radial directions. Due to the different velocities of propagation in directions, this initial shape would be distorted. By using Equations (2-85) and (2-86), the subsequent positions of the wave front can be determined. Figures 2.9-2.12 show the wave front positions at two consecutive instants after $t = 0$ for the in-plane extensional, in-plane shear, bending moment and twisting moment modes, respectively, for the $[0^\circ/45^\circ/0^\circ/-45^\circ/0^\circ]_{2s}$

graphite/epoxy laminated plate. It is noted that for symmetrical laminates, the in-plane modes are uncoupled from the bending modes. The rays along which the normal directions to the wave front are 0° , 45° and 90° , respectively, are also shown in the figures. It is seen that the wave fronts of the in-plane extensional and the in-plane shear modes possess symmetry with respect to x-axis and y-axis. The wave fronts of the bending and twisting moments, however, lose their original symmetry with respect to x-axis and y-axis. This is an indication that in performing analysis of flexural deformation of this laminate, one can not take a quadrant for analysis, a practice followed by many authors dealing with homogeneous and isotropic plates.

From Figures 2.9-2.12, it is also interesting to note that ray geometries for these two groups of wave fronts are quite different. For the in-plane extensional and in-plane shear wave fronts, the rays coincide with the normal directions when $\alpha = 0^\circ$ and 90° . Along other directions, the direction of the ray deviates from the normal direction of the wave front. It was discussed in [2] that the degree of spreading of rays is proportional to the decay of the stress amplitude at the wave front. Thus, from Figures 2.9 and 2.11, one can conclude that the strength of the in-plane extensional and bending moment wave fronts decay more rapidly in the y-direction than in the x-direction.

ORIGINAL PAGE IN
OF POOR QUALITY

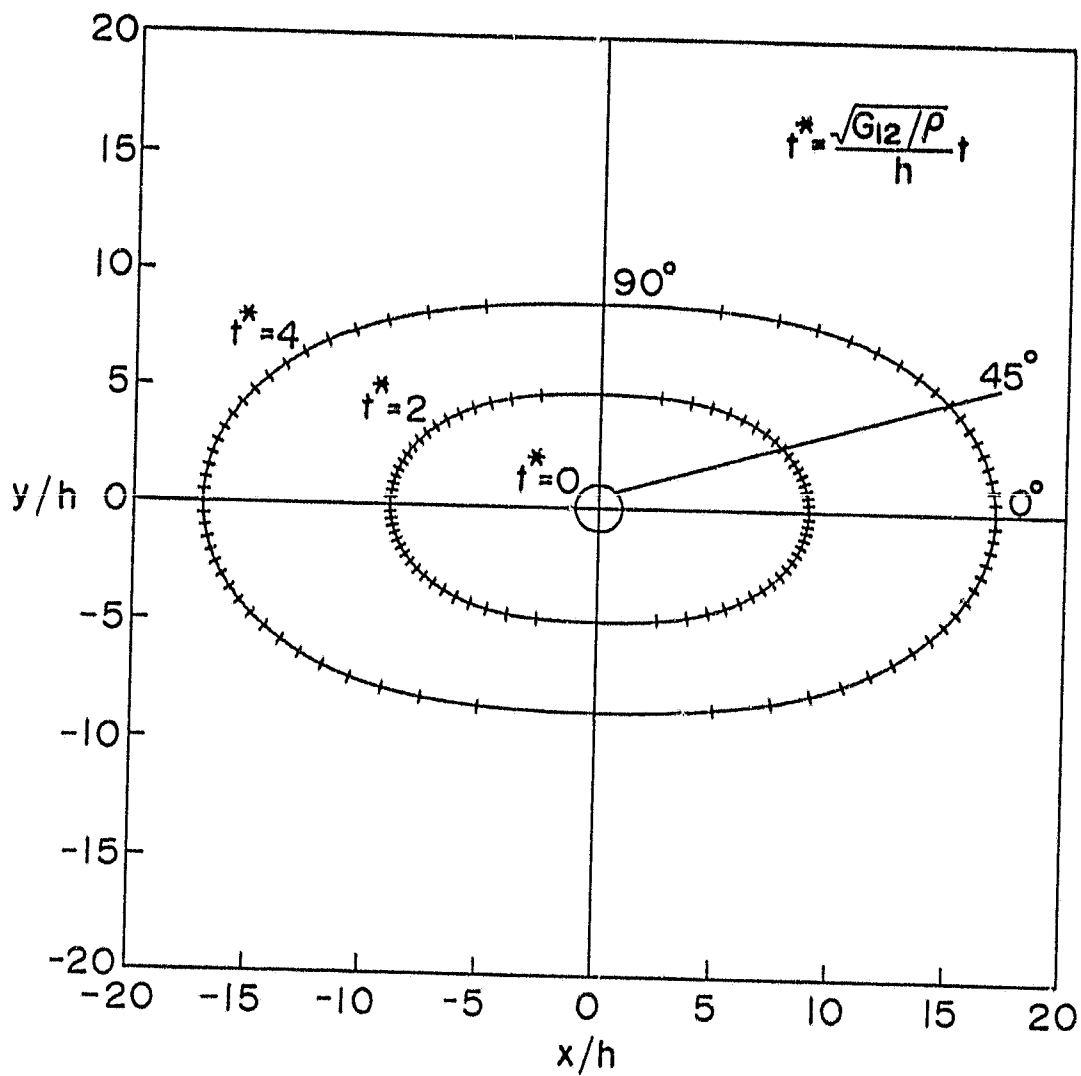


Figure 2.9 Wave front positions at different times and rays for in-plane extensional mode

ORIGINAL PAGE IS
OF POOR QUALITY

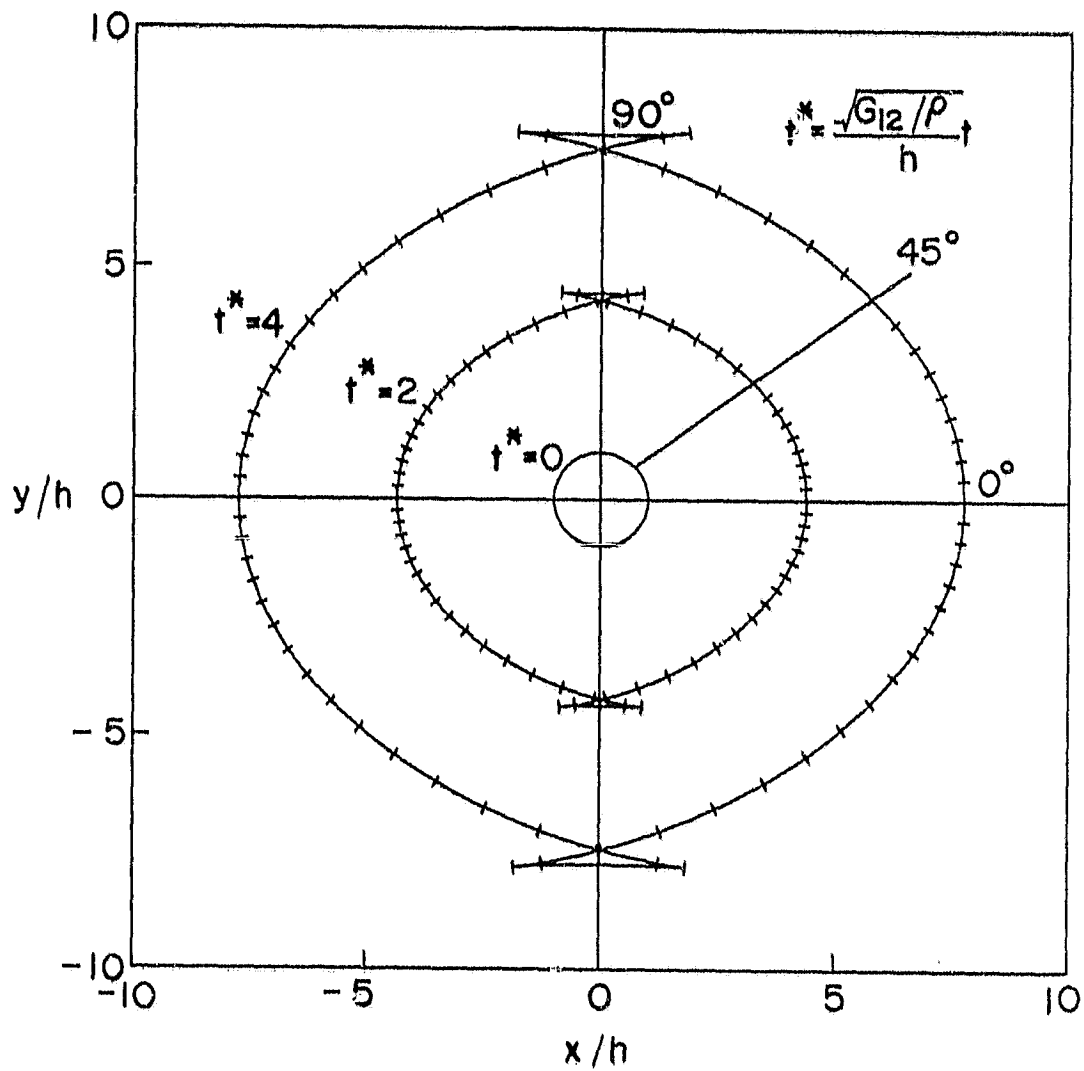


Figure 2.10 Wave front positions at different times and rays for in-plane shear mode

ORIGINAL PAGE IS
OF POOR QUALITY

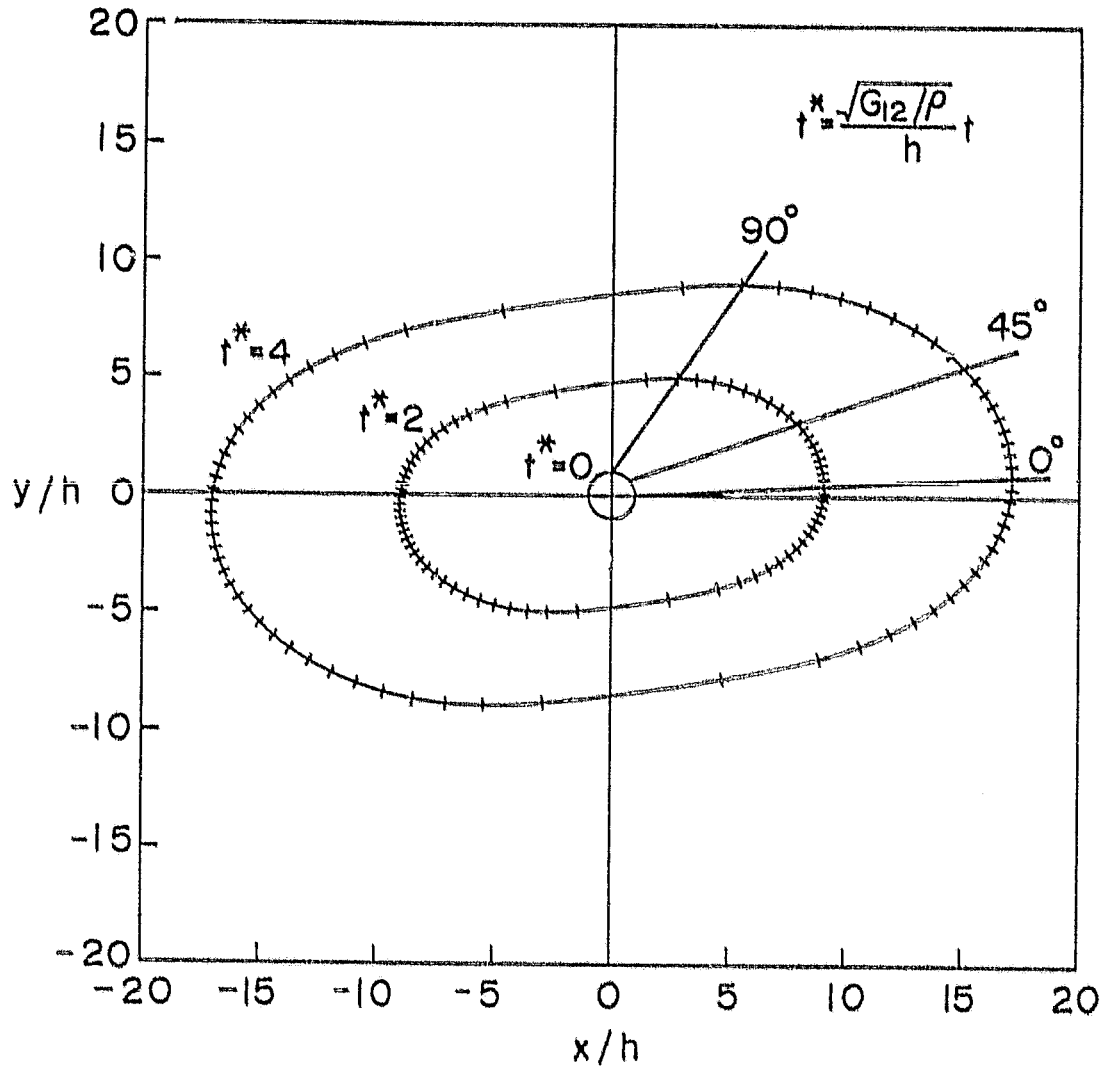


Figure 2.11 Wave front positions at different times and rays for bending mode

ORIGINAL PAGE IS
OF POOR QUALITY

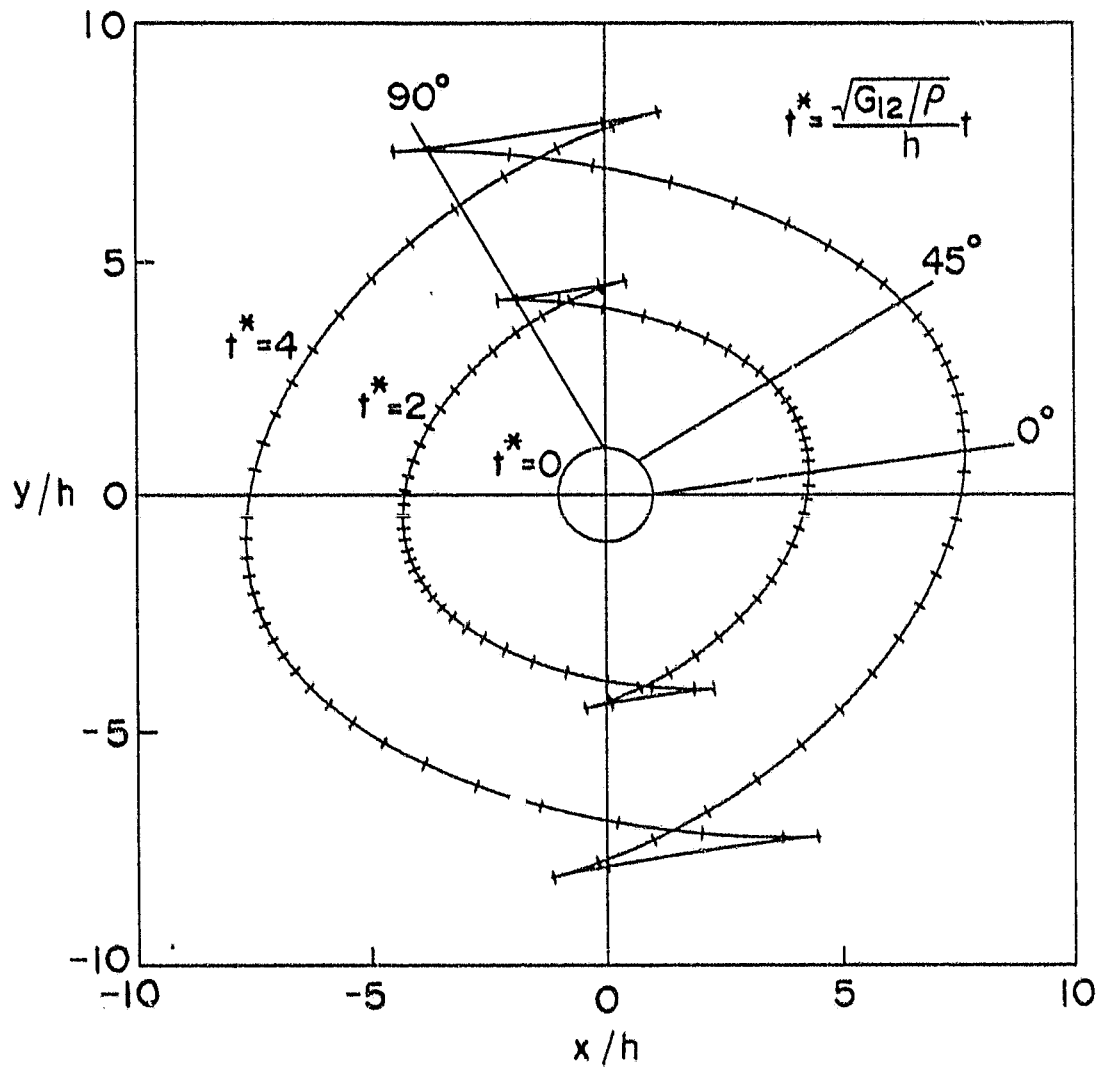


Figure 2.12 Wave front positions at different times and rays for twisting mode

A photoelastic study of anisotropic waves in a fiber reinforced composite has been done by Dally et al. [9]. The waves was produced by a explosive charge in a small hole on the plate. The result showed clearly an elliptic-like stress wave front pattern. This indicates that stress waves in anisotropic materials propagate with different velocities in different directions.

CHAPTER 3

STATICAL INDENTATION LAWS

A brief introduction of the historical development on Impact problem involving homogeneous isotropic materials was given by Goldsmith [12]. Hertz [11] was the first to obtain a satisfactory solution on contact law for two isotropic elastic spherical bodies. When letting the radius of one of the spheres go to infinity, this law then describes the contact behavior between a sphere and an elastic half-space. The Hertzian law, in spite of being static and elastic in nature, has been widely applied to Impact analyses where permanent deformations were produced. The use of this law beyond the elastic limit has been justified on the basis that it appears to predict accurately most of the Impact parameters that can be experimentally verified.

In studying Impact responses of laminated composites, the problem becomes extremely complicated. One may easily realize that the Hertzian contact law which was derived based on homogeneous isotropic materials may not be adequate in describing the contact behavior of laminated composites due to their anisotropic and nonhomogeneous properties. Moreover, most of the laminated composites have finite thickness which can not be represented by a half-space. In

many existing analytical works [25], loadings to the laminates were assumed known, and the responses of the laminates were assumed elastic.

Willis [26] obtained explicit formulas for Hertzian contact law for transversely isotropic half-space pressed by a rigid sphere, and extended it to the application of impact problems. It was shown that

$$F = k\alpha^n \quad (3-1)$$

with $n = 3/2$ is valid for the contact force F and the indentation α , where k is a contact coefficient whose value depends on the material properties of the target and the sphere, and the radius of sphere.

A modified contact law with

$$k = (4/3) \frac{R_s^{1/2}}{\frac{1 - \nu_s^2}{E_s} + \frac{1}{E_t}} \quad (3-2)$$

was used [13] in an analytical study on impact of laminated composites. In Equation (3-2), R_s , ν_s and E_s are the radius, Poisson's ratio and Young's modulus of the sphere, respectively, and E_t is the Young's modulus of the laminates in thickness direction. It was also suggested by Sun et al. [27] that the value of k can be experimentally determined.

ORIGINAL PAGE IS
OF POOR QUALITY

Recently Yang and Sun [14] have conducted static indentation tests on the $[0^\circ/45^\circ/0^\circ/-45^\circ/0^\circ]_{2s}$ graphite/epoxy laminates using spherical steel indenters of 0.25 in. and 0.5 in. diameters. The results were fitted into Equation (3-1) and were found that the 3/2 power is valid. In addition, it was also observed that even for small amounts of load there were significant permanent indentations. This implies that the unloading curve has to be different from the loading curves. In order to account for the permanent deformation, the equation

$$F = F_m \left(\frac{\alpha - \alpha_0}{\alpha_m - \alpha_0} \right)^q \quad (3-3)$$

proposed by Crook [28] was used to model the unloading path where F_m is the contact force at which unloading begins, α_m is the indentation corresponding to F_m , and α_0 denotes the permanent indentation in an unloading cycle. Equation (3-3) can be rewritten as

$$F = s(\alpha - \alpha_0)^q \quad (3-4)$$

In which

$$s = F_m / (\alpha_m - \alpha_0)^q \quad (3-5)$$

is called unloading rigidity. In order to simplify the modeling of the unloading law, it was assumed [14] that the value of s for all the unloading curves remains the same.

Consequently, a constant α_{cr} given by

$$\alpha_{cr} = k/s \quad (3-6)$$

was introduced. It was also shown that $q=5/2$ fitted the unloading path very well, and the permanent indentation α_0 was then related to α_m by

$$\begin{aligned} \alpha_0/\alpha_m &= 1 - (\alpha_{cr}/\alpha_m)^{2/5} && \text{as } \alpha_m > \alpha_{cr} \\ \alpha_0 &= 0 && \text{as } \alpha_m \leq \alpha_{cr} \end{aligned} \quad (3-7)$$

The value of α_{cr} was found to be independent of the size of the indenter and hence can be regarded as a material constant.

It was also mentioned in [14] and [29] that there were some practical difficulties in performing the tests. Since the indentation was measured step by step using a dial gage and readings on the gage were taken about 10 to 20 seconds after the load was increased by one step, the creep effect may cause an appreciable error to the results. Another important problem was that it was almost impossible to measure the permanent indentation accurately using the dial gage. In order to overcome these problems, a Linear Variable Differential Transformer (LVDT) was used in this study to measure the indentation.

The LVDT is an electromechanical transducer that produces an electrical output proportional to the displacement.

Connecting this output and the one from the strain indicator which is used to measure the applied loading to a X-Y plotter, one can obtain a continuous loading-unloading curve. By changing the loading rate which can be applied as fast as 50 lb./sec., it is possible to examine the significance of creep effect on the contact law. The starting point and final point of a loading-unloading cycle, which represent respectively the instants of contact and separation of the indenter and the specimen, can be easily determined from the curve. Thus, the measurements of permanent indentations are much more accurate than those using the dial gage.

3.1 Specimens and Experimental Procedure

Two groups of test specimens were prepared from a $[0^\circ/45^\circ/0^\circ/-45^\circ/0^\circ]_{2s}$ graphite/epoxy laminate. They were cut in the way such that the longitudinal axis of the beam specimen of the first group was parallel to the 0° fiber direction while the second one was perpendicular to it. The latter then becomes $[90^\circ/45^\circ/90^\circ/-45^\circ/90^\circ]_{2s}$ laminated beams. The thickness of the beam was 0.106 in. and the width was approximately 1.25 in.. In all tests, the specimens were clamped at both ends. It was shown in [14] that the span of the specimen in the range of 2 in. to 6 in. has little effect on the contact law. Hence, only one span, i.e. 2 in., was used in the test.

The experimental set-up is shown schematically in Figure 3.1. LVDT was mounted on a 'C' bracket fixed to the loading piston so that only the relative movement between the indenter and the specimen was recorded. The load was applied pneumatically by a plunger and it was measured using a load cell and a strain indicator. Outputs from LVDT and strain indicator were fed into an X-Y plotter so that a continuous force-indentation curve can be obtained. Two spherical steel indenters of diameters 0.5 in. and 0.75 in. were used.

3.2 Experimental Results

3.2.1 Loading Curves

The experimental curves were first digitized into some discrete data points and then fitted into Equation (3-1) using least-squares method. Figures 3.2 and 3.3 show the test data and the fitted curves for 0.5 in. diameter indenter. It can be seen from these figures that the $3/2$ power index gives very good results. However, the contact coefficient k of $[0^\circ/45^\circ/0^\circ/-45^\circ/0^\circ]_{2s}$ specimen is less than the one of $[90^\circ/45^\circ/90^\circ/-45^\circ/90^\circ]_{2s}$ specimen by about 7%. During the test, larger deflections were observed for the second group of specimen due to their lower flexural rigidity. This means that the contact area is also larger and the indentation under same amount of loading should be

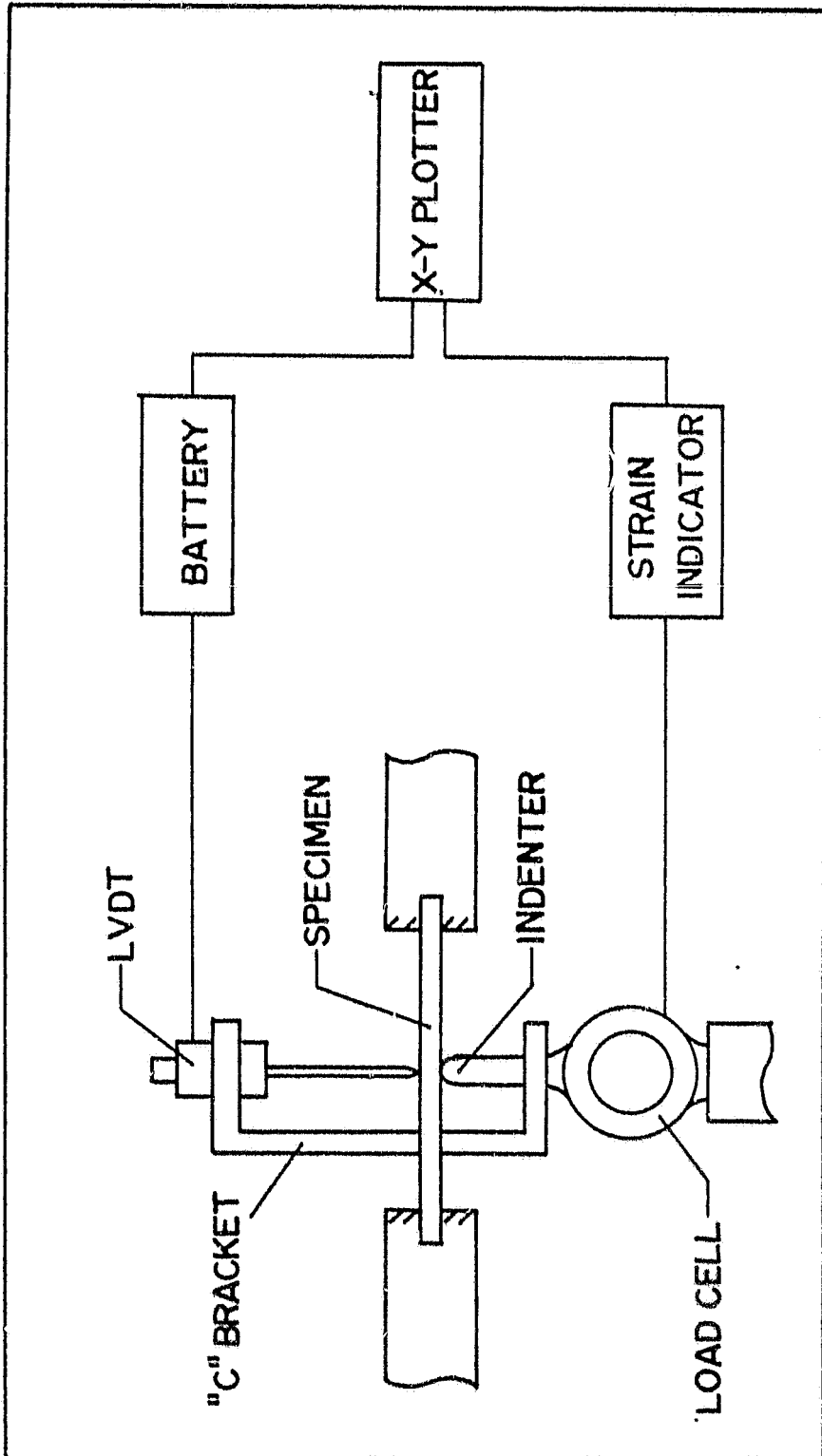


Figure 3.1 Schematic diagram for the indentation test set-up

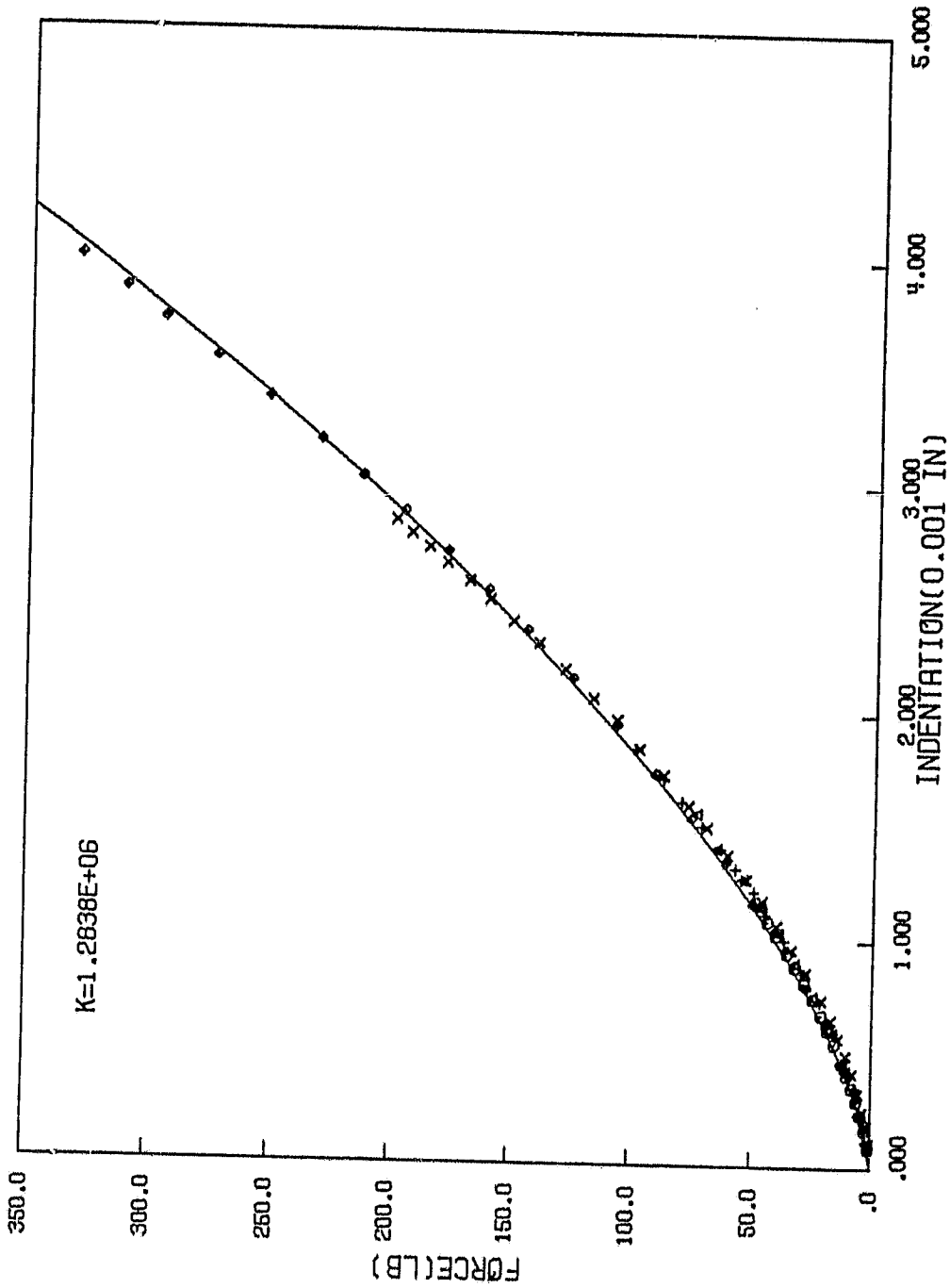


Figure 3.2 Loading curve of $[0^\circ/45^\circ/0^\circ/-45^\circ/0^\circ]_{2s}$ specimens with 0.5 inch indenter ($n=3/2$)

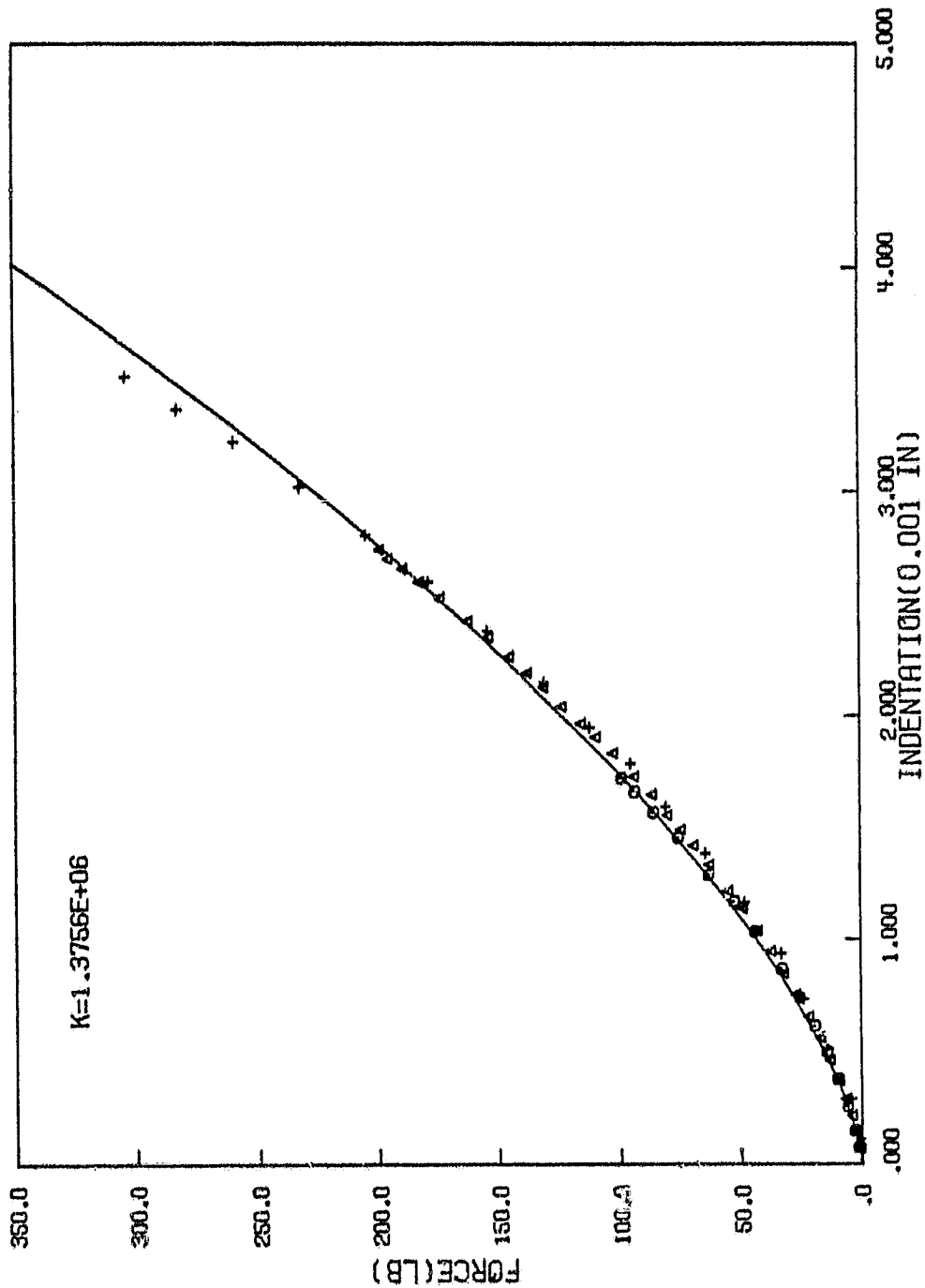


Figure 3.3 Loading curve of $[90^\circ/45^\circ/90^\circ/-45^\circ/90^\circ]_{2s}$ specimens with 0.5 inch indenter ($n=3/2$)

smaller comparing with the first group of specimens. Consequently, the higher value of k for the $[90^\circ/45^\circ/90^\circ/-45^\circ/90^\circ]_{25}$ specimens is reasonable.

The results for 0.75 in. diameter indenter are presented in Figures 3.4 and 3.5. Again, good agreement between the experimental data and fitted curves indicates that the $3/2$ power index for loading law is valid. The values of k for both indenters are summarized in Table 3.1. It should be noted that the average value of k obtained from the two groups of specimens was used later in a finite element analysis of impact responses.

3.2.2 Unloading Curves

By choosing a suitable value for q , it can be seen from Equation (3-5) that once the relation between α_0 and α_m is established, the unloading rigidity s is then determined. Test results show that the permanent indentations α_0 and the corresponding maximum indentations α_m exhibit a rather linear relationship. The equation given by

$$\alpha_0 = s_p (\alpha_m - \alpha_p) \quad (3-8)$$

is obtained from the test data for both 0.5 in. and 0.75 in. indenters using least-squares fitting method, and are plotted in Figure 3.6. In Equation (3-8), α_p can be considered as a critical value of indentation. Once the amount of indentation exceeds α_p , permanent deformation will occur.

ORIGINAL PAGE IS
OF POOR QUALITY

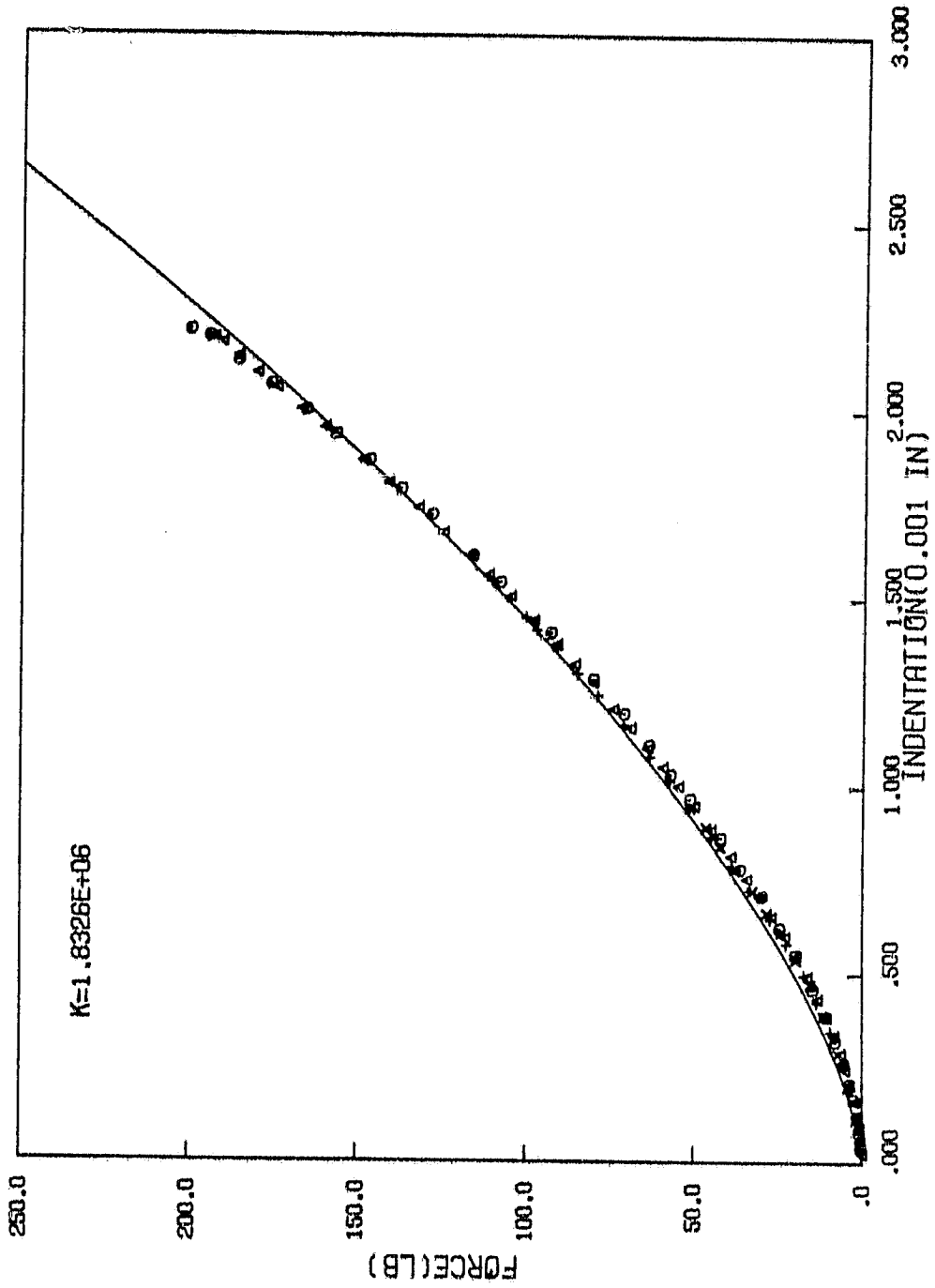


Figure 3.4 Loading curve of $[0^{\circ}/45^{\circ}/0^{\circ}/-45^{\circ}/0^{\circ}]_{2s}$ specimens with 0.75 inch indenter ($n=3/2$)

ORIGINAL PAGE IS
OF POOR QUALITY

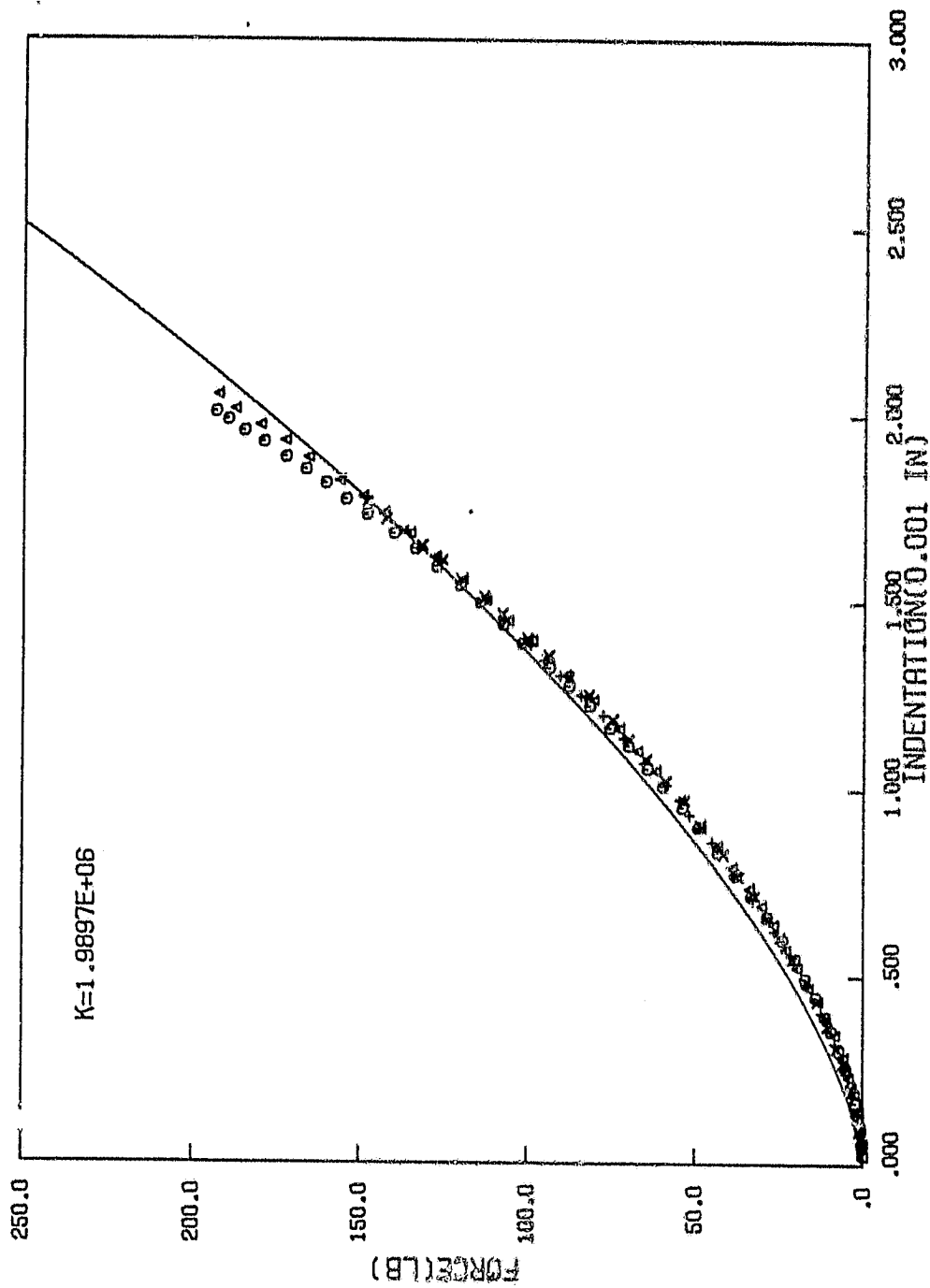


Figure 3.5 Loading curve of [90°/45°/90°/-45°/90°]_{2s} specimens with 0.75 inch indenter (n=3/2)

ORIGINAL PAGE 13
OF POOR QUALITY

Table 3.1
Contact coefficient k of loading law $F = k\alpha^{1.5}$

Size of Indenter (in)	0.5		0.75	
	Group 1 ⁺	Group 2 [‡]	Group 1 ⁺	Group 2 [‡]
k (lb/in ^{1.5})	1.284×10^6	1.376×10^6	1.833×10^6	1.990×10^6
Average k	1.330×10^6		1.912×10^6	
Ref. [14]	9.694×10^5			

⁺ $[0^\circ/45^\circ/0^\circ/-45^\circ/0^\circ]_{28}$ specimens

[‡] $[90^\circ/45^\circ/90^\circ/-45^\circ/90^\circ]_{28}$ specimens

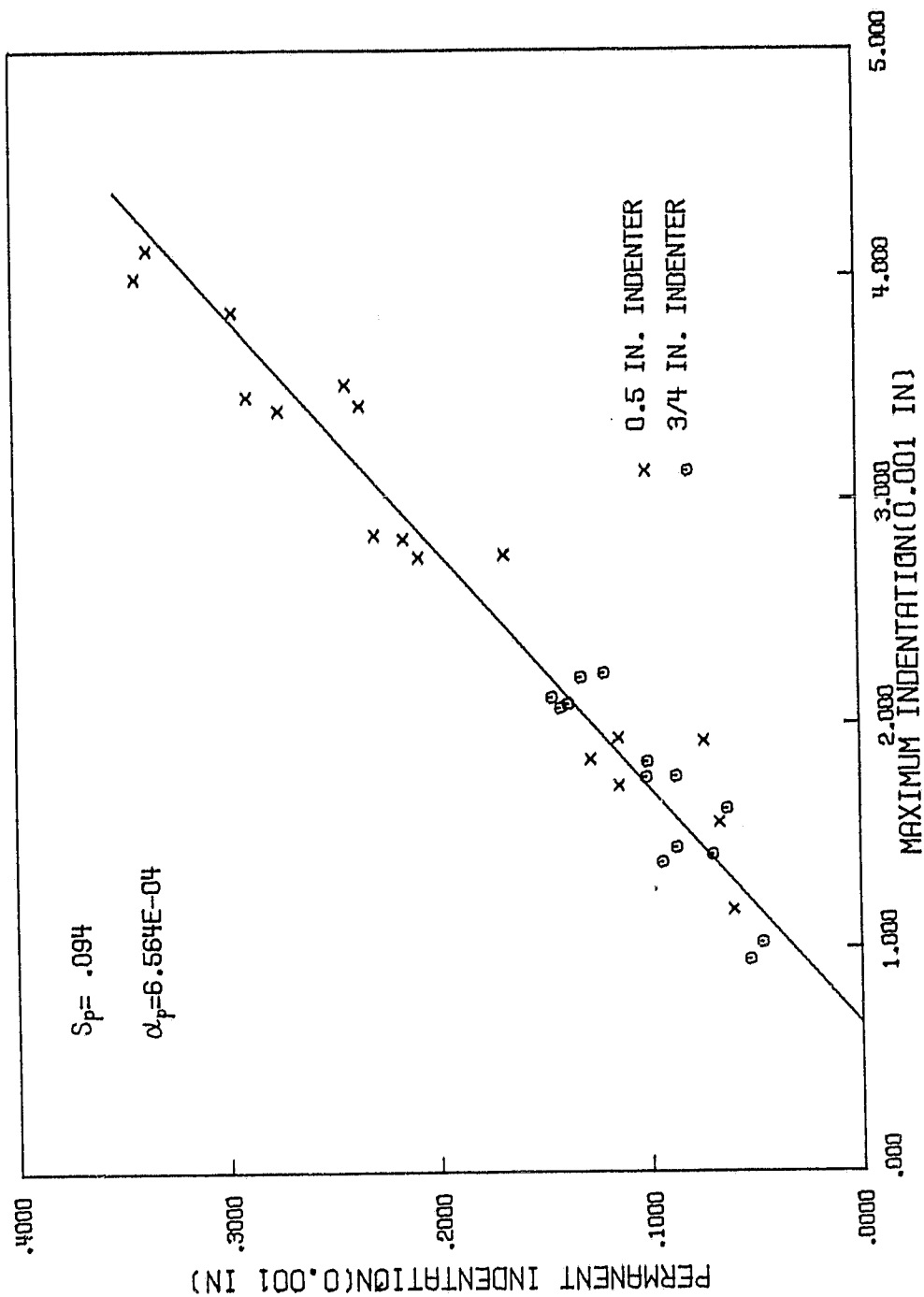


Figure 3.6 Relation between permanent indentation and maximum indentation

Substitution of Equation (3-8) and (3-1) into Equation (3-5) yields

$$s = \frac{k\alpha_m^{3/2}}{[(1 - s_p)\alpha_m + s_p\alpha_p]^q} \quad \text{if } \alpha_m \geq \alpha_p \quad (3-9)$$

$$s = \frac{k\alpha_m^{3/2}}{\alpha_m^q} \quad \text{if } \alpha_m < \alpha_p \quad (3-10)$$

These two equations along with Equation (3-4) are then used to fit the experimental unloading curves in finding the value of q .

Yang [14] has shown that $q = 2.5$ fits the test results for both 0.25 in. and 0.5 in. indenters quite well. In this study, however, the values of 2.2 and 1.8 were found to give the best fitting for 0.5 in. and 0.75 in. indenters, respectively using the aforementioned method (Figures 3.7-3.10). For convenience, $q = 2.5$ was used for 0.5 in. indenter while $q = 2.0$ was chosen for 3/4 in. indenter. The results of the curve-fitting are presented in Figures 3.11-3.14. Further discussions on the unloading law will be given in Section 3.3.

ORIGINAL PAGE IS
OF POOR QUALITY

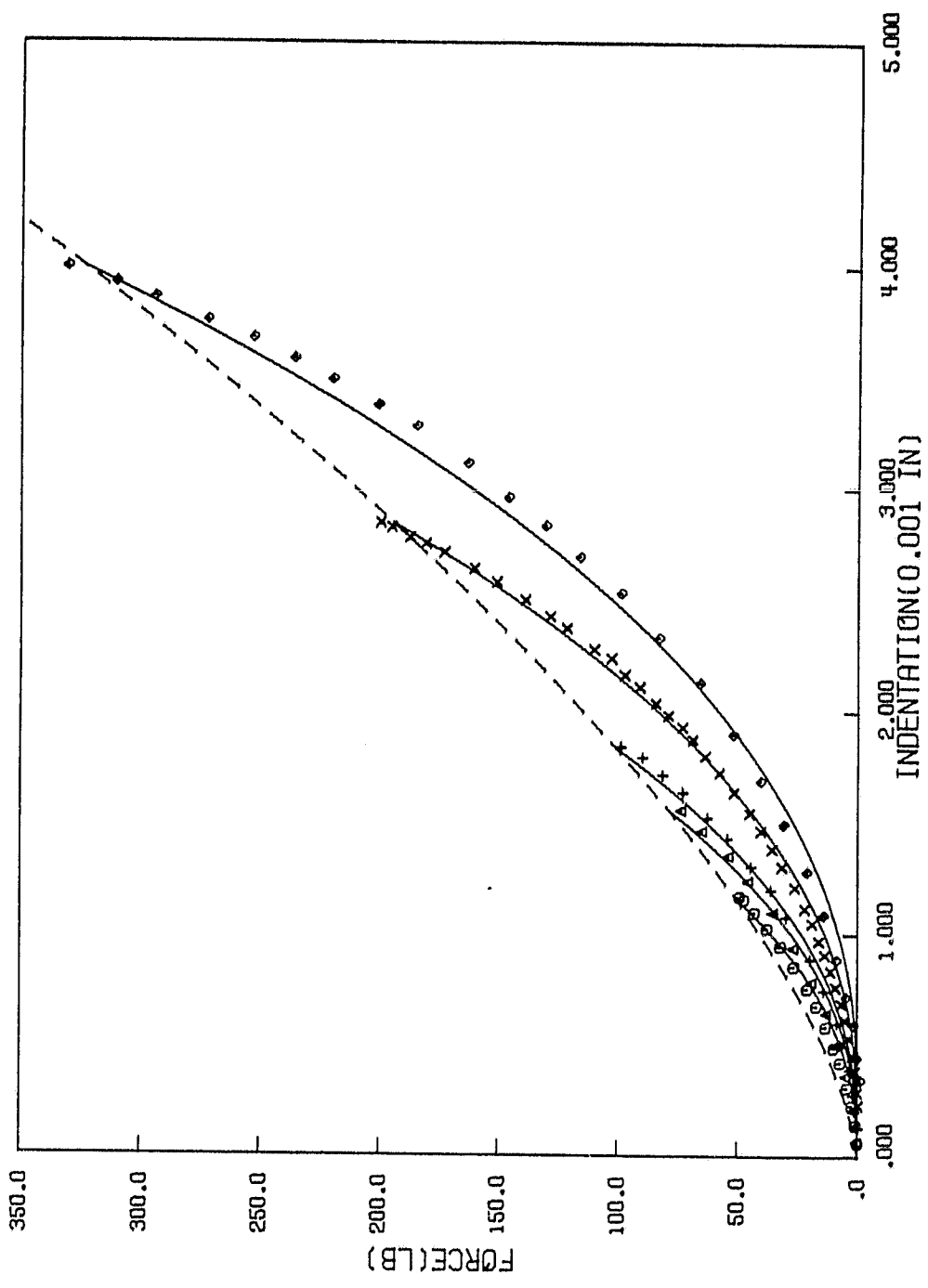


Figure 3.7 Unloading curves of $[0^\circ/45^\circ/0^\circ/-45^\circ/0^\circ]_{2s}$ specimens with 0.5 inch indenter ($q=2.2$)

ORIGINAL PAGE IS
OF POOR QUALITY

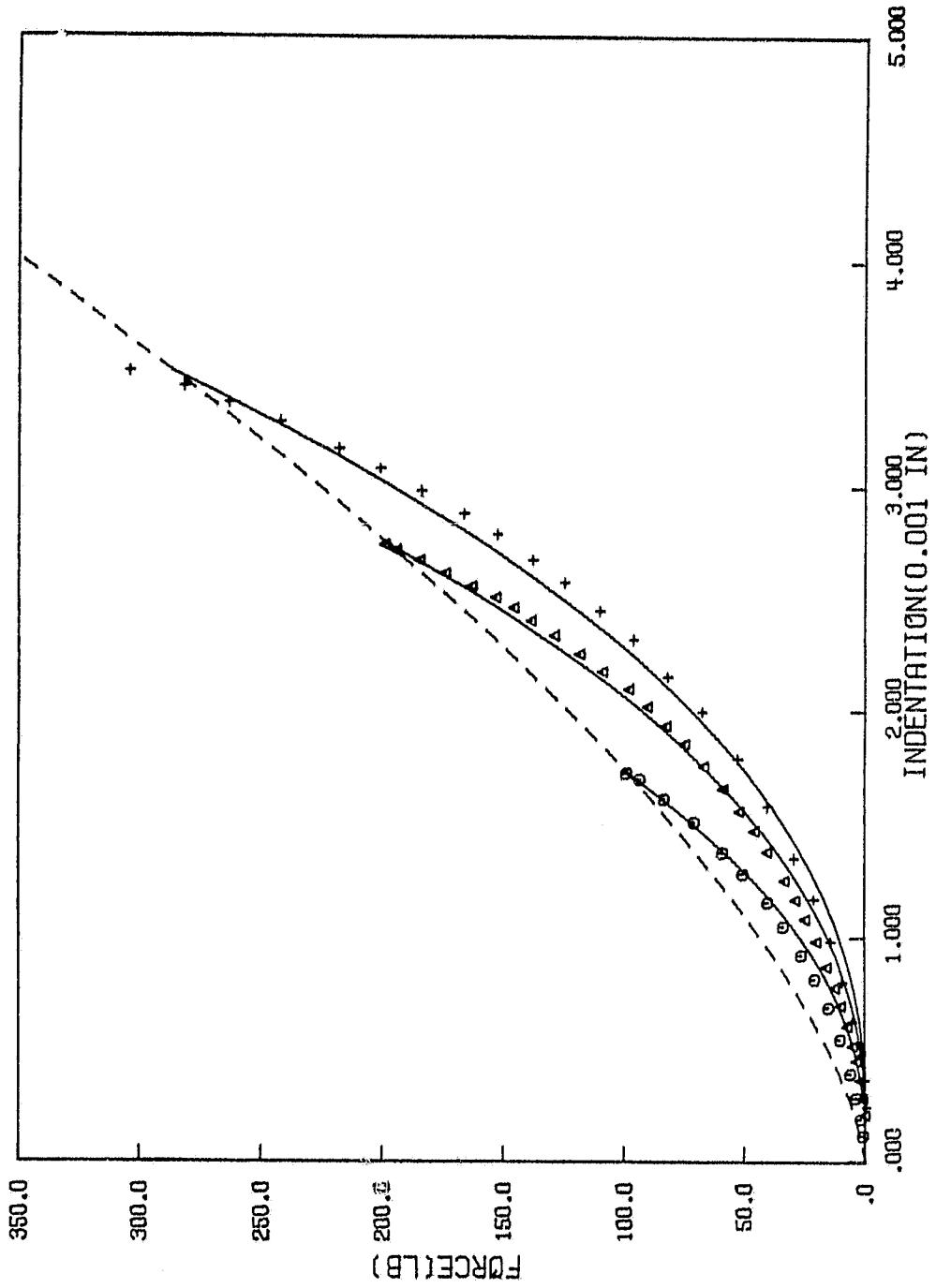


Figure 3.8 Unloading curves of $[90^\circ/45^\circ/90^\circ/-45^\circ/90^\circ]_{2s}$ specimens with 0.5 inch indenter ($q=2.2$)

ORIGINAL PAGE 19
OF POOR QUALITY

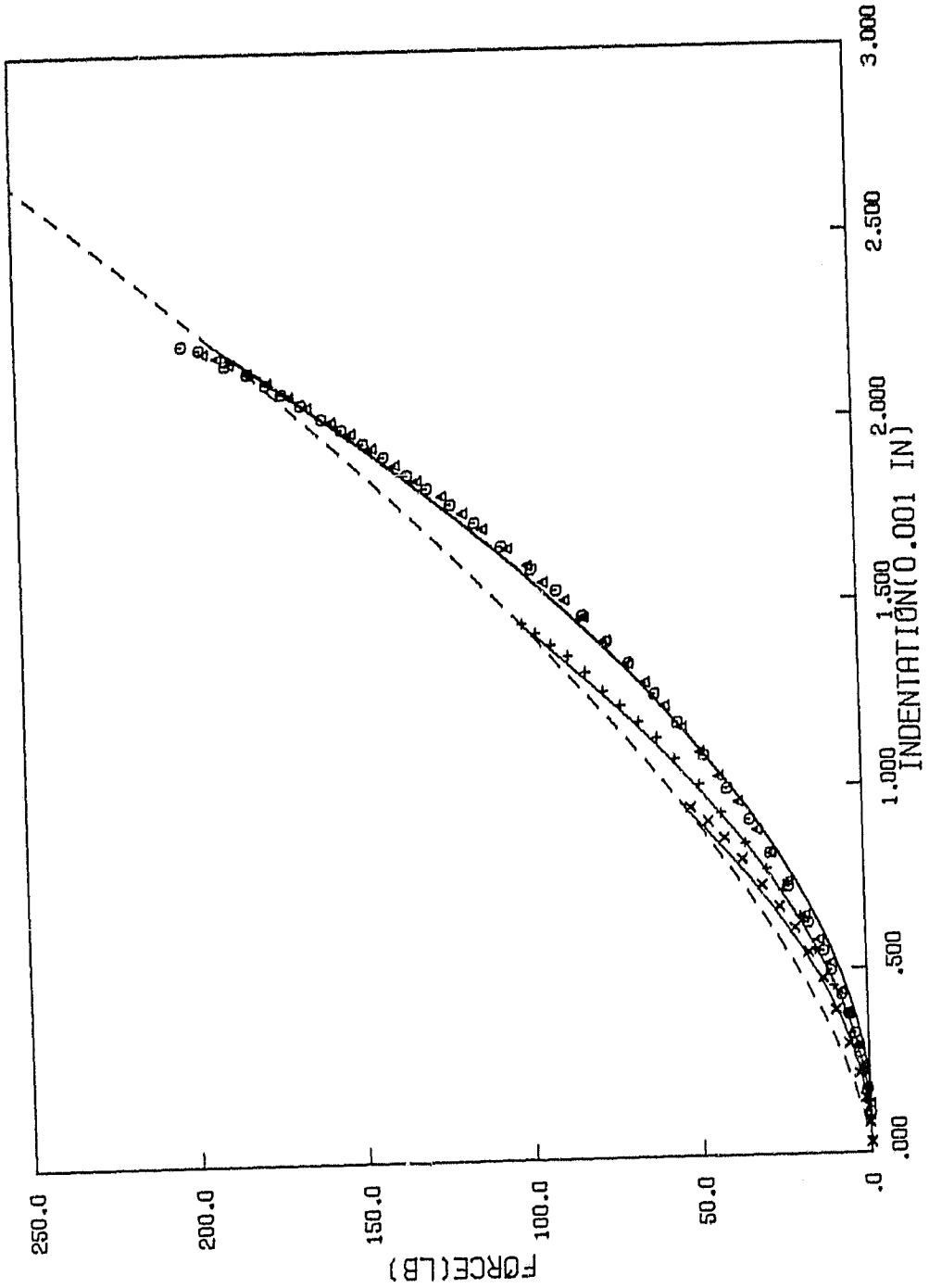


Figure 3.9 Unloading curves of $[0^\circ/45^\circ/0^\circ/-45^\circ/0^\circ]_{2s}$ specimens with 0.75 inch indenter ($q=1.8$)

ORIGINAL PAGE IS
OF POOR QUALITY

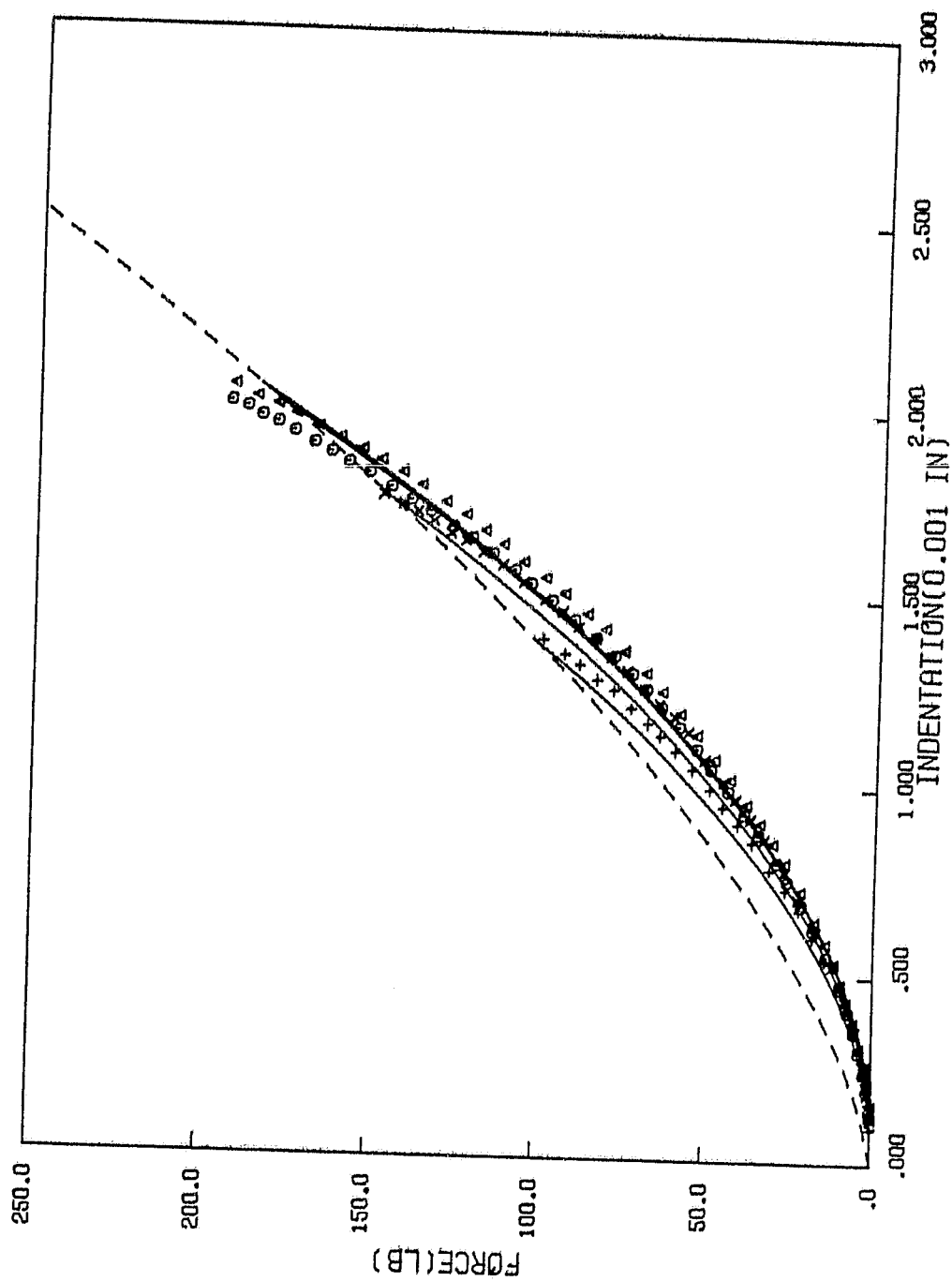


Figure 3.10 Unloading curves of $[90^\circ/45^\circ/90^\circ/-45^\circ/90^\circ]_{2s}$ specimens with 0.75 inch indenter ($q=1.8$)

ORIGINAL PAGE IS
OF POOR QUALITY

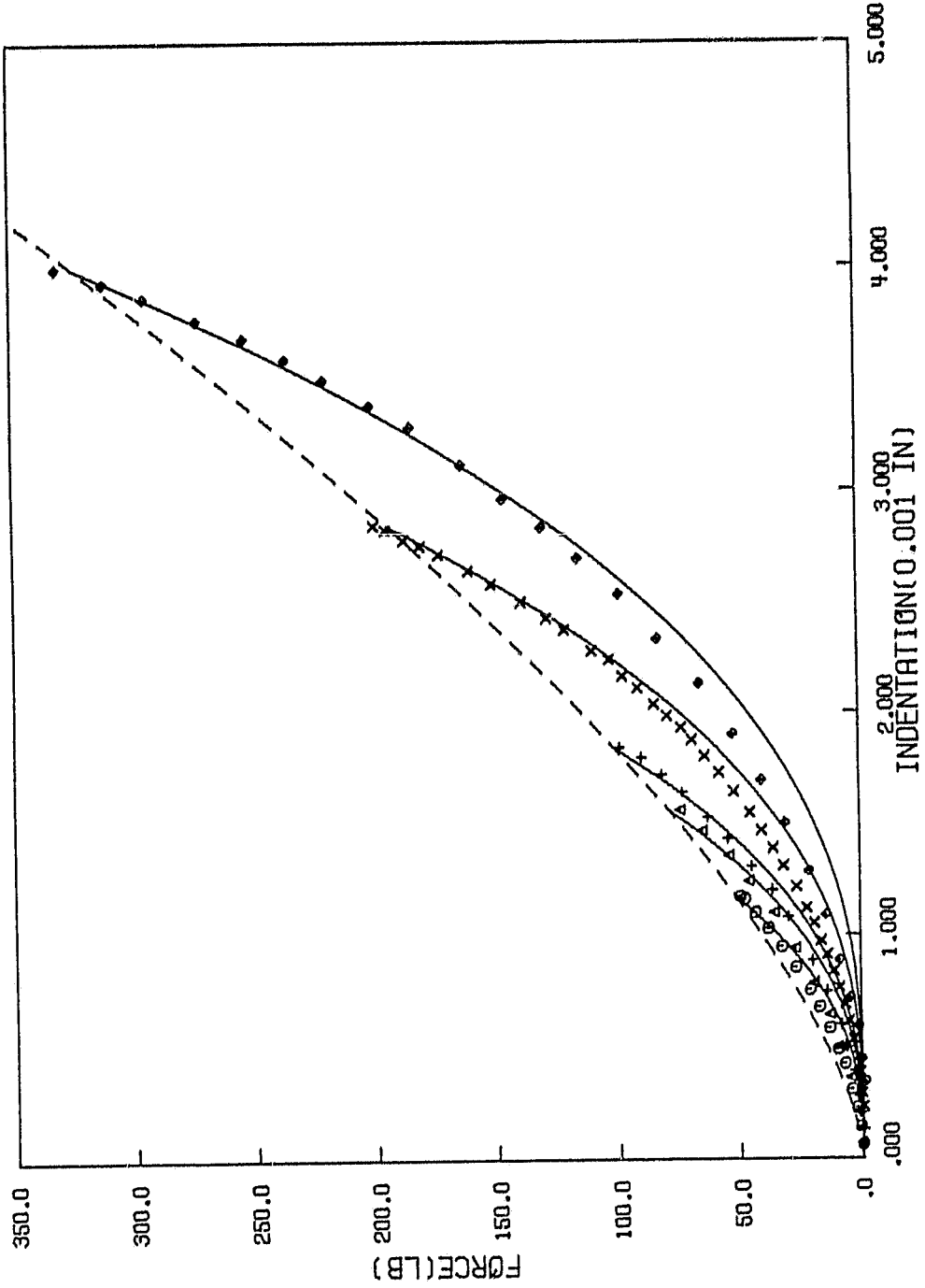


Figure 3.11 Unloading curves of $[0^\circ/45^\circ/0^\circ/-45^\circ/0^\circ]_{2s}$ specimens with 0.5 inch indenter ($q=2.5$)

ORIGINAL PAGE IS
OF POOR QUALITY

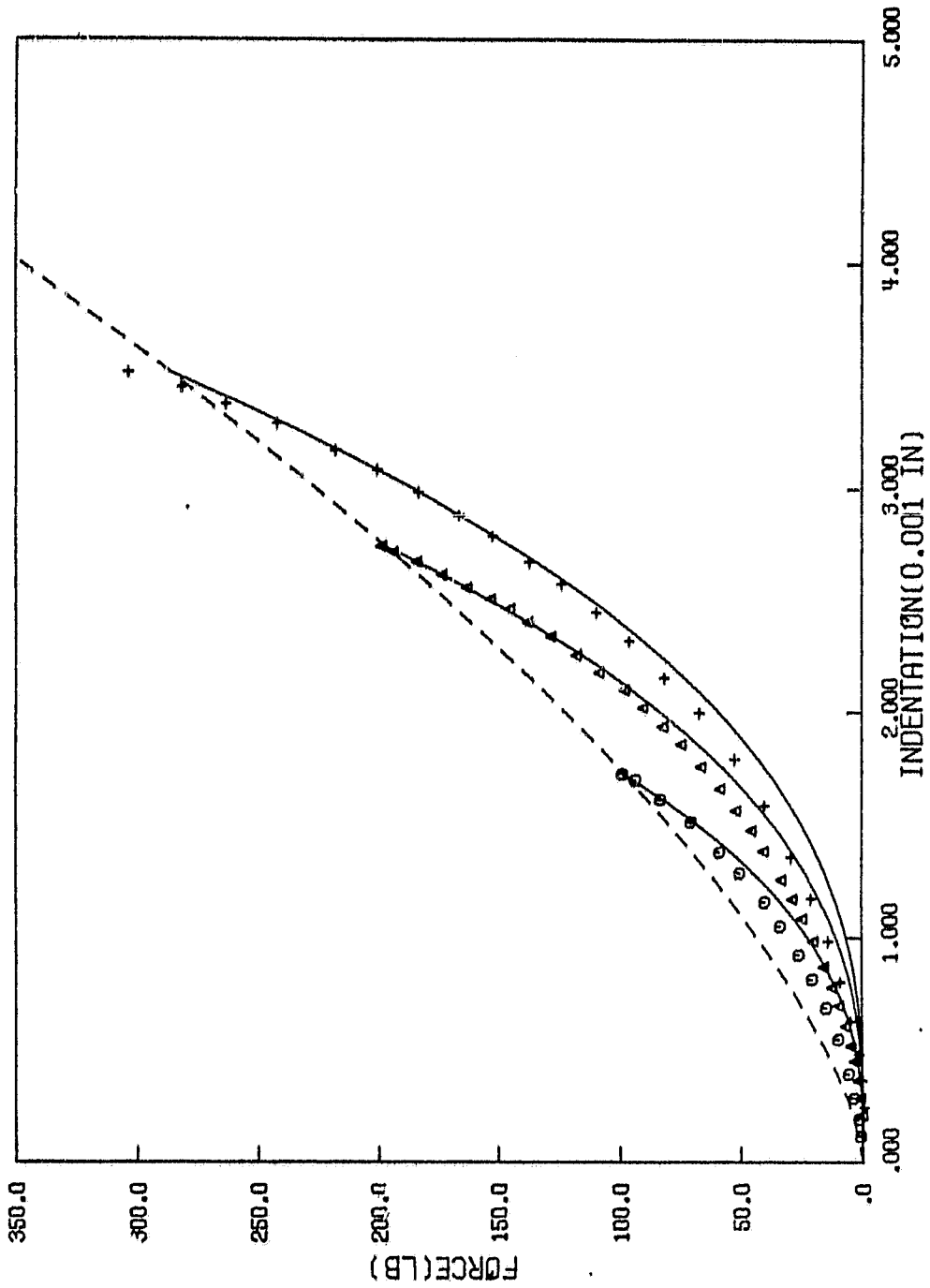


Figure 3.12 Unloading curves of $[90^\circ/45^\circ/90^\circ/-45^\circ/90^\circ]_{2s}$ specimens with 0.5 inch indenter ($q=2.5$)

ORIGINAL PAGE IS
OF POOR QUALITY

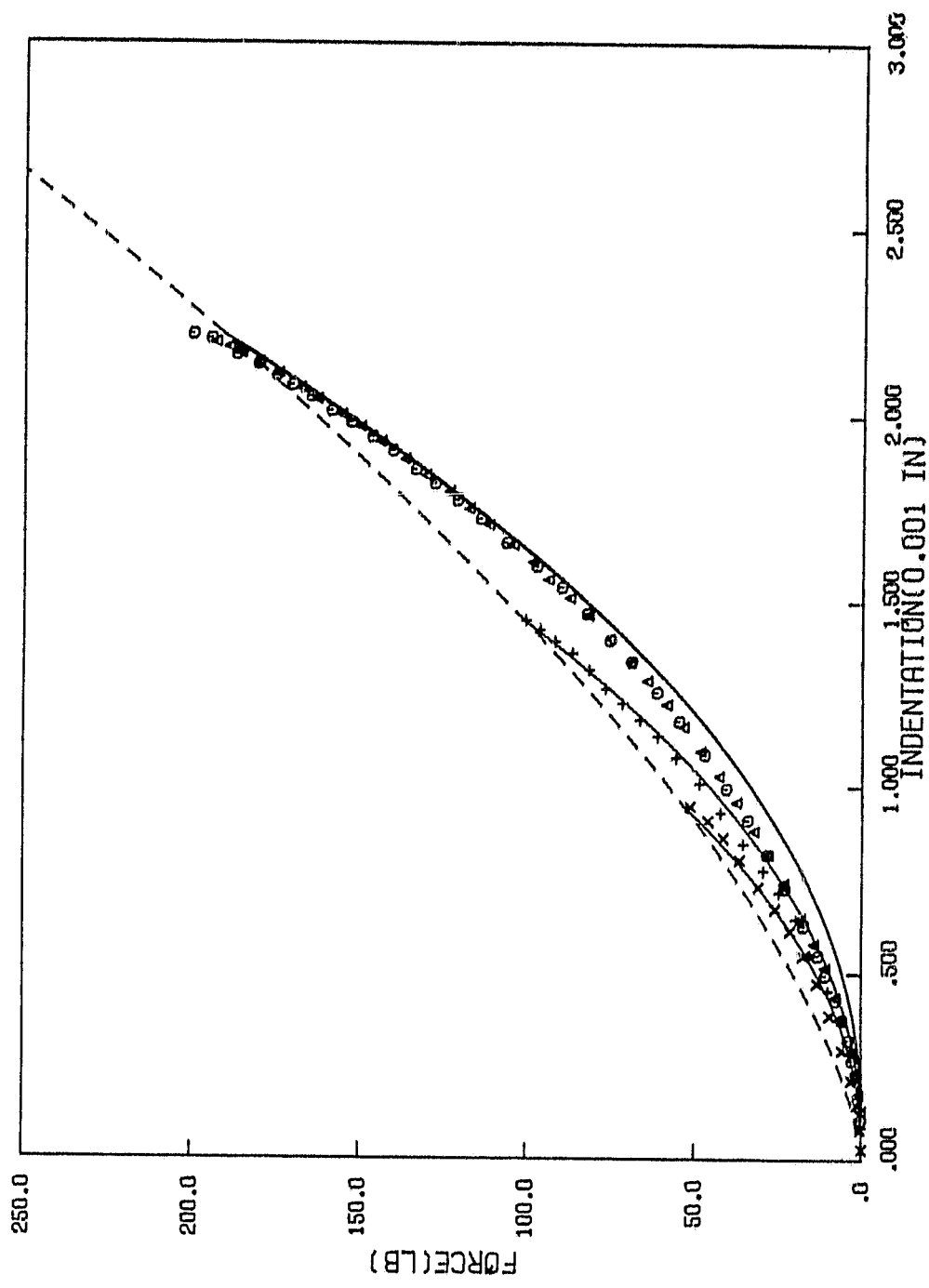


Figure 3.13 Unloading curves of $[0^\circ/45^\circ/0^\circ/-45^\circ/0^\circ]_{2s}$ specimens with 0.75 inch indenter ($q=2.0$)

ORIGINAL PAGE IS
OF POOR QUALITY

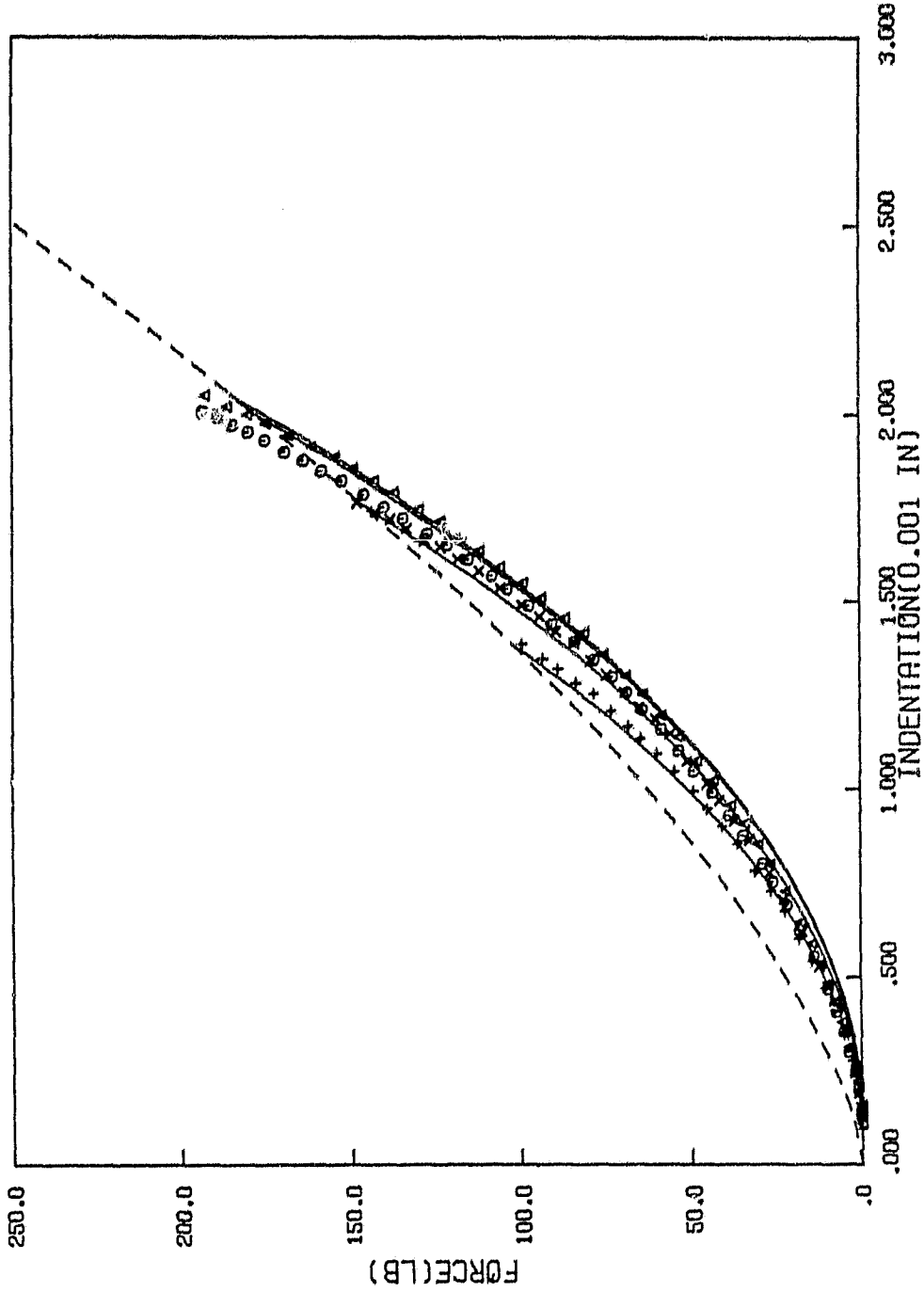


Figure 3.14 Unloading curves of $[90^\circ/45^\circ/90^\circ/-45^\circ/90^\circ]_{2s}$ specimens with 0.75 inch indenter ($q=2.0$)

3.2.3 Reloading Curves

ORIGINAL PAGE IS
OF POOR QUALITY

The equation

$$F = k_1 (\alpha - \alpha_0)^p \quad (3-11)$$

suggested by Yang [14] was used to model the reloading curve, where k_1 is called reloading rigidity and $p = 3/2$ was found to fit the experimental data quite well. It was also observed that the reloading curve always returns to where the unloading began, and hence the reloading rigidity can be determined by

$$k_1 = \bar{F}_m / (\alpha_m - \alpha_0)^{3/2} \quad (3-12)$$

In other words, the reloading test is not necessary provided the unloading condition is specified. Some reloading curves obtained following Equations (3-11) and (3-12), and the experimental data are presented in Figures 3.15-3.18.

3.3 Discussion

As mentioned before, due to creep the loading rate may affect the contact law (i.e. the value of k). A series of tests with different loading rates was performed to examine this point. The maximum loading rate the test equipment can apply without exceeding its capacity is about 50 lb/sec.. It was found that in the range of 5 lb/sec. to 50 lb/sec., the values of k showed very little scatter, and the effect

ORIGINAL PAGE IS
OF POOR QUALITY

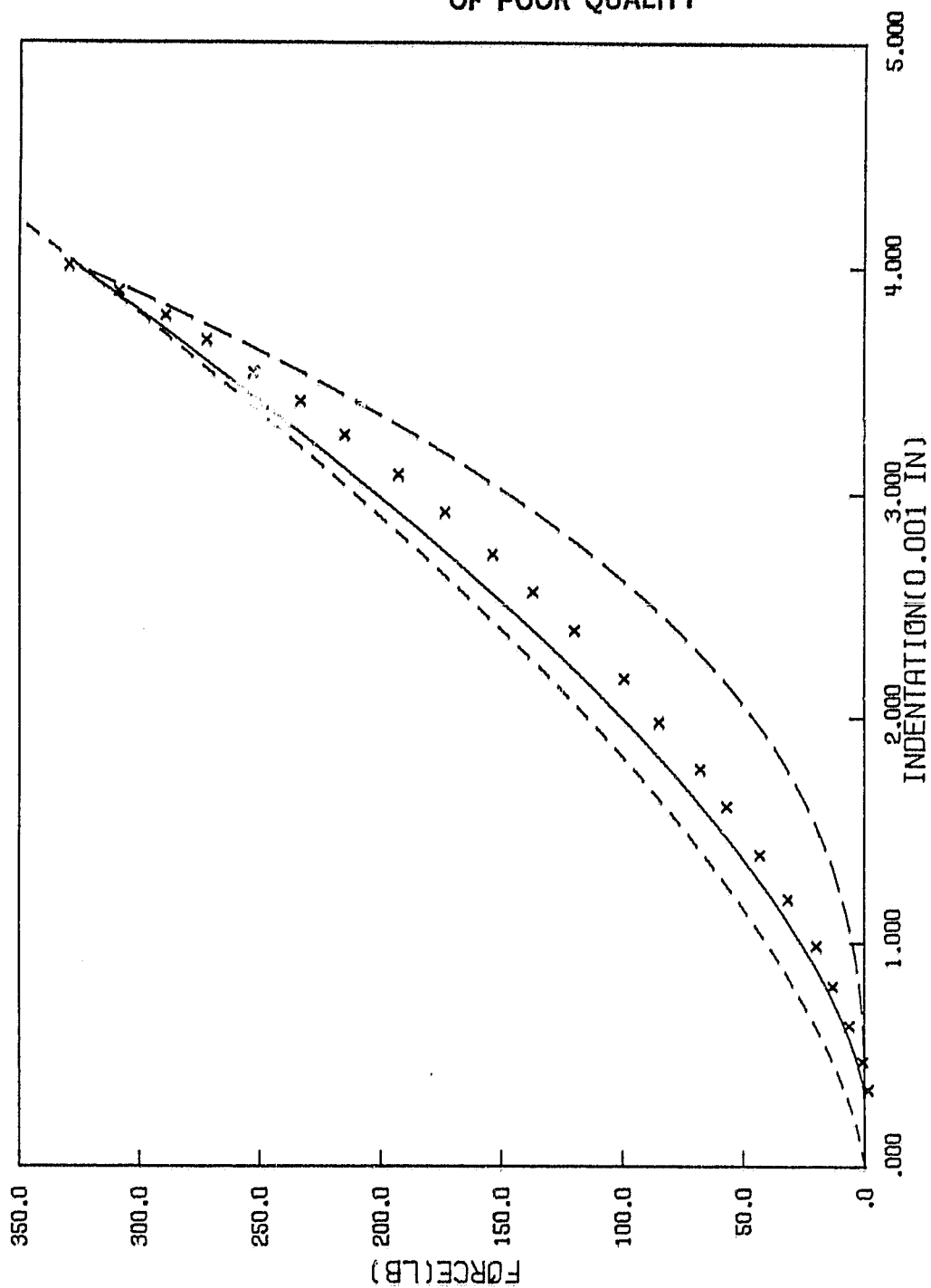


Figure 3.15 Reloading curve of $[0^\circ/45^\circ/0^\circ/-45^\circ/0^\circ]_{2s}$ specimens with 0.5 inch indenter ($p=1.5$)

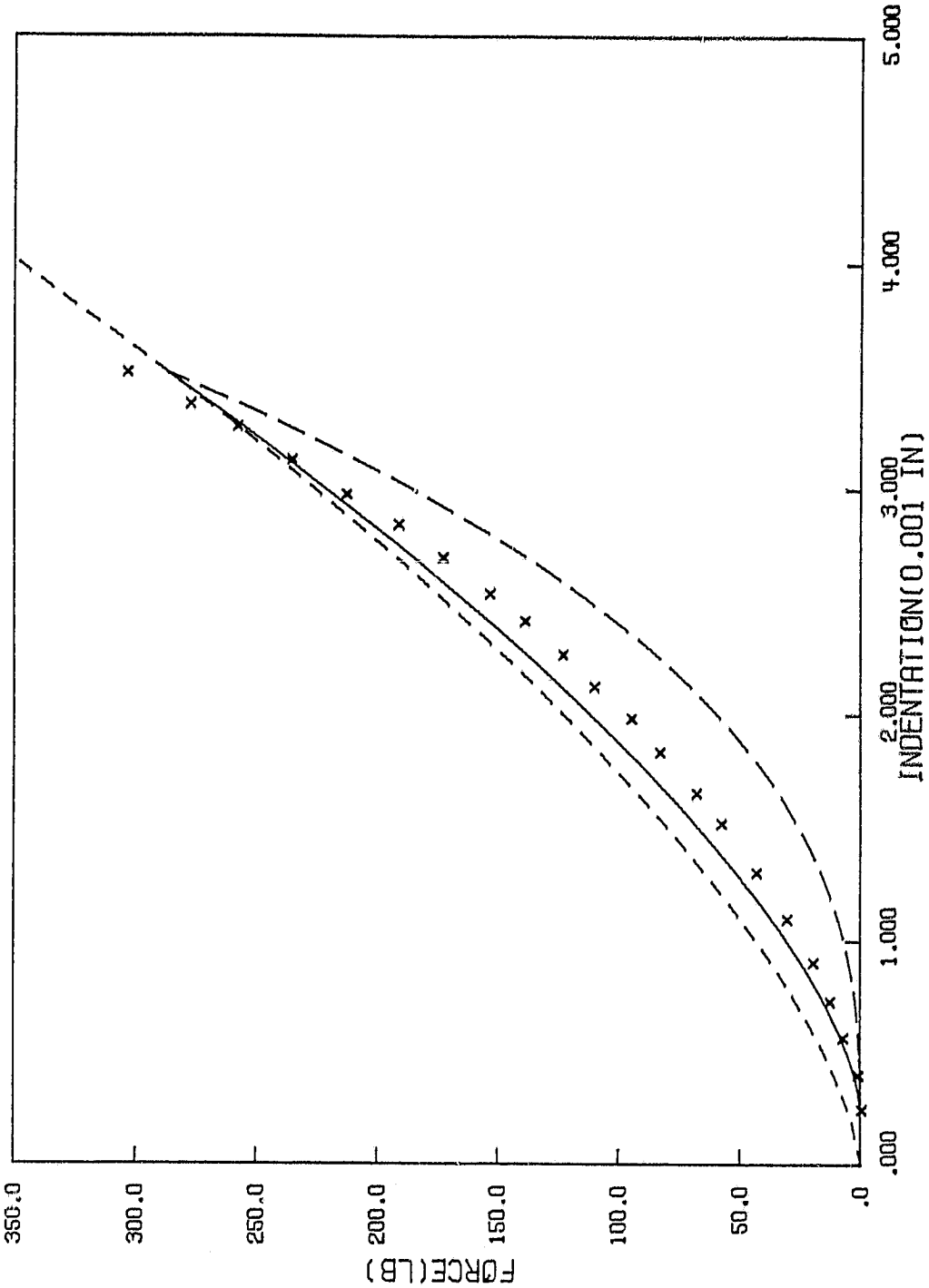


Figure 3.16 Reloading curve of $[90^\circ/45^\circ/90^\circ/-45^\circ/90^\circ]_{2s}$ specimens with 0.5 inch indenter ($p=1.5$)

ORIGINAL PAGE IS
OF POOR QUALITY

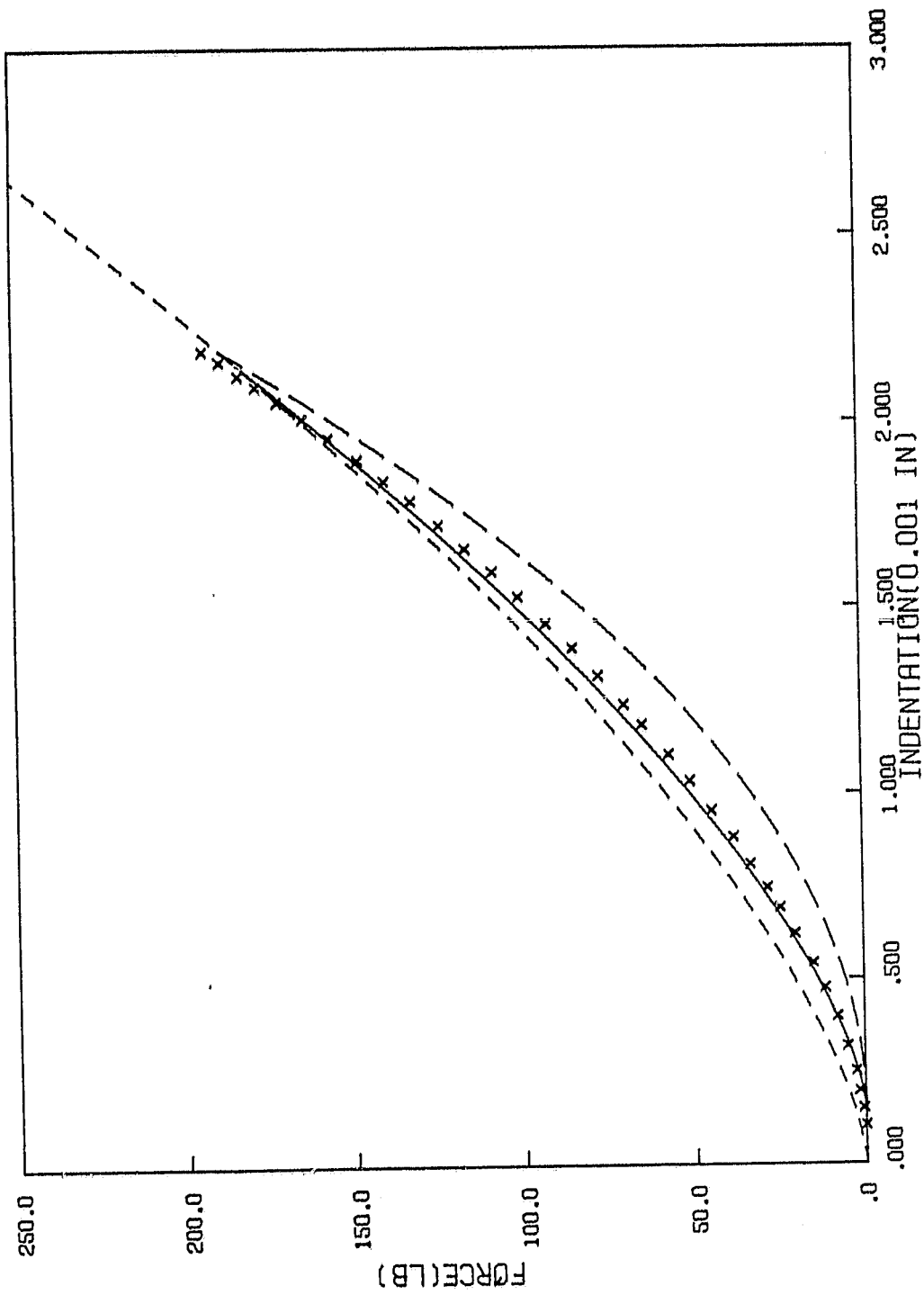


Figure 3.17 Reloading curve of $[0^\circ/45^\circ/0^\circ/-45^\circ/0^\circ]_{2s}$ specimens with 0.75 inch indenter ($p=1.5$)

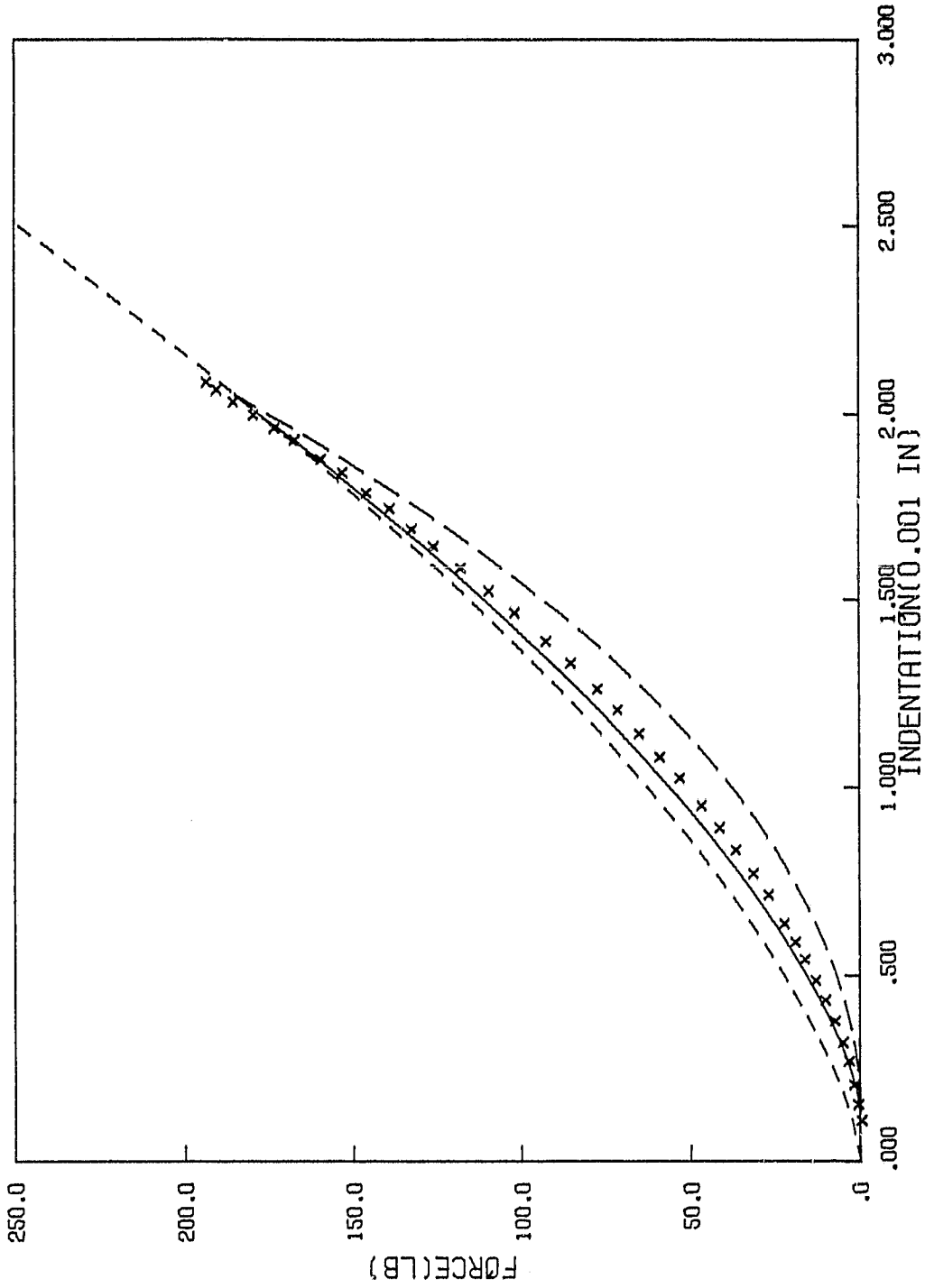


Figure 3.18 Reloading curve of $[90^\circ/45^\circ/90^\circ/-45^\circ/90^\circ]_{2s}$ specimens with 0.75 inch indenter ($p=1.5$)

due to local material nonhomogeneity in the composite may be even greater than the one due to the loading rate. However, an appreciable decrease of the value k was observed when the loading rate was lower than 1 lb/sec.. In some extreme cases where loadings were applied as slow as 10 lb/min., the average value of k for 0.5 in. indenter was very close to the one obtained previously by Yang [14] using dial gage to measure the indentation. In this study, the loading rates for all tests were approximately equal to 10 lb/sec..

Unlike the exponent n of the loading law for which the value of $3/2$ seems to yield good agreement with all experimental data, the exponent q of the unloading law (Equation 3-3 or 3-4) reveals much wider deviation for different sizes of indenter. Value of $q = 3/2$ corresponding to an elastic recovery according to the Hertzian theory was previously used by Crook [28] in a study of impacts between metal bodies. The experimental results from [14] and present study show that the value of q varies from 1.5 to 2.5. Local plastic deformation, anisotropic properties of composite material and unloading rate are all possible causes for this deviation. Obviously, an analytical study to determine the value of q as function of aforementioned factors is impracticable. Since the purpose of this study is to establish a contact law that can be used in the analysis of impact, the validity of this law must be verified from impact experiment. This will be investigated

In the next chapter.

ORIGINAL PAGE IS
OF POOR QUALITY

From Equation (3-3) or (3-4), it can be seen that α_0 plays an essential role in the unloading law and hence the value of it must be estimated accurately. Both of Equation (3-7) used by Yang [14] and Equation (3-8) used in this study for calculating α_0 were obtained experimentally, in which $\alpha_{c,r}$ and α_p are considered to be material constants and were determined using α_0 and α_m from test data. However, it was pointed out in [14] that the values of α_0 might not be the true permanent indentations. They were the values which could make the power law given by Equation (3-4) fit the total data under the unloading path. In fact, the load corresponding to the value of $\alpha_{c,r} = 3.16 \times 10^{-3}$ in. obtained in [14] is about 200 lb. for 0.5 in. indenter, which is apparently too high. The value of $\alpha_p = 6.564 \times 10^{-4}$ in. obtained in this study, which corresponds to about 20 lb of loading, seems more reasonable as a critical value in indentation. For comparison, the relations between unloading rigidity s and maximum indentation α_m using Equation (3-7) with $\alpha_{c,r} = 3.16 \times 10^{-3}$ in. and Equation (3-8) with $\alpha_p = 6.564 \times 10^{-4}$ in., respectively, are plotted in Figure 3.19. It is interesting to see that these two equations give almost the same values of s up to $\alpha_m = 4 \times 10^{-3}$ in. which is approximately the maximum indentation before failure could occur to the specimen. The advantage of using Equation (3-7) for the formulation of the unloading law is

ORIGINAL PAGE IS
OF POOR QUALITY

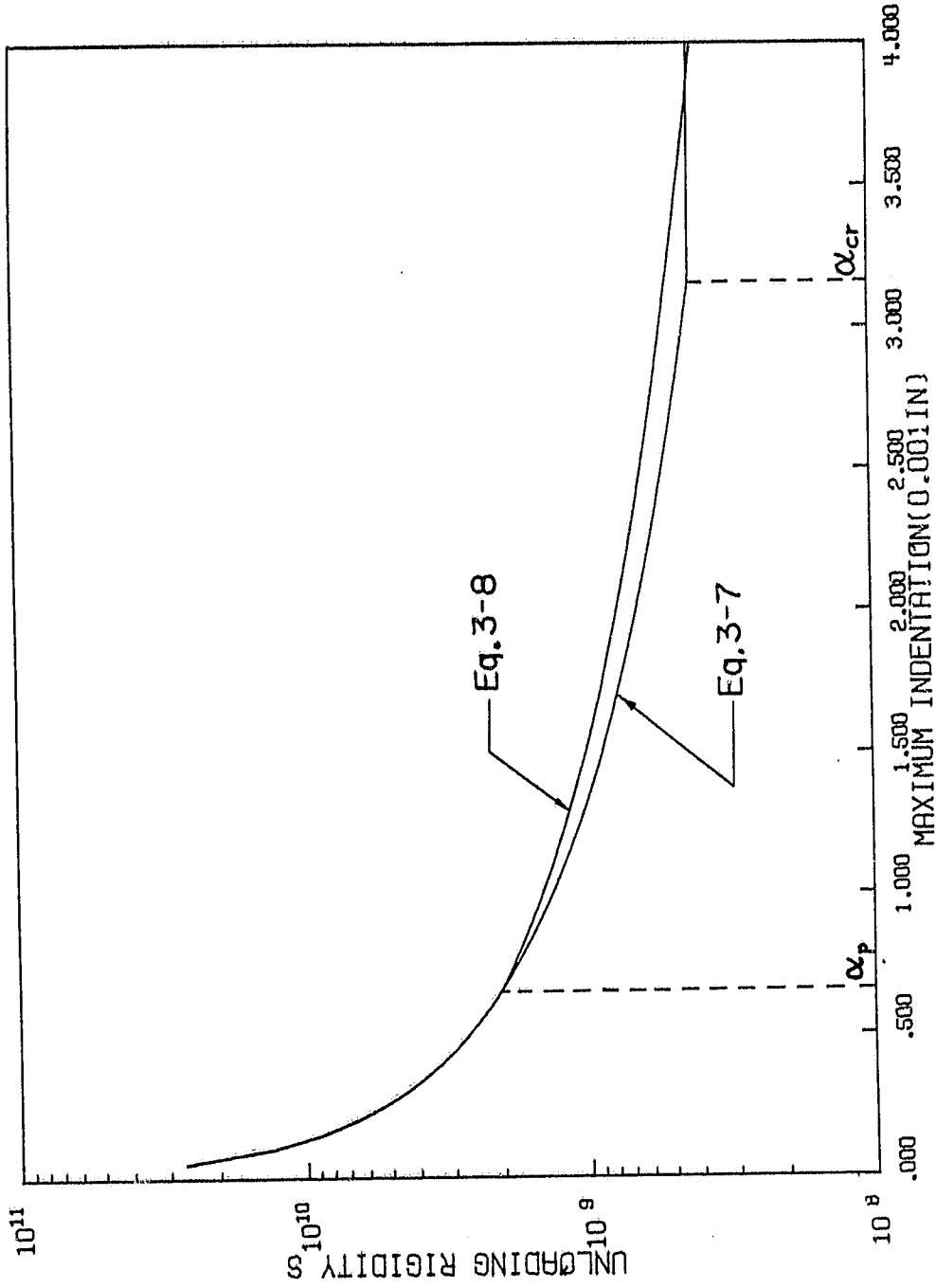


Figure 3.19 Unloading rigidity s as function of maximum indentation

that the value of s is constant for any α_m once the indentation passes α_{cr} , and only one unloading test is necessary to determine α_{cr} provided the load is high enough to produce permanent indentations. The use of Equation (3-9) needs performing many tests to obtain a proper relation between α_0 and α_m according to Equation (3-8). However, it should be noted that Equation (3-7) is valid only if $q = 5/2$ is used in the unloading equation (3-4), while Equation (3-8) has no such restriction.

ORIGINAL PAGE IS
OF POOR QUALITY

ORIGINAL PAGE IS
OF POOR QUALITY

CHAPTER 4 IMPACT EXPERIMENTS

High velocity impacts usually result in very small contact time and the material under impact loadings may behave differently from static contact due to the strain rate effect. The statically determined contact laws presented in the previous chapter thus must be verified experimentally before it can be applied to the impact analysis. Wang [15] has conducted many impact experiments on laminated composite beams and plates using spherical steel balls as impacters. The strain response histories at various points on the specimens were recorded and compared with the finite element analysis with which the contact laws obtained by Yang [14] was incorporated. The results showed that the test data agreed with the predictions using the statical indentation laws quite well. In this chapter, an attempt was made to measure the contact force directly so that the applicability of statical contact laws in impact analysis can be further evaluated.

4.1 Experimental Procedure

A 6 in. by 4 in. laminated plate cut from a $[0^\circ/45^\circ/0^\circ/-45^\circ/0^\circ]_{2s}$ graphite/epoxy panel was used as the impact target. The 0° -direction was arranged to parallel the long side of the plate. Seven strain gages (Micro Measurement Company TYPE EA-13-062 AQ 350) were placed at different locations as shown in Figure 4.1 to record the dynamic strain histories. One of the gages was placed on the surface directly opposite to the impact point to trigger the oscilloscope. This plate was hung with two strings at two corners to achieve the free boundary condition.

The projectile was made of an impact-force transducer with a spherical steel cap of 0.75 inch in diameter glued on the impact side and a steel rod of 5/8 inch in diameter glued on the other side as shown in Figure 4.2. It was then attached to a thin rod to form a pendulum which could produce impact velocities up to 150 in/sec. The total mass of the projectile is 0.000181 lb-sec²/in .

The schematic diagram for this impact experimental set-up is shown in Figure 4.3. Signals from gages and transducer were amplified by a 3A9 Textronix amplifier and displayed on the screen of an oscilloscope.

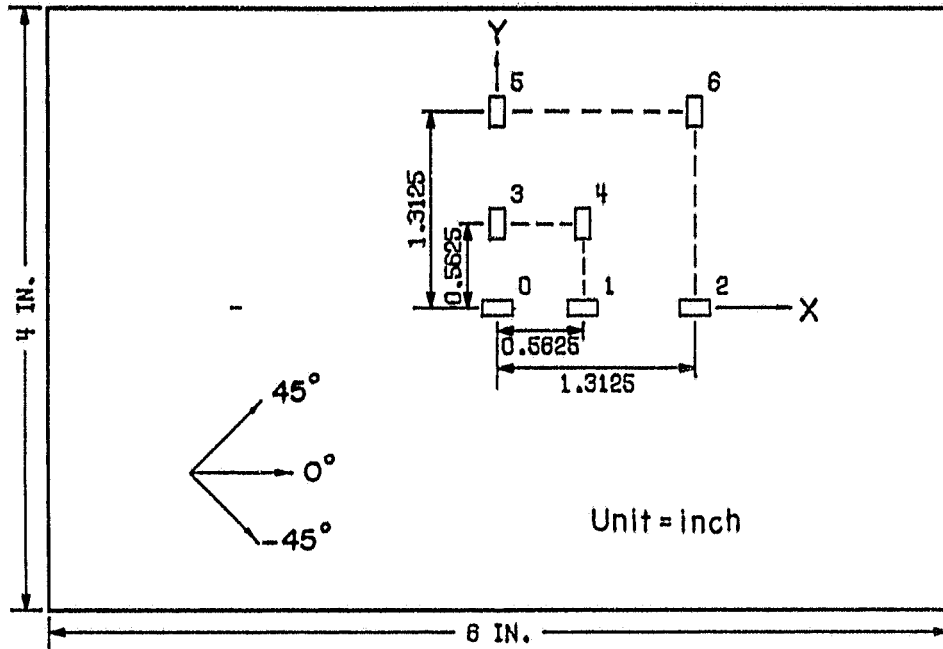
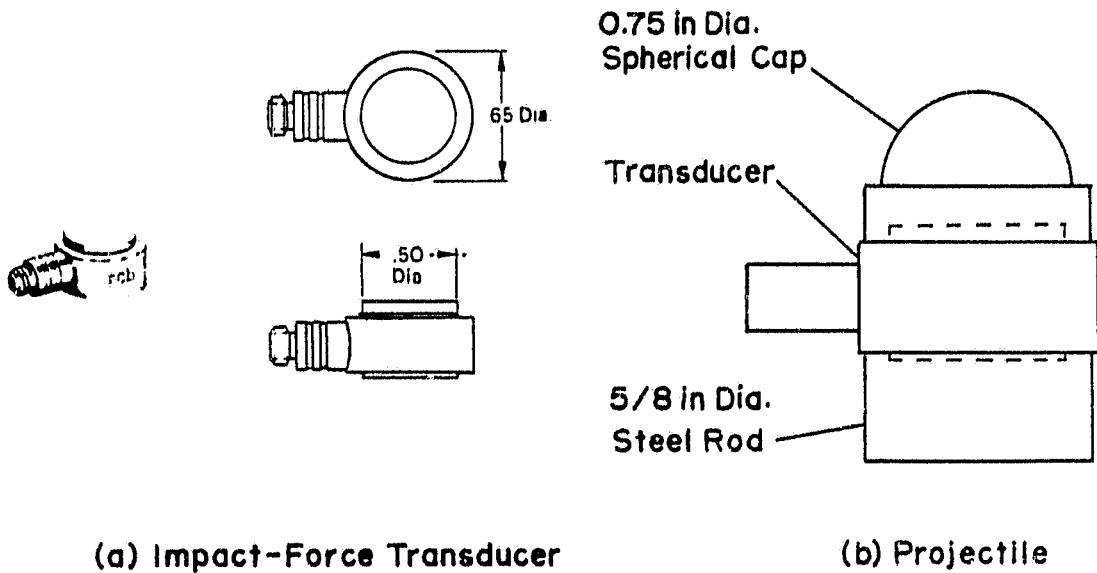


Figure 4.1 Laminate dimension and strain gage locations



(a) Impact-Force Transducer

(b) Projectile

Figure 4.2 Graphical illustration of Impact projectile

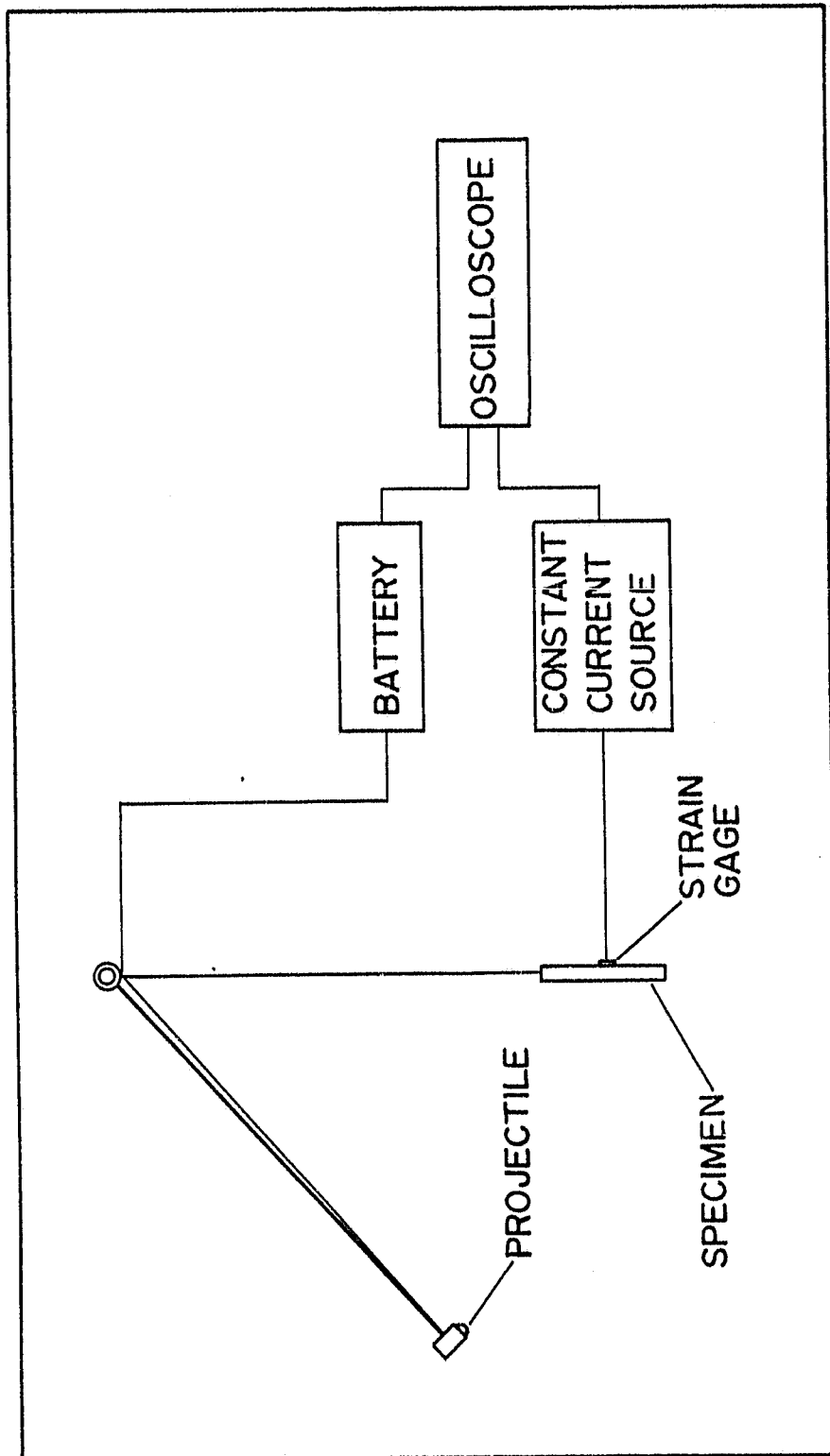


Figure 4.3 Schematic diagram for the impact experimental set-up

4.2 Calibration of Impact-Force Transducer

ORIGINAL PAGE IS
OF POOR QUALITY

The Impact-force transducer used was Modal 200A05 marketed by PCB Piezotronics Inc. Some of its specifications are shown in Table 4.1 [30]. The structure of this transducer contains two thin quartz disks operating in a thickness compression mode and sandwiched between hardened steel cylindrical members. A built-in amplifier can reduce the high impedance of the voltage from the quartz element and provides an output voltage which can be read out on oscilloscope, recorder, etc.. The impact force is then computed using the equation,

$$F = V_F / c_F \quad (4-1)$$

where V_F is the output voltage and c_F is the sensitivity of the transducer. Since the value of c_F in Table 4.1 was obtained under quasi-static condition [30], it must be verified under impact condition first so that later the results from impact experiment can be correctly interpreted.

A circular cylindrical steel rod of 2 inch in diameter and 1.19 inch long hung on strings was used as the impact target to calibrate the transducer. The acceleration of the rod was measured by using a Model 302A accelerometer which was mounted on the end of the rod opposite to the impacted end as shown in Figure 4.4. The total weight of the target is 1.105 lb.

ORIGINAL LISTING
OF POOR QUALITY

Table 4.1
Specifications for Model 200A05 Impact-Force Transducer

Range, Compression (5V output)	lb.	5,000
Maximum Compression	lb.	10,000
Resolution (200 μ V p-p noise)	lb.	0.2
Stiffness	lb/ μ in	100
Sensitivity	mV/lb	1.0
Resonant Frequency (no load)	Hz	70,000
Rise Time	μ sec	10
Discharge Time Constant (T.C.)	sec	2,000
Low-Frequency (-5%)	Hz	0.0003
Linearity, B.F.S.L.	%	1
Output Impedance	ohms	100
Excitation (thru C.C.diode)	VDC/mA	+18 to 24/2 to 20
Temperature Coefficient	%/ $^{\circ}$ F	0.03
Temperature Range	$^{\circ}$ F	-100 to +250
Shock (no load)	g	10,000

ORIGINAL PAGE IS
OF POOR QUALITY

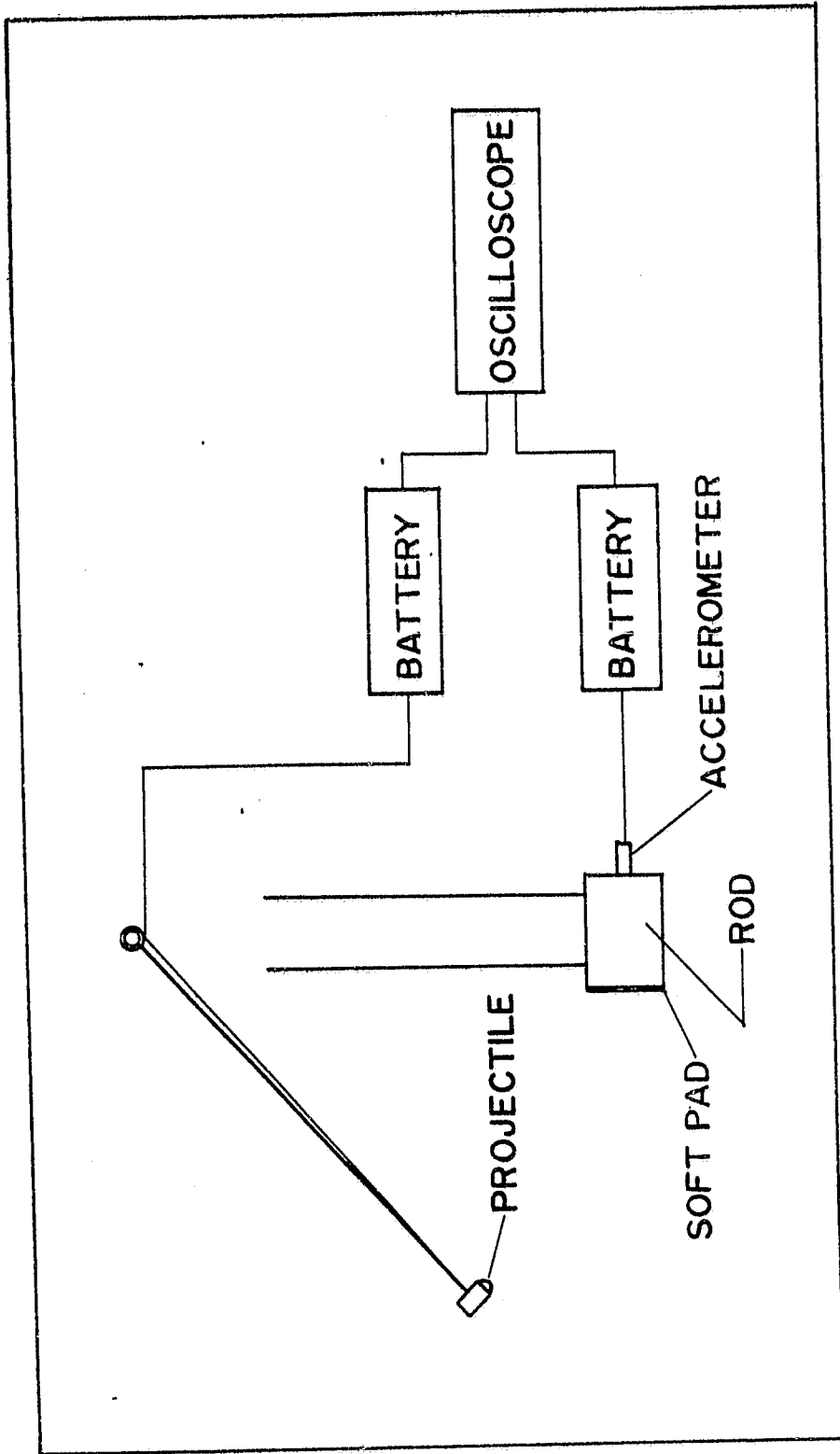


Figure 4.4 Experimental set-up for the calibration of impact-force transducer

C-2

Using Equation (4-1) and

$$a = V_a/c_a \quad (4-2)$$

$$F = ma \quad (4-3)$$

we obtain

$$c_F = (c_a/m)(V_F/V_a) \quad (4-4)$$

where V_a and c_a are the output voltage and the sensitivity of the accelerometer, respectively, a is acceleration of the target, and m is the mass of the target.

When impacting a metal projectile on a metal target with no pad on the impact surface, a high frequency ringing can be seen at the output of the transducer. In order to obtain smooth output curves, a soft pad was placed on the impact region of the target to eliminate the high frequency ringing. The cause of this ringing phenomenon will be discussed later. Typical output voltages of transducer and accelerometer read from the oscilloscope are shown in Figure 4.5. Values of V_F were plotted vs the corresponding values of V_a taken from these two curves at several discrete points in time and then fitted into a straight line as shown in Figure 4.6. The slope of this line represents the ratio of V_F/V_a which is then substituted in Equation (4-4) to calculate the sensitivity c_F .

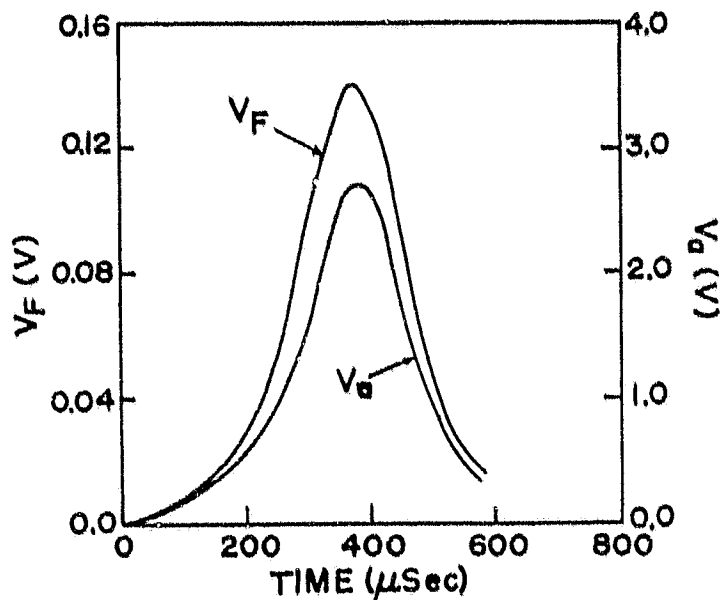


Figure 4.5 Typical output voltages from transducer and accelerometer

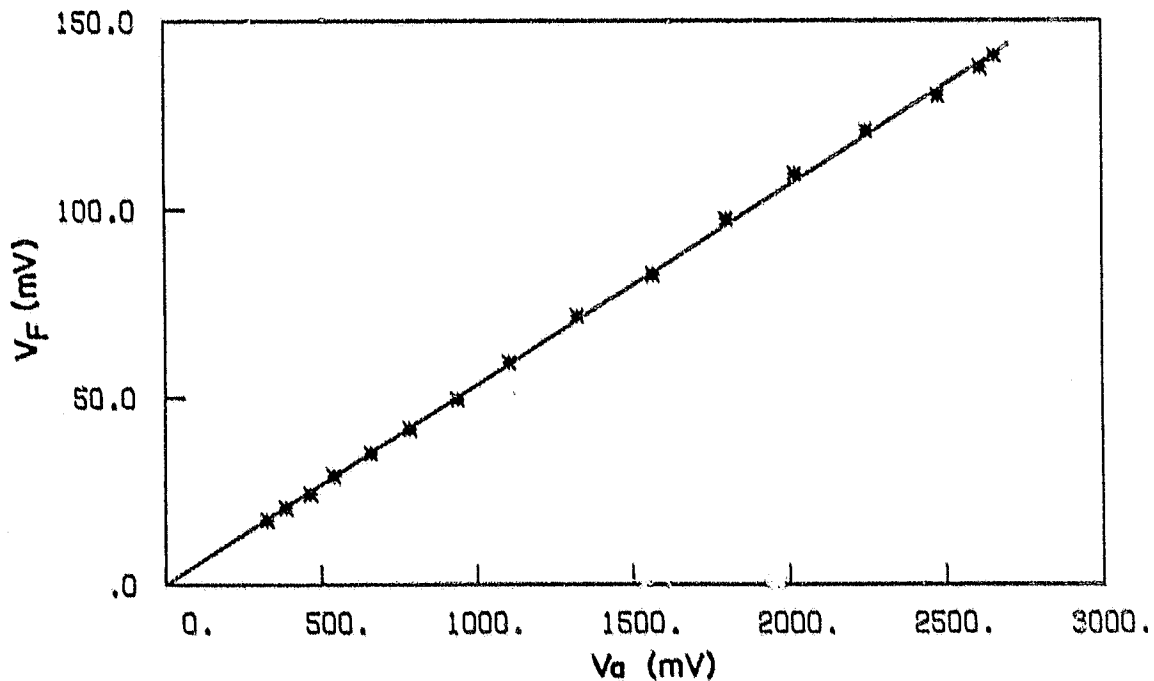


Figure 4.6 Relation between V_F and V_a

Assuming the sensitivity of the accelerometer c_a is correct, and using Equation (4-4) and the test data, the average value of c_f calculated was 0.494 mV/lb.. A comparison with the value of 1.0 mV/lb from Table 4.1 shows that the test result has more than 50% error. However, since the quartz elements are located at the center of the projectile while the impact force is applied at the end, we were not certain that the force history picked up by the quartz elements did represent the real history of the impact force. The following simple analysis was performed to examine this uncertainty.

Consider a 1 in. long steel rod with free-free boundary conditions. For a impulse loading given by

$$F(t) = F_0 \text{ EXP}[-(t-\tau)^2/4b^2] \quad (4-5)$$

at one end, the force history at the midpoint of the rod, $F_m(t)$, was computed and plotted in Figure 4.7 together with the applied force history. It should be noted that the values of $F_0 = 1000$ lb., $\tau = 200 \times 10^{-6}$ sec. and $b = 40 \times 10^{-6}$ sec. were chosen in Equation (4-5) so that the applied force history is similar to the experimental loading history. From Figure 4.7, it can be seen that $F_m(t)$ is only about half of the applied force $F(t)$. The average ratio of $F_m(t)/F(t)$ was obtained to be 0.498, which is very close to the value of c_f obtained previously. The accelerations at the two ends and the midpoint of the rod were also

ORIGINAL PAGE IS
OF POOR QUALITY

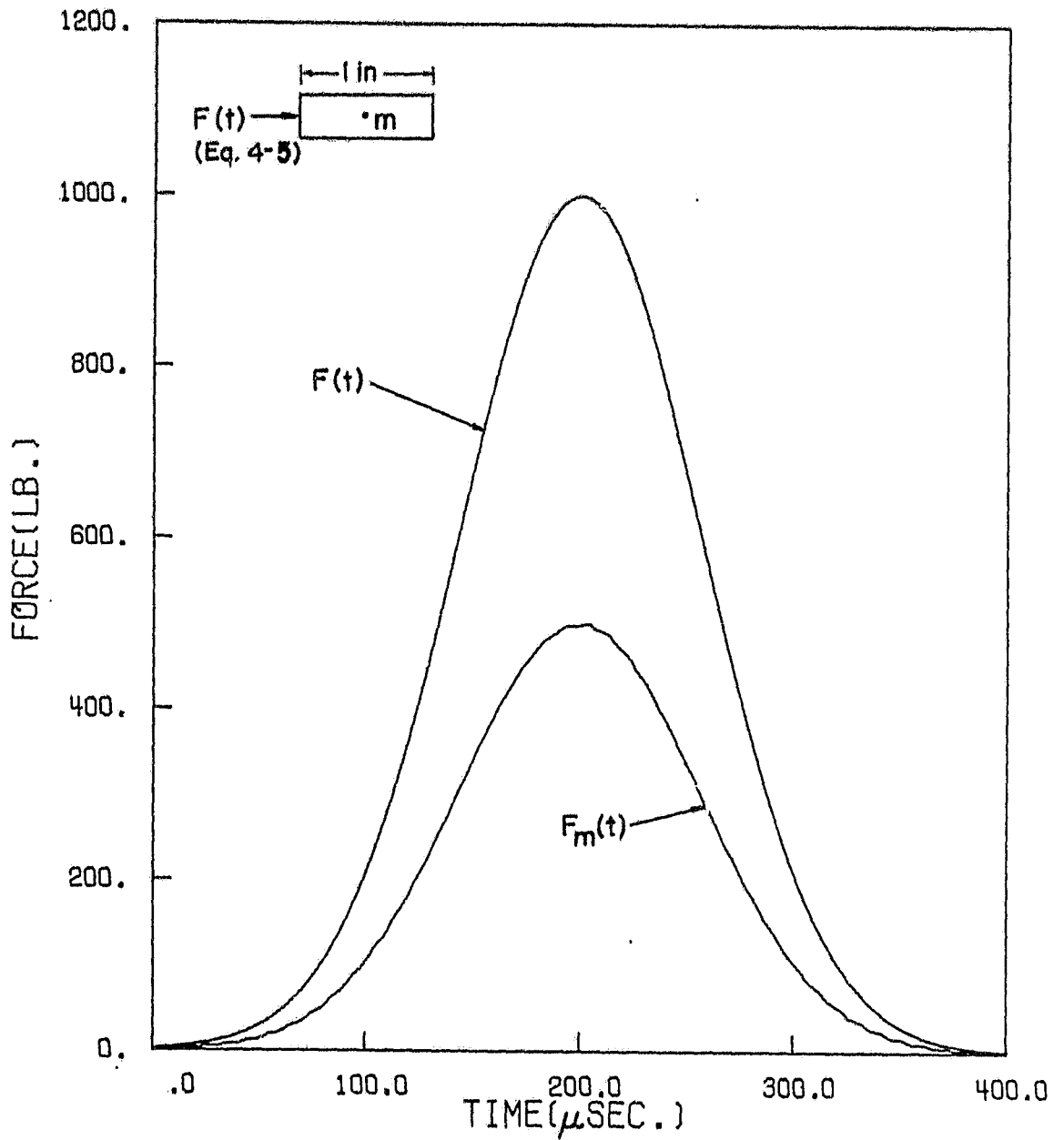


Figure 4.7 Assumed exponential impulsive loading and the response history at the midpoint of the rod

calculated and plotted in Figure 4.8. It shows that the magnitudes of acceleration at any position of the rod have virtually no difference. This indicates that the accelerometer did measure the real acceleration of the target while the impact-force transducer only picked up the force history at the point of its own position. In other words, the wave motion in the projectile can not be neglected, hence it must be treated as an elastic body.

Repeating the previous analysis by changing the impulse loading of Equation (4-5) to

$$F(t) = F_0 \sin(\pi t/b) \quad (4-6)$$

and letting $F_0 = 1000$ lb. and $b = 400 \times 10^{-6}$ sec., we obtain the force history at the midpoint of the rod as shown in Figure 4.9. Comparing Figure 4.9 with Figure 4.8, it is clear that the initial slope of the impulse forcing function would affect the amplitude of ringing. The steeper the initial slope is, the higher the amplitude of ringing will be. When impacting the steel projectile on graphite/epoxy surface, this ringing phenomenon was also observed.

ORIGINAL PAGE IS
OF POOR QUALITY

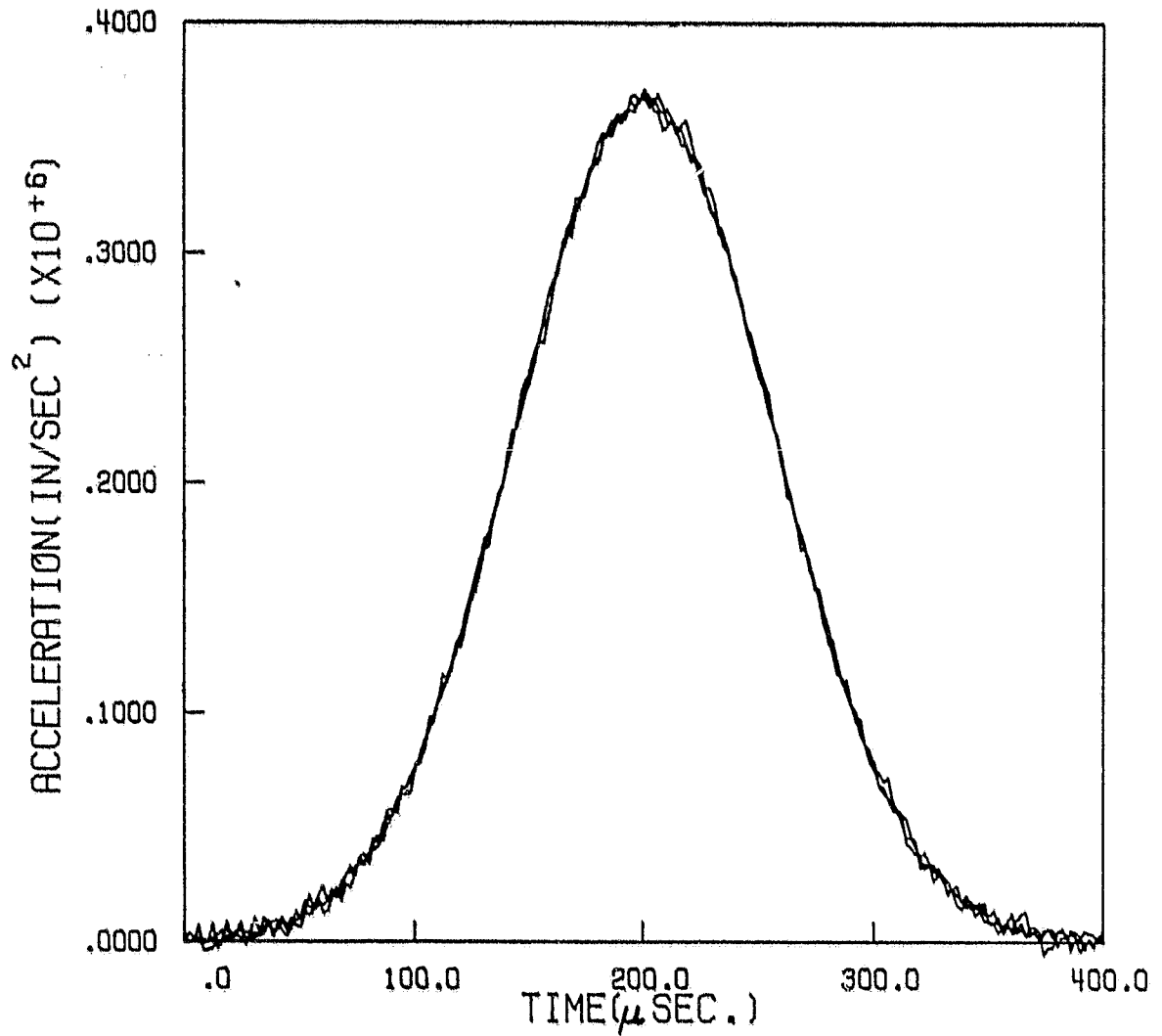


Figure 4.8 Accelerations of rod for assumed exponential impulsive loading

ORIGINAL PAGE IS
OF POOR QUALITY

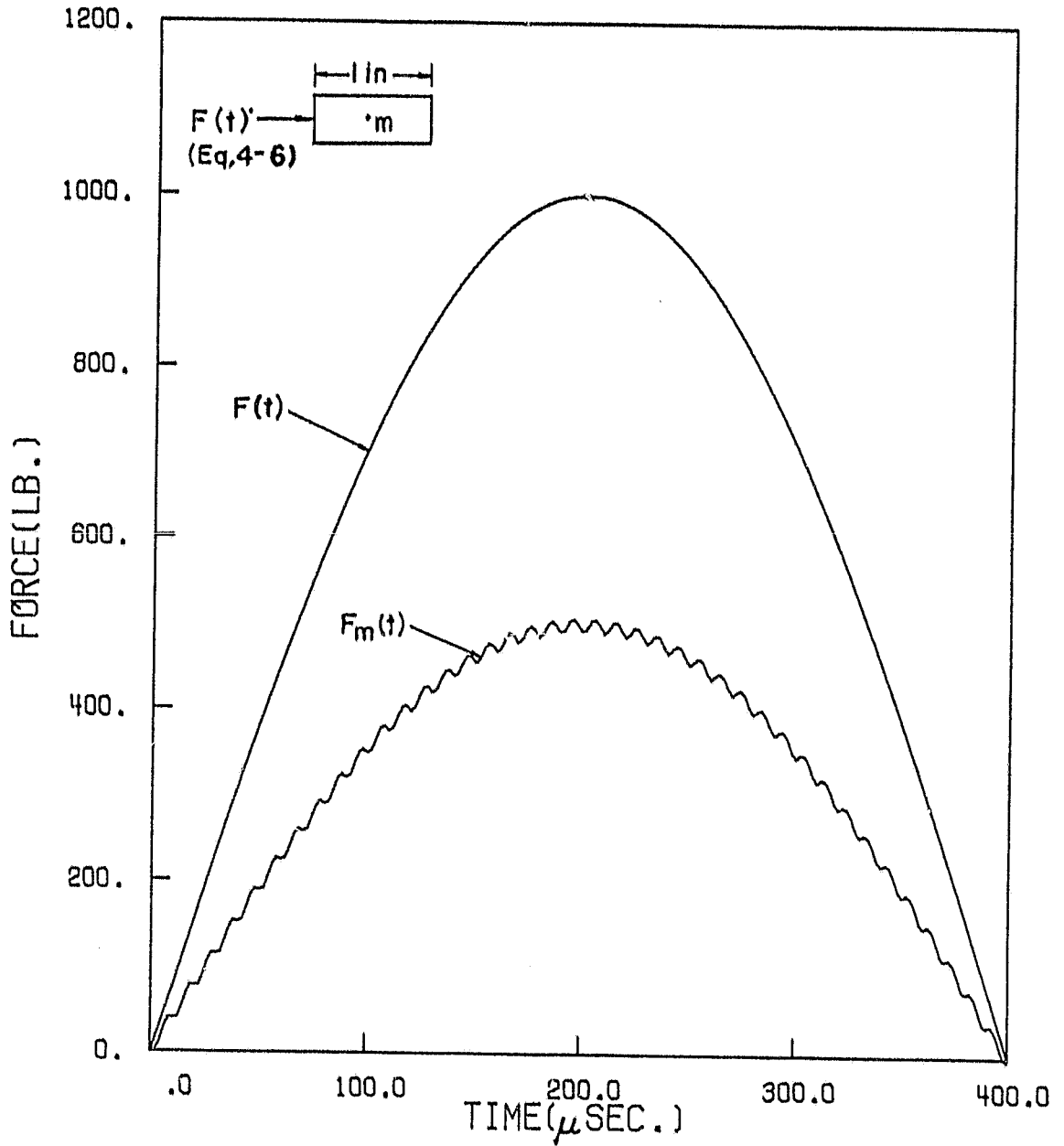


Figure 4.9 Assumed sine-function impulsive loading and the response history at the midpoint of the rod

4.3 Finite Element Analysis

ORIGINAL PAGE IS
OF POOR QUALITY

4.3.1 Plate Finite Element

A 9-node isoparametric plate finite element (see Figure 4.10) developed by Yang [31] based upon the laminate theory of Whitney and Pagano [18] was used to model the dynamic motion of the laminated plate. At each node there are five degrees of freedom. Among them, u^0 , v^0 and w are displacement components of mid-plane in the x -, y - and z -direction, respectively, and ϕ_x and ϕ_y are rotations of the cross-sections perpendicular to the x - and y -axis, respectively. For symmetric laminates, the flexural deformation is uncoupled from the in-plane extensional and shear deformations, and hence, the degrees of freedom corresponding to u^0 and v^0 can be neglected in the transverse impact problem.

The isoparametric plate finite element is developed using the following shape functions:

For corner nodes:

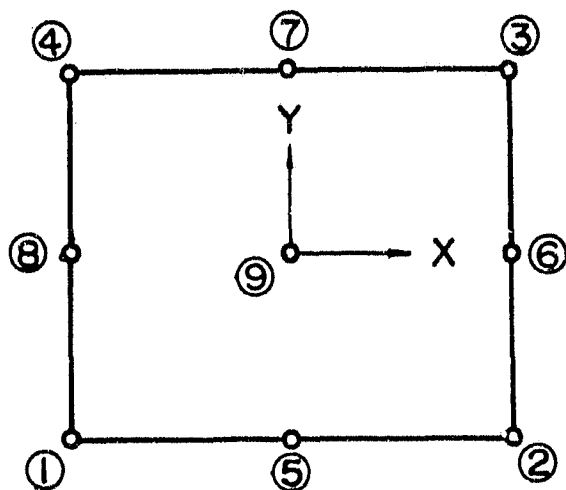
$$S_1 = (1/4)(1+\xi_0)(1+\eta_0)(\xi_0+\eta_0-1) + (1/4)(1-\xi^2)(1-\eta^2) \quad (4-7)$$

For nodes at $\xi = 0$ and $\eta = \pm 1$:

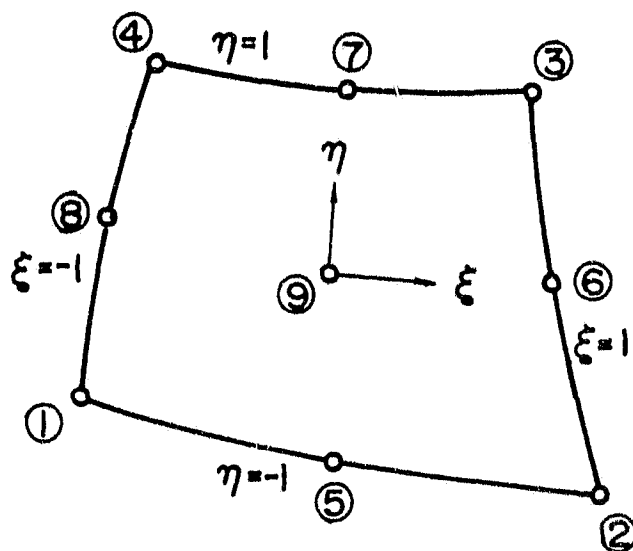
$$S_1 = (1/2)(1-\xi^2)(\eta_0+\eta^2) \quad (4-8)$$

For nodes at $\xi = \pm 1$ and $\eta = 0$:

Original PAGE IS
OF POOR QUALITY



(a) PARENT ELEMENT



(b) DISTORTED ELEMENT

Figure 4.10 9-node isoparametric plate element

$$S_1 = (1/2)(\xi_0 + \xi^2)(1 - \eta^2)$$

ORIGINAL PAGE IS
OF POOR QUALITY

(4-9)

For the center node:

$$S_1 = (1/2)(1 - \xi^2)(1 - \eta^2)$$

(4-10)

In the above shape functions, ξ and η are normalized local coordinates, and

$$\xi_0 = \xi\xi_1, \quad \eta_0 = \eta\eta_1 \quad (4-11)$$

where ξ_1 and η_1 are the natural coordinates of node 1 (Figure 4.10).

Using the shape functions, the plate displacements w , ϕ_x and ϕ_y are approximated by

$$\begin{Bmatrix} w \\ \phi_x \\ \phi_y \end{Bmatrix} = \sum_{i=1}^9 [S_i] \{q_p\}_i \quad (4-12)$$

where $\{q_p\}_i$ is the nodal displacement vector at node i and

$$[S]_i = S_i [I]^{3 \times 3} \quad (4-13)$$

The stiffness and mass matrices are obtained by numerical integration using Gauss quadrature. Following standard finite element procedures, the system stiffness matrix $[K_p]$ and mass matrix $[M_p]$ are assembled from the element matrices. The equations of motion are expressed in matrix

ORIGINAL PAGE IS
OF POOR QUALITY

form as

$$[M_p]\{\ddot{q}_p\} + [K_p]\{q_p\} = \{P_p\} \quad (4-14)$$

where

$$\{P_p\}^T = \{0, \dots, F, \dots, 0\} \quad (4-15)$$

is the force vector in which F is the contact force associated with the degree of freedom corresponding to the w -displacement at the impact point. The subscript p in Equations (4-12) through (4-15) denotes those are quantities corresponding to laminated plate.

4.3.2 Modeling of Projectile

In Section 4.2 we showed that in order to interpret the experimental transducer response, it is necessary to treat the projectile as an elastic body. A higher order rod finite element developed by Yang and Sun [32] was used to model the projectile. This element has two degrees of freedom at each node, namely the axial displacement u and its first derivative $\partial u / \partial x$. It has been shown that this higher order element is far more superior than the elements with less degrees of freedom in the analysis of dynamic problems. The displacement function is taken as

$$u = a_1 + a_2x + a_3x^2 + a_4x^3 \quad (4-16)$$

where a_i are constant coefficients. Solving these coefficients in terms of the nodal degrees of freedom and substituting into Equation (4-16), we obtain

$$u = \{N\}^T \{q_r\}_e \quad (4-17)$$

where

$$\{q_r\}_e^T = \{(u)_1, (\partial u / \partial x)_1, (u)_2, (\partial u / \partial x)_2\} \quad (4-18)$$

is the vector of element nodal degrees of freedom, and

$$\{N\}^T = \{f_1(x), f_2(x), f_3(x), f_4(x)\} \quad (4-19)$$

In which

$$f_1(x) = (1 - x/L)^2(1 + 2x/L)$$

$$f_2(x) = x(1 - x/L)^2$$

$$f_3(x) = x^2/L^2(3 - 2x/L)$$

$$f_4(x) = x^2/L(x/L - 1)$$

are shape functions. The subscript r in Equation (4-17) denotes quantities corresponding to the rod.

Using variational principle, the equations of motion for one element are obtained as

$$[m_r] \{\ddot{q}_r\}_e + [k_r] \{q_r\}_e = \{p_r\}_e \quad (4-20)$$

where $\{p_r\}_e$ is the vector of the generalized forces associated with the nodal degrees of freedom $\{q_r\}_e$, $[m_r]$ is the element mass matrix whose entries are given by

$$(m_r)_{ij} = \rho A \int_0^L f_i f_j dx \quad i, j = 1, 2, 3, 4 \quad (4-21)$$

and $[k_r]$ is the element stiffness matrix whose entries are given by

$$(k_r)_{ij} = EA \int_0^L f_i' f_j' dx \quad i, j = 1, 2, 3, 4 \quad (4-22)$$

In Equations (4-21) and (4-22), ρ , E and A are mass density, Young's modulus and cross-sectional area of the projectile, respectively, and L is the length of the element. The explicit forms of $[k_r]$ and $[m_r]$ are given by

$$[k_r] = \frac{EA}{30L} \begin{bmatrix} 36 & 3L & -36 & 3L \\ 3L & 4L^2 & -3L & -L^2 \\ -36 & -3L & 36 & -3L \\ 3L & -L^2 & -3L & 4L^2 \end{bmatrix} \quad (4-23)$$

and

$$[m_r] = \frac{\rho AL}{420} \begin{bmatrix} 156 & 22L & 54 & -13L \\ 22L & 4L^2 & 13L & -3L^2 \\ 54 & 13L & 156 & -22L \\ -13L & -3L^2 & -22L & 4L^2 \end{bmatrix} \quad (4-24)$$

Following the usual manner, the system stiffness and mass matrices are assembled from the element stiffness and mass matrices, and the system equations of motion are expressed as

ORIGINAL PAGE IS
OF POOR QUALITY

$$[M_r]\{\ddot{q}_r\} + [K_r]\{q_r\} = \{P_r\} \quad (4-25)$$

where

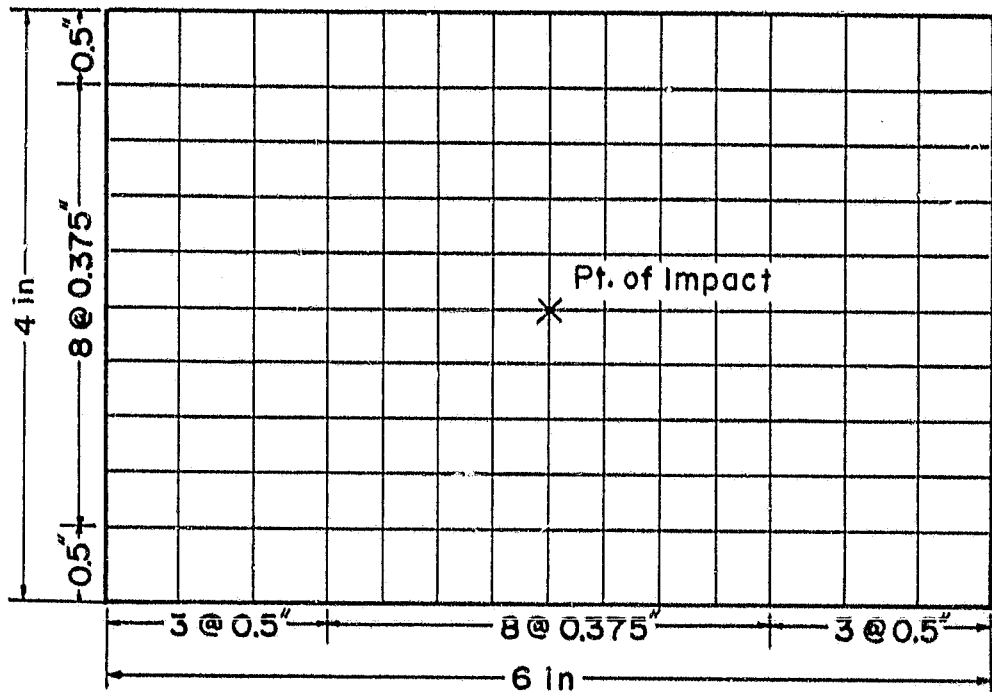
$$\{P_r\}^T = \{F, 0, \dots, 0\} \quad (4-26)$$

In which F is the contact force applied at the impacting end of the projectile.

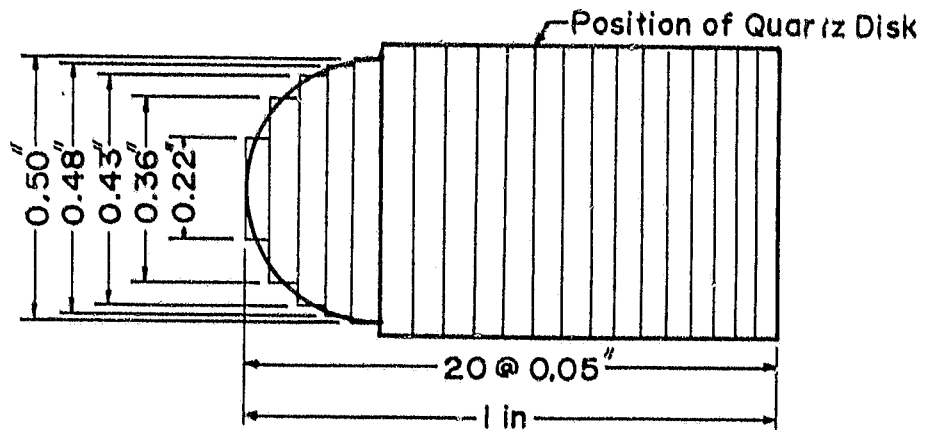
4.4. Results and Discussion

The 6 in. by 4 in. graphite/epoxy laminate was modeled by 140 (14 x 10 mesh) plate elements while the projectile was modeled by 20 rod elements (see Figure 4.11). The two sets of equations (4-14) and (4-25) along with the contact laws given by Equations (3-1), (3-3) and (3-11) were solved simultaneously. The finite difference method with $\Delta t = 0.2 \mu\text{sec.}$ was used to integrate the time variable. A coarser finite element mesh for plate was used and it was found that the present mesh yielded converged solutions. A 3-Dimensional analysis using 112 axisymmetric finite elements to model the projectile was also performed, and the results showed the the response at the midpoint of the projectile to have no significant difference comparing with the one obtained by using rod elements.

An impact velocity of 115 in/sec was used in the experiment. Figures 4.12-4.17 show the strain response histories at the six locations picked up by the strain



(a) Plate



(b) Projectile

Figure 4.11 Finite element mesh for laminated plate and projectile

gages. The results obtained using the finite element methods and the contact laws are also shown in these figures. It is evident that the finite element solutions agree with the experimental data very well.

In Figure 4.18, the experimental transducer responses and the computed transducer responses using finite element are plotted against time as curve I and curve II, respectively. The computed contact force history is also plotted as curve III. It can be seen that the magnitudes of curve I and curve II agree fairly well. The frequencies of ringing for these two curves, however, are quite different. For the finite element results, the time interval between two consecutive peaks of ringing is approximately equal to the time that the longitudinal stress wave needed to travel the distance between two ends of the projectile. This indicates that the ringing is simply caused by the transient wave travelling back and forth in the projectile.

From Figure 4.18 we can see that curve I has exact 9 peaks in 180 microseconds, and the time interval between two consecutive peaks is about 20 microseconds. It is noted that this transducer has a rise time of 10 microseconds (see Table 4.1), which is the time it needs to reach the maximum response. Any input signal with period smaller than twice of this value will be smoothed out by the transducer, and the output signal may appear to have lower frequency. In other words, the period of the output signal will be at

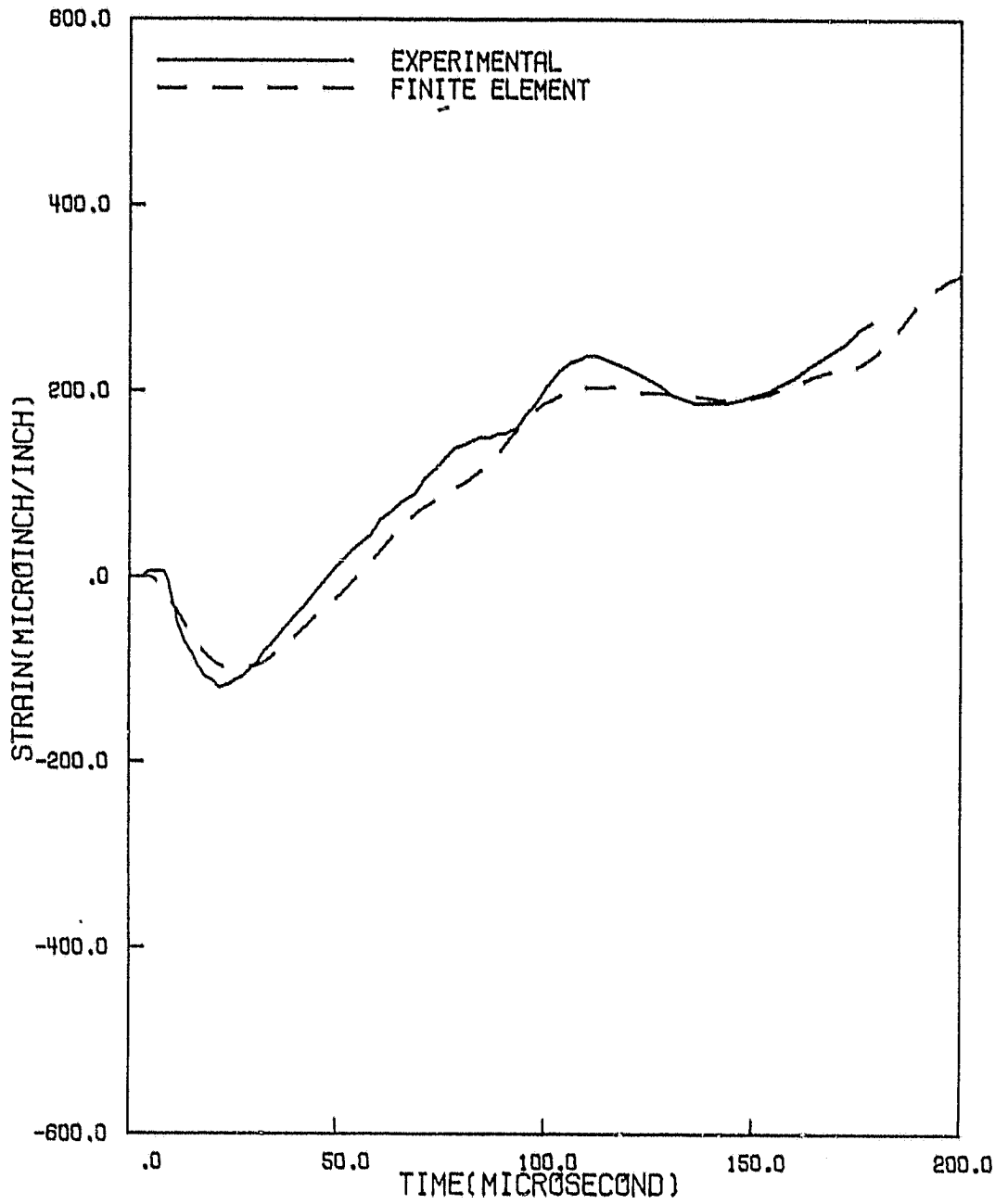


Figure 4.12 Strain response history at gage No.1

ORIGINAL PAGE IS
OF POOR QUALITY

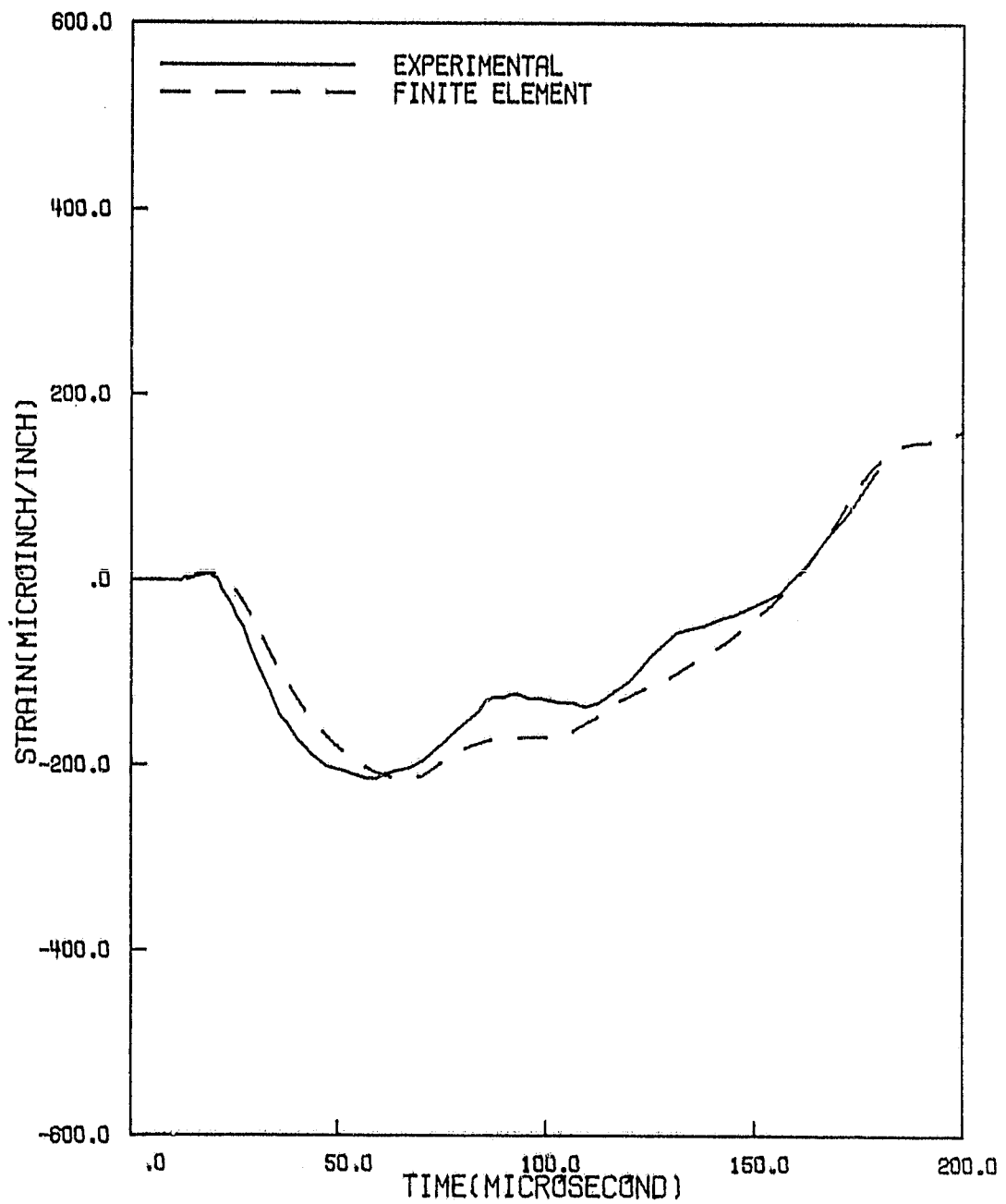


Figure 4.13 Strain response history at gage No.2

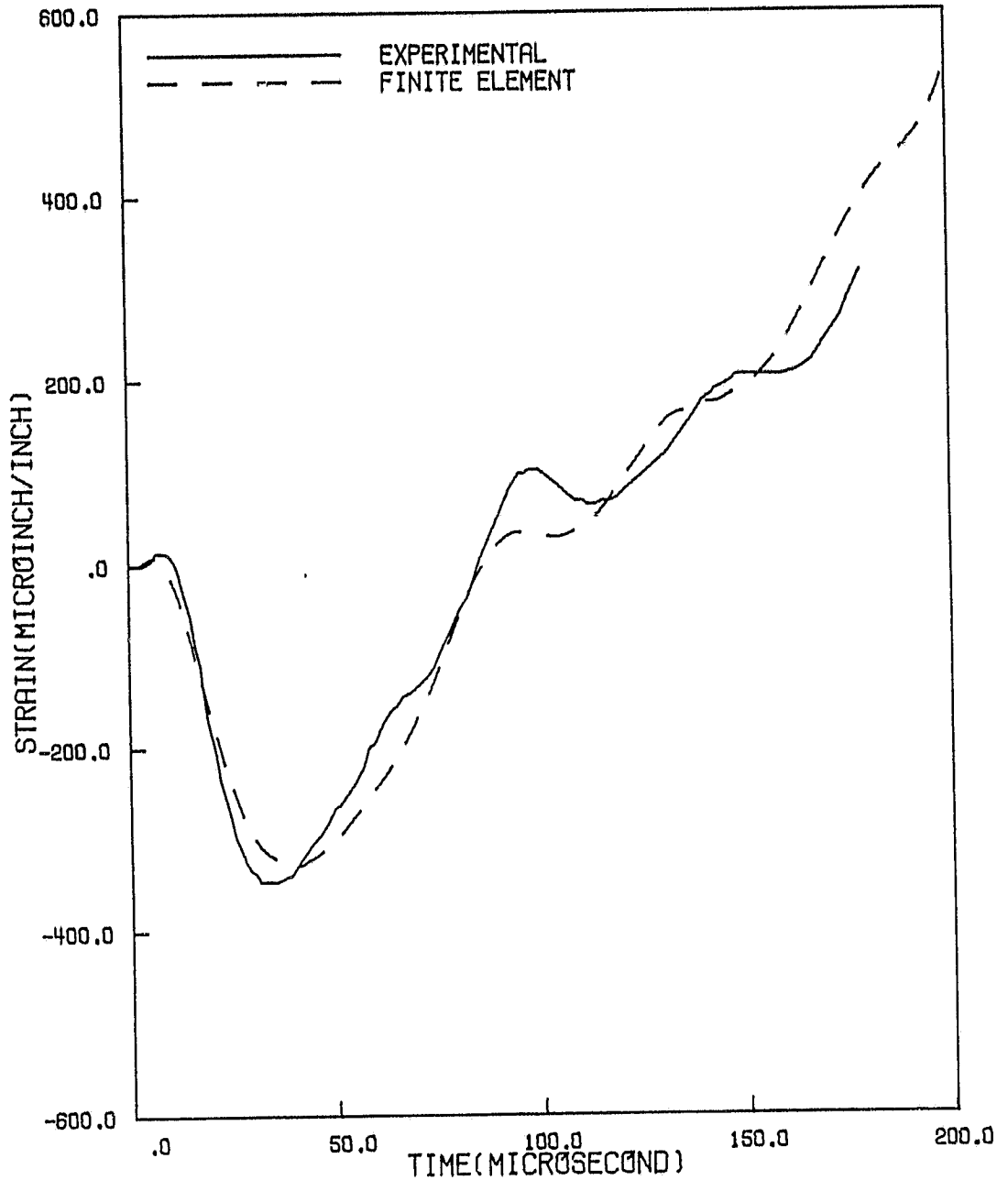


Figure 4.14 Strain response history at gage No.3

ORIGINAL PAGE IS
OF POOR QUALITY

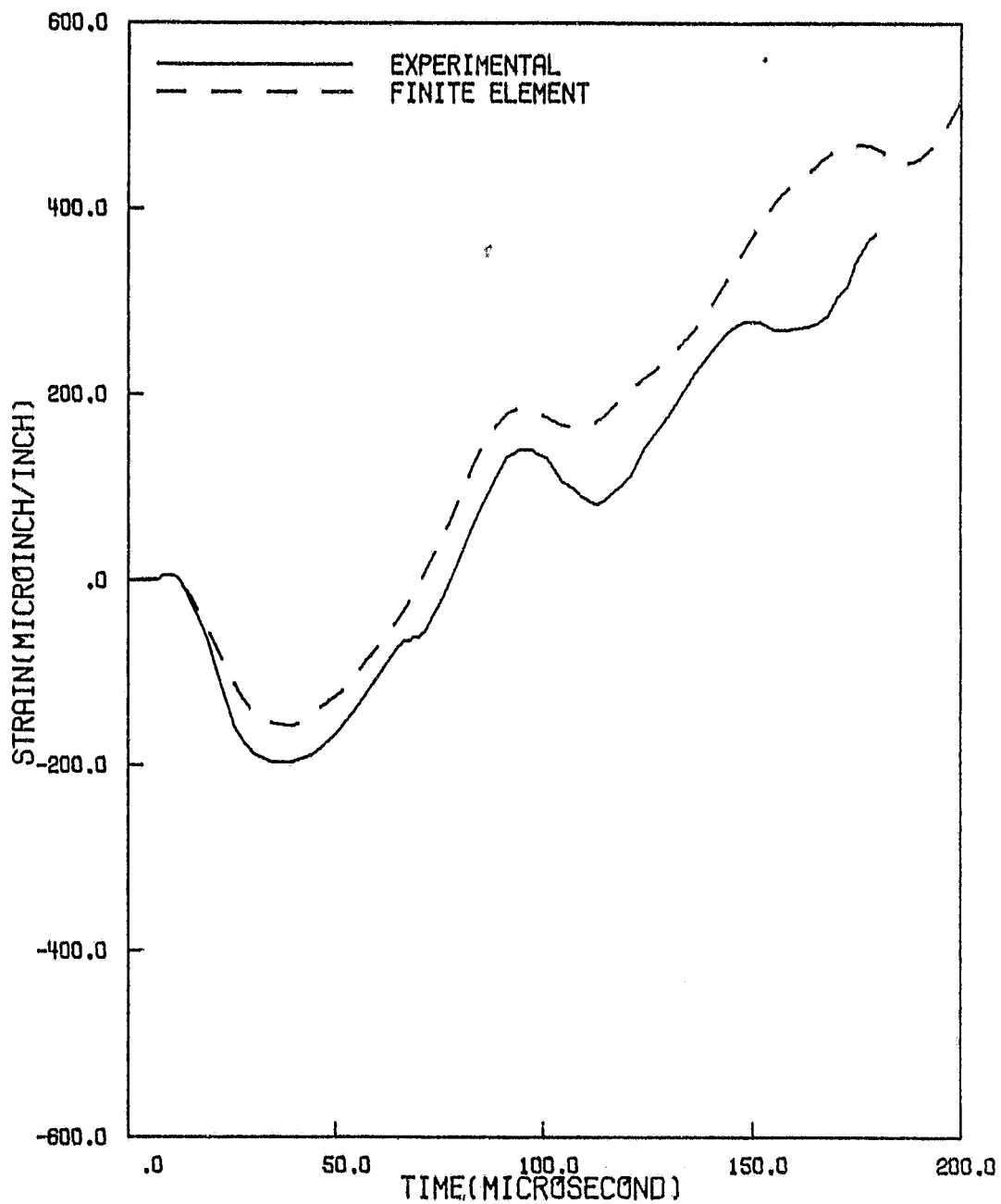


Figure 4.15 Strain response history at gage No.4

ORIGINAL PAGE IS
OF POOR QUALITY

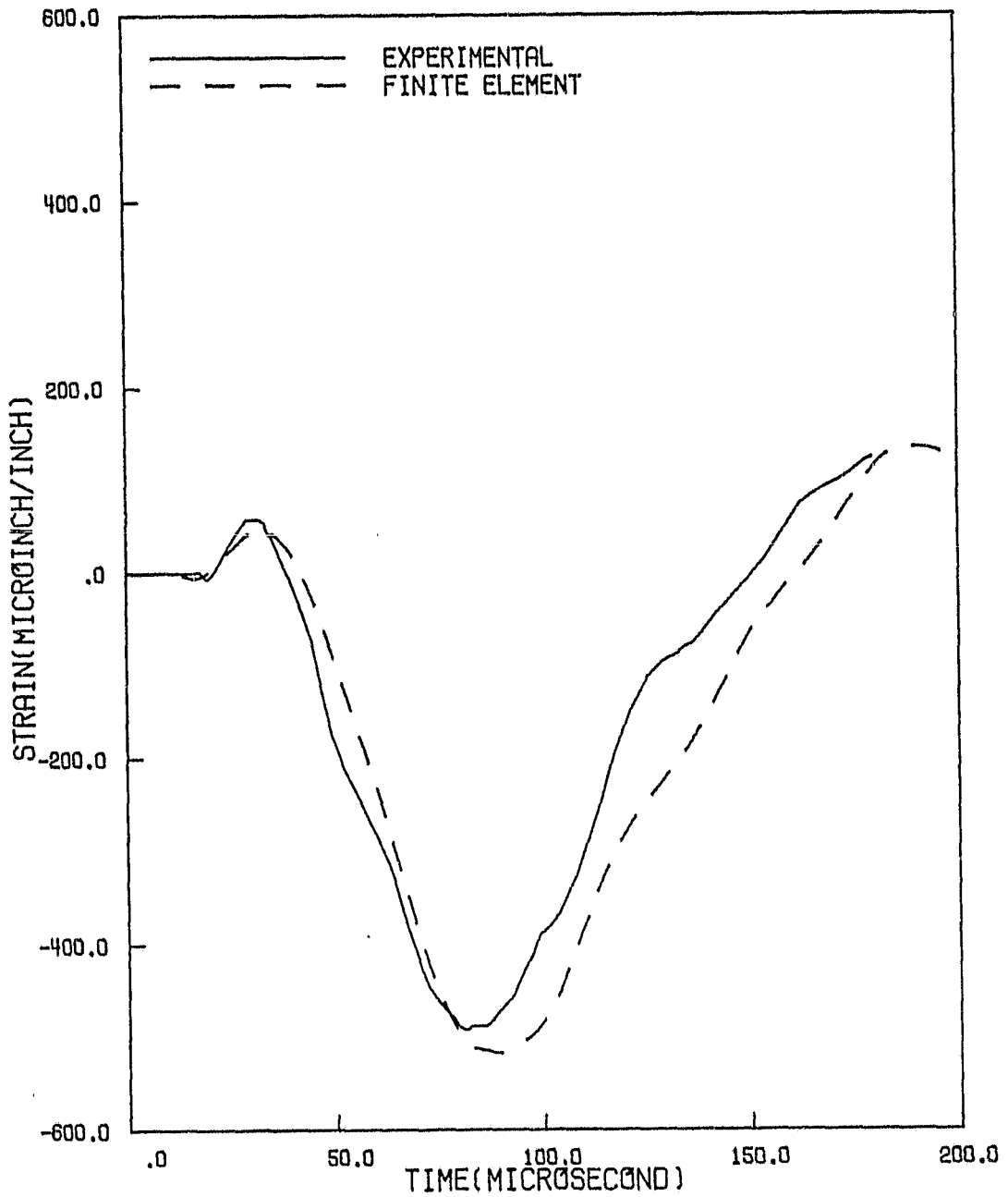


Figure 4.16 Strain response history at gage No.5

ORIGINAL PAGE IS
OF POOR QUALITY

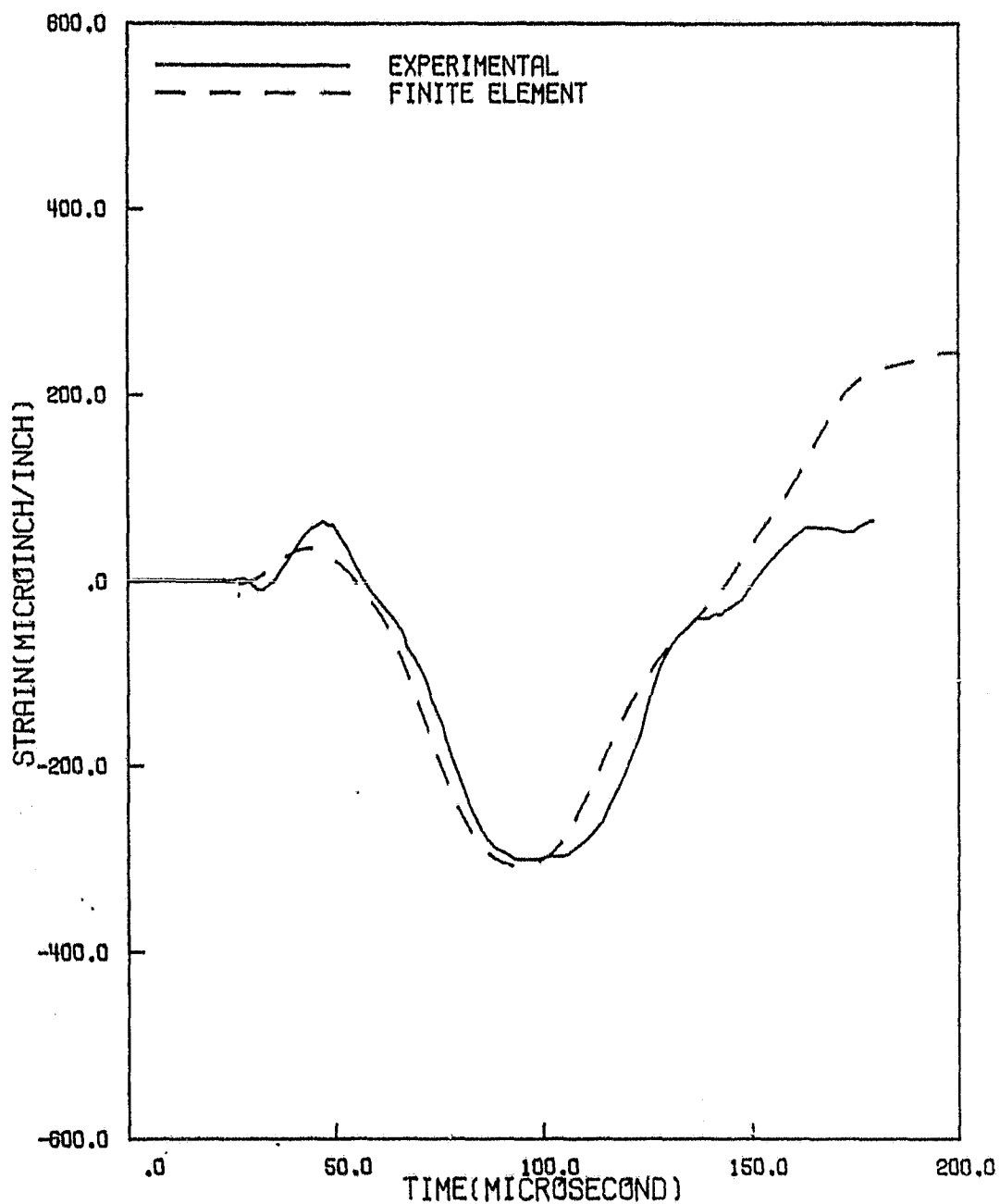


Figure 4.17 Strain response history at gage No.6

ORIGINAL PAGE IS
OF POOR QUALITY

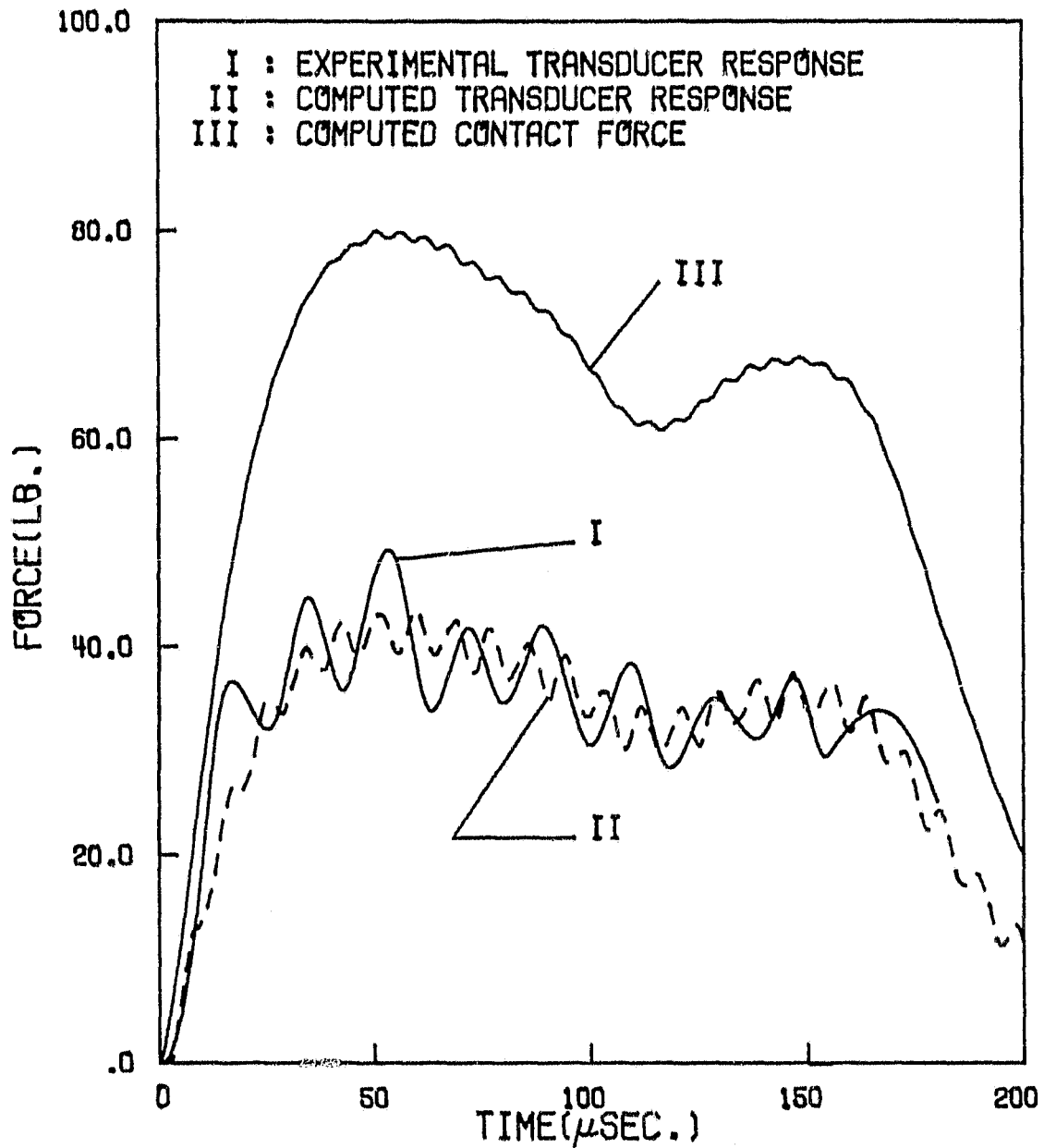


Figure 4.18 Transducer response and contact force histories from experimental and finite element results

least 20 microseconds. This might explain the lower frequency of ringing in the output voltage from the transducer.

The total duration of contact for this impact test is about 800 microseconds, and multiple contact is also observed from the test data. Figure 4.19 shows the experimental transducer responses and the computed transducer responses up to 800 microseconds. Although these two results do not match very well after the end of the first contact, it is evident that the finite element analysis does predict the multiple contact phenomenon, and the calculated total duration of contact is also approximately the same as the test result.

Figure 4.20 presents a number of deformed configurations of the laminated plate after impact. It is seen that at the point of impact, there is a strong discontinuity in slope of the transverse displacement indicating the presence of a significant transverse shear deformation.

**ORIGINAL PAGE IS
OF POOR QUALITY**

ORIGINAL PAGE IS
OF POOR QUALITY

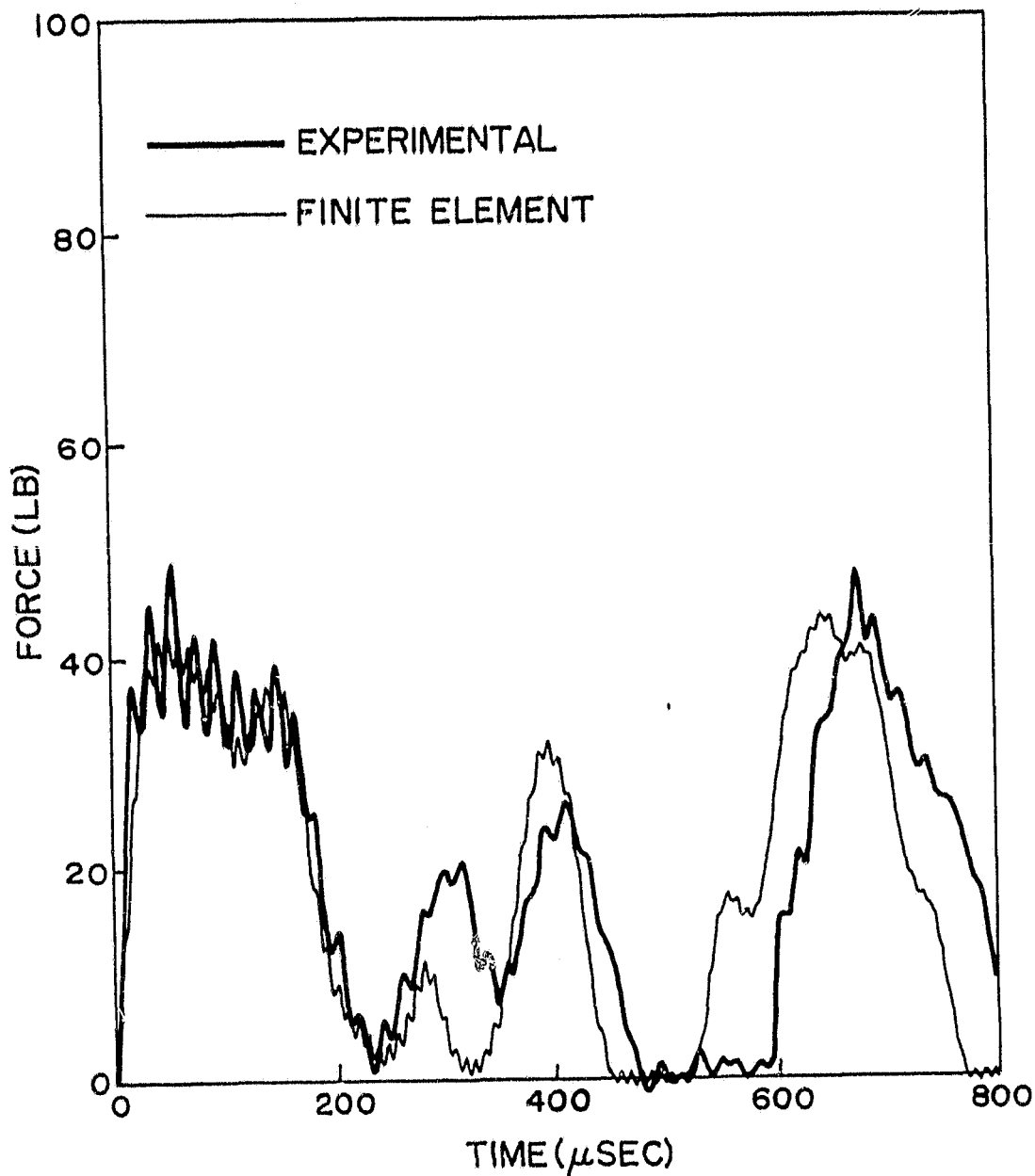


Figure 4.19 Transducer response histories from experimental and finite element results up to 800 microseconds

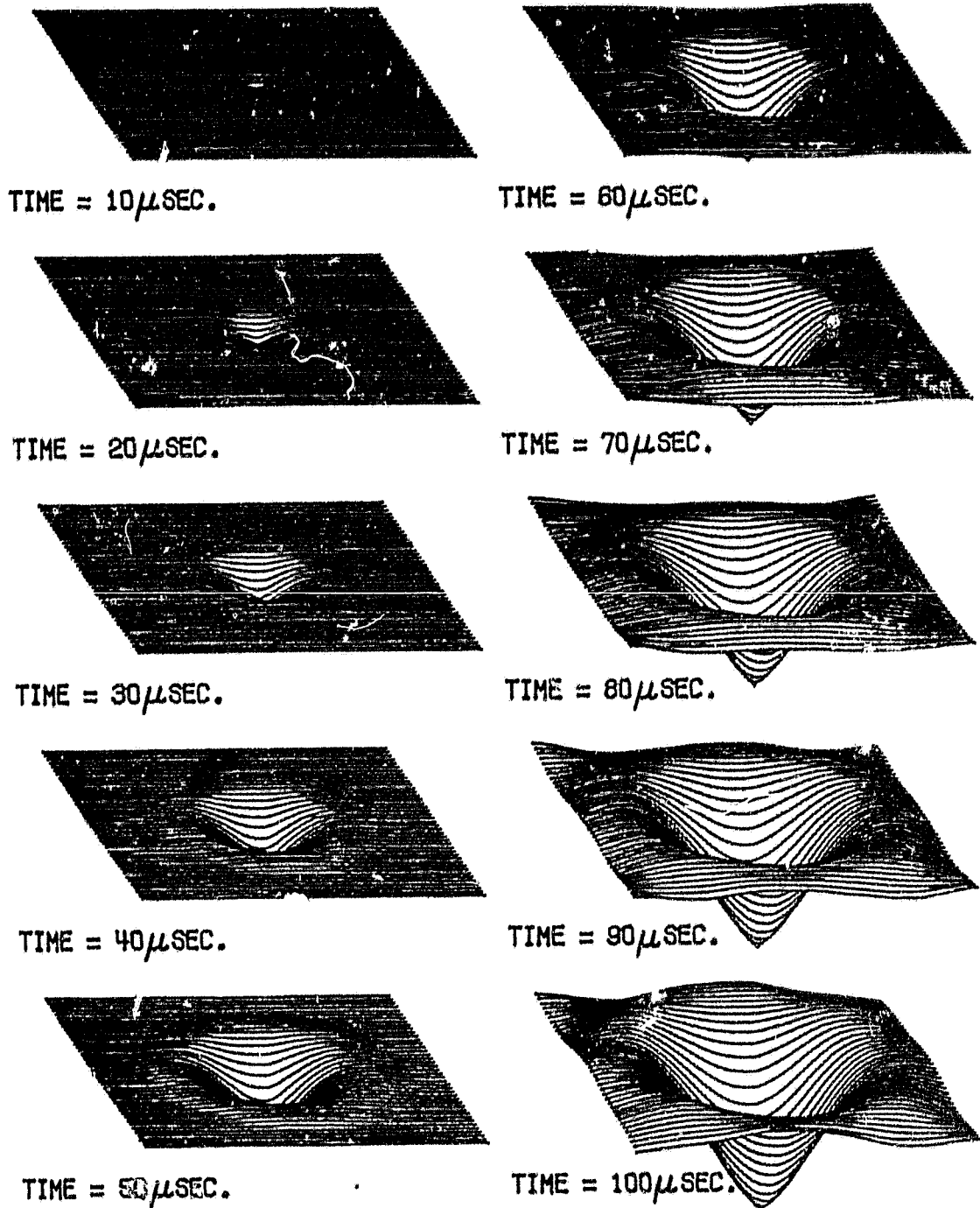


Figure 4.20 Deformed configurations of laminated plate after impact

ORIGINAL PAGE IS
OF POOR QUALITY

CHAPTER 5
SUMMARY AND CONCLUSION

The laminate theory developed by Whitney and Pagano was employed for studies of harmonic wave and propagation of wave front in a $[0^\circ/45^\circ/0^\circ/-45^\circ/0^\circ]_{2S}$ graphite/epoxy laminate. The dispersion properties of flexural waves were investigated. The wave front surface was constructed using ray theory. It was shown that due to the anisotropic properties of composite laminate, the transient wave would propagate with different velocities in different directions. The growth and decay of the wave front strength were also discussed.

The contact laws between 0.5 inch and 0.75 inch spherical steel indenters and the graphite/epoxy laminate were determined experimentally by means of a statical indentation test. Loading, unloading and reloading curves were fitted into power equations. Linear relation was found between the permanent indentation and the maximum indentation at unloading, which is seen to be independent of the size of indenters. This relation was then used to determine the coefficient of the unloading law. It was demonstrated that there was no need to perform reloading experiments once the loading and unloading laws were established. Test results

showed loading and reloading curves followed the power laws with power indices of 1.5 very well, while the power indices for unloading curves varied from 1.5 to 2.5.

The statically determined contact laws were incorporated into an existing 9-node isoparametric plate finite element program to study the dynamic response of a graphite/epoxy laminated plate subjected to impact of a hard object. An impact experiment was conducted to verify the validity of statical contact laws in the dynamical impact analysis. It was shown that the strain responses predicted using the finite element method agreed with the test results very well. The contact force history of the impact test was measured by an impact-force transducer, which was also seen to match the finite element result in magnitude as well as contact duration.

The indentation tests have been used ever since the beginning of the century to determine the static and dynamic hardnesses of metals in terms of the applied loading, the size of the indenter, and the chordal diameter of the permanent indentation [33]. If similar systematic indentation tests are performed on the laminated composite materials, then the relations between contact coefficients and the sizes of the indenters could be determined more rigorously, and the usefulness of the contact laws could be further extended.

**ORIGINAL PAGE IS
OF POOR QUALITY**

As the verification of the contact laws has been limited to low velocity impacts in this study, their accuracy under high velocity impact conditions is not clear. Besides the contact behavior which may be significantly different from the static one, the damage induced by waves could be quite extensive which needs to be included in the analysis. While the present study tried to establish experimentally contact laws which can be used in the analysis of low velocity impact, the damage of laminate due to impact loading has not been discussed. It is apparent that more work needs to be done so that the failure mechanism in laminated composites due to impact can be better understood. Stress waves propagating in thickness direction, which may be responsible for the delamination of laminates, is one of the important subjects that should be investigated. Strength and fatigue life degradations of laminates after impact, which have been examined briefly by Wang [15], also need more extensive study.

ORIGINAL PAGE IS
OF POOR QUALITY

LIST OF REFERENCES

- [1] Moon, F.C., "A Critical Survey of Wave Propagation and Impact in Composite Material", NASA CR-121226, 1973.
- [2] Sun, C.T., "Propagation of Shock Waves in Anisotropic Composite Plates", Journal of Composite Materials, Vol.7, 1973, pp.366-382.
- [3] Moon, F.C., "Wave Surfaces Due to Impact on Anisotropic Plates", Journal of Composite Materials, Vol.6, 1972, pp.62-79.
- [4] Chow, T.S., "On the Propagation of Flexural Waves in an Orthotropic Laminated Plate and Its Response to an Impulsive Load", Journal of Composite Materials, Vol.5, 1971, pp.306-319.
- [5] Greszczuk, L.B., "Response of Isotropic and Composite to Particle Impact", Foreign Object Impact Damage to Composite, ASTM STP 568, American Society for Testing and Materials, 1975, pp.183-211.
- [6] Sun, C.T. and Huang, S.N., "Transverse Impact Problems by Higher Order Beam Finite Element", Computers & Structures, Vol.5, 1975, pp.297-303.
- [7] Kim, B.S. and Moon, F.C., "Impact Induced Stress Waves in an Anisotropic Plate", AIAA Journal, Vol.17, No.10, 1979, pp.1126-1133.
- [8] Daniel, I.M., Liber, T. and LaBedz, R.H., "Wave Propagation in Transversely Impacted Composite Laminates", Experimental Mechanics, January 1979, pp.9-16.
- [9] Dally, J.W., Link, J.A. and Prabhakaran, R., "A Photoelastic Study of Stress Waves in Fiber Reinforced Composites", Developments in Mechanics, Vol.6, Proceedings of the 12th Midwestern Mechanics Conference, 1971, pp.937-949.

- [10] Takeda, N., Sierakowski, R.L. and Malvern, L.E., "Wave Propagation Experiments On Ballistically Impacted Composite Laminates", Journal of Composite Materials, Vol.15, 1981, pp.157-174.
- [11] Hertz, H., "Uber die Berührung fester elastischer Körper", Journal Reine Angew Math, (Crelle), Vol.92, 1881, p.155.
- [12] Goldsmith, W., Impact, Edward Arnold, London, 1960.
- [13] Sun, C.T., "An Analytical Method for Evaluation of Impact Damage Energy of Laminated Composites", ASTM STP 617, American Society for Testing and Materials, 1977, pp.427-440.
- [14] Yang, S.H. and Sun, C.T., "Indentation Law for Composite Laminates", NASA CR-165460, July 1981, also to appear in ASTM STP series, American Society for Testing and Materials.
- [15] Wang, T., "Dynamic Response and Damage of Hard Object Impact on a Graphite/Epoxy Laminate", Ph.D. Dissertation, Purdue University, 1982.
- [16] Yang, P.C., Norris, C.H. and Stavsky, Y., "Elastic Wave Propagation in Heterogeneous Plates", International Journal of Solids and Structures, Vol.2, 1966, pp.665-683.
- [17] Mindlin, R.D., "Influence of Rotatory Inertia and Shear on Flexural Motions of Isotropic, Elastic Plates", Journal of Applied Mechanics, Vol.18, 1951, pp.31-38.
- [18] Whitney, J.M. and Pagano, N.J., "Shear Deformation in Heterogeneous Anisotropic Plates", Journal of Applied Mechanics, Vol.37, 1970, pp.1031-1036.
- [19] Sun, C.T. and Whitney, J.M., "On Theories for the Dynamic Response of Laminated Plates", Proceedings AIAA/ASME/SAE 13th Structures, Structural Dynamics, and Materials Conference, 1972, AIAA Paper No.72-398.
- [20] Kraut, E., "Advances in the Theory of Anisotropic Elastic Wave Propagation", Review of Geophysics, Vol.1, No.3, 1963, pp.401-448.
- [21] Keller, H.B., "Propagation of Stress Discontinuities in Inhomogeneous Elastic Media", SIAM Review, Vol.6, No.4, 1964, pp.356-382.

- [22] Vlaar, N.J., "Ray Theory for an Anisotropic Inhomogeneous Elastic Medium", Bulletin of the Seismological Society of America, Vol.58, No.6, 1968, pp.2053-2072.
- [23] Thomas, T.Y., Plastic Flow and Fracture in Solids, Academic Press, 1961, p.10.
- [24] Courant, R. and Hilbert, D., Methods of Mathematical Physics, Vol.II, Interscience Publishers, 1962.
- [25] Foreign Object Impact Damage to Composite, ASTM STP 568, American Society for Testing and Materials, 1973.
- [26] Willis, J.R., "Hertzian Contact of Anisotropic Bodies", Journal of Mechanics and Physics of Solids, Vol.14, 1966, pp.163-176.
- [27] Sun, C.T. and Chattopadhyay, S., "Dynamic Response of Anisotropic Laminated Plates Under Initial Stress to Impact of a Mass", Journal of Applied Mechanics, Vol.42, 1975, pp.693-698.
- [28] Crook, A.W., "A Study of Some Impacts Between Metal Bodies by a Piezoelectric Method", Proceedings of Royal Society, London, A 212, 1952, p.377.
- [29] Sun, C.T., Sankar, B.V. and Tan, T.M., "Dynamic Response of SMC to Impact of a Steel Ball", Advances in Aerospace Structures and Materials, The Winter Annual Meeting of the American Society of Mechanical Engineers, Washington, D.C., 1981.
- [30] Operating Instructions, Model No. 200A05 Transducer, PCB Piezotronics, INC.
- [31] Yang, S.H., "Static and Dynamic Contact Behavior of Composite Laminates", Ph.D. Dissertation, Purdue University, 1981.
- [32] Yang, T.Y. and Sun, C.T., "Finite Elements for the Vibration of Framed Shear Walls", Journal of Sound and Vibration, Vol.27, No.3, 1973, pp.297-311.
- [33] Tabor, D., The Hardness of Metal, Oxford University Press, 1951.
- [34] Zienkiewicz, O.C., The Finite Element Method, 3rd edition, McGraw-Hill, 1977, Chapter 24, pp.677-757.

ORIGINAL PAGE IS
OF POOR QUALITY

APPENDIX
COMPUTER PROGRAM AND USER INSTRUCTIONS

The computer program used in this research was written following the program by Professor R. L. Taylor [34] with some necessary modification in order to solve the impact problems of laminated plates. A brief instruction of the input data for solving the impact problem specified in Chapter 4 of this report is given in this appendix. The detailed descriptions of data input as well as the macro instructions for solving various types of problems can be found in [34]. The listing of input is shown at the end of this appendix, followed by the listing of program.

I. Title and control information:

1. Title card-Format(20A4)

Columns Description

1-4 Must contain FECM

5-80 Alphanumeric information to be printed with output as page header.

2. Control information card-Format(6I5)

Columns Description

1-5 Number of nodes (NUMNP)

6-10 Number of elements (NUMEL)

ORIGINAL PAGE IS
OF POOR QUALITY

- 11-15 Number of layers (LAYER)
- 16-20 Spatial dimension (NDM)
- 21-25 Number of unknowns per node (NDF)
- 26-30 Number of nodes per element (NEN)

II. Mesh and Initial Information:

The input of each segment in this part of data is controlled by the alphanumeric value of macros, which must be followed immediately by the appropriate data. Except for the END card which must be the last card of this part, the data segments can be in any order. Each segment is terminated with blank card(s). The meaning of each macro is given by the following:

<u>Macro</u>	<u>Data to be Input</u>
COOR	Coordinate data
ELEM	Element data
BOUN	Boundary condition data
MATE	Material data
ROD	Initial condition of the projectile
EXPE	Experimental indentation laws data
END	Must be the last card of this part, terminates mesh and initial information input.

1. Coordinate data-Format(2I5,2F10.0)

<u>Columns</u>	<u>Description</u>
1-5	Nodal number
6-10	Generation increment

ORIGINAL PAGE IS
OF POOR QUALITY

11-20 X-coordinate
21-30 Y-coordinate

2. Element data-Format(11I5)

Columns Description

1-5 Element number
6-10 Node 1 number
11-15 Node 2 number
etc. .
46-50 Node 9 number
51-55 Generation increment

3. Boundary condition data-Format(7I5)

Columns Description

1-5 Node number
6-10 Generation increment
11-15 DOF 1 boundary code
16-20 DOF 2 boundary code
21-25 DOF 3 boundary code
26-30 DOF 4 boundary code
31-35 DOF 5 boundary code

4. Initial condition of the projectile-Format(2I5,F10.0)

Columns Description

1-5 The node at which the projectile hits
6-10 DOF corresponding to the direction of impact
11-20 Initial impact velocity

5. Experimental indentation laws data-Format(4F10.0)

Columns Description

1-10	Contact coefficient k
11-20	Critical indentation α_p
21-30	Constant s_p of Equation 3-9
31-40	Power index q of the unloading law

6. Material data

Card 1-format(3I5,F10.0)

Columns Description

1-5	Order of Gauss quadrature for the numerical integration of the bending energy
6-10	Order of Gauss quadrature for the numerical integration of the transverse shear energy
11-15	Order of Gauss quadrature for strain outputs at Gauss points if >0 at nodal points if <0
16-25	Total thickness of the laminate

Card 2-Format(7F10.0)

Columns Description

1-10	Mass density
11-20	Poisson's ratio ν_{12}
21-30	Longitudinal Young's modulus E_1
31-40	Transverse Young's modulus E_2
41-50	Shear modulus G_{12}
11-20	Shear modulus G_{13}
11-20	Shear modulus G_{23}

Card 3,4,... Format(I5,F5.0,F10.0)

Columns Description

1-5 Layer number

6-10 Fiber angle

11-20 Thickness of the layer

ORIGINAL PAGE IS
OF POOR QUALITY

III. Macro Instructions:

The first instruction must be a card with MACR in columns 1 to 4. The macro instructions needed to solve the problem specified in Chapter 4 of this report are shown in the listing of input. Cards must be input in the precise order. The following is the explanation of each macro:

<u>Columns</u> <u>1-4</u>	<u>Columns</u> <u>5-10</u>	<u>Columns</u> <u>11-15</u>	<u>Description</u>
LMAS			Lumped mass formulation
DT		V	Set time increment to value V
LOOP		N	Execute N times the instructions between this macro and macro NEXT
TIME			Advance time by DT value
RODP		N	Integration of the equations of motion using the finite difference method. Contact force, indentation and element strain will be stored every N steps in loop
DISP		N	Nodal displacements will be stored every N steps in loop
NEXT			End of loop instructions

END

End of macro program Instructions

IV. Termination of program execution

A card with STOP in columns 1 to 4 must be supplied at the end of the input data in order to properly terminate the execution.

The values of contact force, indentation, element strain, nodal displacement and the response of the projectile at each requested output time step are stored in program files which can be saved (say, copy to a magnetic tape) at the end of execution. Three program files, i.e.; tape3, tape8 and tape9 are used for data saving:

Tape3: Nodal displacement - Format(6E12.4)

Nodal displacements, from node 1 to node NUMNP, are saved on tape3 at each requested output time step according to the format.

Tape8: Element strain - Format(2I6,5E12.4)

Element strains, from element 1 to element NUMEL, and then from node 1 to node NEN of each element, are saved on on tape8 at each requested output time step.

Columns Data saved

1-6	Element number
7-12	Node number of element
13-24	Bending strain κ_x
25-36	Bending strain κ_y

- 37-48 Bending strain κ_{xy}
- 49-60 Transverse shearing strain γ_{yz}
- 49-60 Transverse shearing strain γ_{xz}

Tape9: Contact force, Indentation and the response of the projectile - Format(6E12.4)

The following information is saved on tape9 at each requested output time step:

Columns Data saved

- 1-12 Contact force
- 13-24 Indentation
- 25-36 'Transducer' response (see Chapter 4)
- 37-48 Displacement of the projectile at the impacted end
- 37-48 Velocity of the projectile at the impacted end
- 37-48 Acceleration of the projectile at the impacted end

ORIGINAL PAGE IS
OF POOR QUALITY

LISTING OF INPUT DATA

FECM **LOW VELOCITY IMPACT OF LAMINATED PLATE**

609	140	20	2	5	9
COORD					
1	1		0.0		0.0000
7	1		1.5		0.0000
23	1		4.5		0.0000
29	0		6.0		0.0000
30	1		0.0		0.2500
36	1		1.5		0.2500
52	1		4.5		0.2500
58	0		6.0		0.2500
59	1		0.0		0.5000
65	1		1.5		0.5000
81	1		4.5		0.5000
87	0		6.0		0.5000
88	1		0.0		0.6875
94	1		1.5		0.6875
110	1		4.5		0.6875
116	0		6.0		0.6875
117	1		0.0		0.8750
123	1		1.5		0.8750
139	1		4.5		0.8750
145	0		6.0		0.8750
146	1		0.0		1.0625
152	1		1.5		1.0625
168	1		4.5		1.0625
174	0		6.0		1.0625
175	1		0.0		1.2500
181	1		1.5		1.2500
197	1		4.5		1.2500
203	0		6.0		1.2500
204	1		0.0		1.4375
210	1		1.5		1.4375
226	1		4.5		1.4375
232	0		6.0		1.4375
233	1		0.0		1.6250
239	1		1.5		1.6250
255	1		4.5		1.6250
261	0		6.0		1.6250
262	1		0.0		1.8125
268	1		1.5		1.8125
284	1		4.5		1.8125
290	0		6.0		1.8125
291	1		0.0		2.0000
297	1		1.5		2.0000
313	1		4.5		2.0000
319	0		6.0		2.0000
320	1		0.0		2.1875
326	1		1.5		2.1875
342	1		4.5		2.1875
348	0		6.0		2.1875
349	1		0.0		2.3750
355	1		1.5		2.3750
371	1		4.5		2.3750
377	0		6.0		2.3750
378	1		0.0		2.5625
384	1		1.5		2.5625
400	1		4.5		2.5625
406	0		6.0		2.5625
407	1		0.0		2.7500
413	1		1.5		2.7500
429	1		4.5		2.7500
435	0		6.0		2.7500
436	1		0.0		2.9375
442	1		1.5		2.9375

458	1	4.5	2.9375
464	0	6.0	2.9375
465	1	0.0	3.1250
471	1	1.5	3.1250
487	1	4.5	3.1250
493	0	6.0	3.1250
494	1	0.0	3.3125
500	1	1.5	3.3125
516	1	4.5	3.3125
522	0	6.0	3.3125
523	1	0.0	3.5000
529	1	1.5	3.5000
545	1	4.5	3.5000
551	0	6.0	3.5000
552	1	0.0	3.7500
558	1	1.5	3.7500
574	1	4.5	3.7500
580	0	6.0	3.7500
581	1	0.0	4.0000
587	1	1.5	4.0000
603	1	4.5	4.0000
609	0	6.0	4.0000

ELEM

1	1	3	61	59	2	32	60	30	31	2
15	59	61	119	117	60	90	118	88	89	2
29	117	119	177	175	118	148	176	146	147	2
43	175	177	235	233	176	206	234	204	205	2
57	233	235	293	291	234	264	292	262	263	2
71	291	293	351	349	292	322	350	320	321	2
85	349	351	409	407	350	380	408	378	379	2
99	407	409	467	465	408	438	466	436	437	2
113	465	467	525	523	466	496	524	494	495	2
127	523	525	583	581	524	554	582	552	553	2

BOUN

1	1	-1	-1	0	0	0
609	0	1	1	0	0	0

ROD

305	3	115.0
-----	---	-------

EXPE

1912000.	0.0006564	0.094	2.0
----------	-----------	-------	-----

MATE

3	3	-3	.106					
0.000148		0.3	17500000.	1150000.	800000.	800000.	800000.	
1	0.	0.0053						
2	45.	0.0053						
3	0.	0.0053						
4	-45.	0.0053						
5	0.	0.0053						
6	0.	0.0053						
7	45.	0.0053						
8	0.	0.0053						
9	-45.	0.0053						
10	0.	0.0053						
11	0.	0.0053						
12	-45.	0.0053						
13	0.	0.0053						
14	45.	0.0053						
15	0.	0.0053						
16	0.	0.0053						
17	-45.	0.0053						
18	0.	0.0053						
19	45.	0.0053						
20	0.	0.0053						

END

MACR
LMAS
DT
LOOP
TIME
RODP
DISP
NEXT
END
STOP

.2E-6
10
5
5

ORIGINAL PAGE IS
OF POOR QUALITY

ORIGINAL PAGE IS
OF POOR QUALITY

LISTING OF PROGRAM

```

PROGRAM MAIN(INPUT, OUTPUT, TAPES=INPUT, TAPE6=OUTPUT, TAPE2, TAPE3,
1          TAPE8, TAPE9)
C**** MAIN PROGRAM
LOGICAL PCOMP
COMMON /PSIZE/ MAX
COMMON /CTDATA/ O, HEAD(20), NUMNP, NUMEL, LAYER, NEG, IPR
COMMON /LABELS/ PDIS(6), A(6), BC(2), DI(6), CD(3), FD(3)
COMMON /LODATA/ NDF, NDM, NEN, NST, NKM
COMMON /PARATS/ NPAR(14), NEND
DIMENSION TITL(20), WD(3)
COMMON G(39000)
DIMENSION M(39000)
EQUIVALENCE (G(1), M(1))
MAX=39000
WD(1)=4HFECM
WD(2)=4HMOCR
WD(3)=4HSTOP
999 READ(5, 1000) TITL
IF(PCOMP(TITL(1), WD(1))) GO TO 100
IF(PCOMP(TITL(1), WD(2))) GO TO 200
IF(PCOMP(TITL(1), WD(3))) STOP
GO TO 999
100 DO 101 I=1, 20
101 HEAD(I)=TITL(I)
READ(5, 1001) NUMNP, NUMEL, LAYER, NDM, NDF, NEN
WRITE(6, 2000) HEAD, NUMNP, NUMEL, LAYER, NDM, NDF, NEN
PDIS(2)=A(NDM)
NST=NEN*NDF
DO 110 I=1, 14
110 NPAR(I)=1
NPAR(1)=1
NPAR(2)=NPAR(1)+3*NST*IPR
NPAR(3)=NPAR(2)+NDM*NEN*IPR
NPAR(4)=NPAR(3)+NST
NPAR(5)=NPAR(4)+NST*IPR
NPAR(6)=NPAR(5)+NEN*NUMEL
NPAR(7)=NPAR(6)+NDF*NUMNP
NPAR(8)=NPAR(7)+NDM*NUMNP*IPR
NPAR(9)=NPAR(8)+NDF*NUMNP*IPR
NPAR(10)=NPAR(9)+NDF*NUMNP
CALL SETMEM(NPAR(9))
CALL PZERO(G(1), NPAR(9))
CALL PMESH(M(NPAR(3)), G(NPAR(2)), M(NPAR(5)), M(NPAR(6)),
1 G(NPAR(7)), G(NPAR(8)), M(NPAR(9)), NDF, NDM, NEN, NKM)
NPAR(10)=NPAR(9)+NEG
NPAR(11)=NPAR(10)+NDF*NUMNP*IPR
NEND=NPAR(11)+NEG*IPR
NE=NEND
CALL SETMEM(NE)
CALL PZERO(G(NPAR(10)), NE-NPAR(10))
GO TO 999
200 CALL PMOCR(G(NPAR(1)), G(NPAR(2)), M(NPAR(3)), G(NPAR(4)),
1 M(NPAR(5)), M(NPAR(6)), G(NPAR(7)), G(NPAR(8)), M(NPAR(9)),
2 G(NPAR(10)), G(NPAR(11)), G(NE), NDF, NDM, NEN, NST)
CALL PZERO(G, MAX)
GO TO 999
1000 FORMAT(20A4)
1001 FORMAT(16I5)
2000 FORMAT(1H1, 20A4//
1 5X, #C O N T R O L   I N F O R M A T I O N S#//
2 10X, 35HNUMBER OF NODAL POINTS           =, I6/
3 10X, 35HNUMBER OF ELEMENTS               =, I6/
4 10X, 35HNUMBER OF MATERIAL LAYERS        =, I6/
5 10X, 35HDIMENSION OF COORDINATE SPACE    =, I6/
6 10X, 35HDEGREES OF FREEDOM FOR EACH NODE =, I6/
7 10X, 35HNODES PER ELEMENT (MAXIMUM)      =, I6/
END

```

C	BLOCK DATA	BLOC 1
C****	BLOCK DATA	BLOC 2
	COMMON /CTDATA/ O,HEAD(20),NUMNP,NUMEL,LAYER,NEG,IPR	BLOC 3
	COMMON /LABELS/ PDIS(6),A(6),BC(2),DI(6),CD(3),FD(3)	BLOC 4
	DATA O/1H1/,IPR/1/	BLOC 5
	DATA PDIS/4H(I10,2H, ,4HF13.,4H4, ,4HGE13,4H.4) /	BLOC 6
	DATA A/2H,1,2H,2,2H,3,2H,4,2H,5,2H,6/	BLOC 7
	DATA BC/4H B.C,2H. /	BLOC 8
	DATA DI/4H DIS,2HPL,4H VEL,2HOC,4H ACC,2HEL/	BLOC 9
	DATA CD/4H COO,4HRDIN,4HATES/	BLOC 10
	DATA FD/4H FOR,4HCE/D,4HISPL/	BLOC 11
	END	BLOC 12
C	SUBROUTINE PMACR(UL,XL,LD,P,IX,ID,X,F,JDIAG,DR,B,CT,NDF,NDM, ^ NEN,NST)	PMAC 1
C****	MACRO INSTRUCTION ROUTINE	PMAC 2
	LOGICAL PCOMP	PMAC 3
	COMMON G(1)	PMAC 4
	DIMENSION M(1)	PMAC 5
	EQUIVALENCE (G(1),M(1))	PMAC 6
	COMMON /CTDATA/ O,HEAD(20),NUMNP,NUMEL,LAYER,NEG,IPR	PMAC 7
	COMMON /PROLOD/ PROP	PMAC 8
	COMMON /TMDATA/ TIME,DT,DDT,FORCE,ALPHA	PMAC 9
	COMMON /ISWIDX/ ISW	PMAC 10
	COMMON /PARATS/ NPAR(14),NEND	PMAC 11
	COMMON /RODATA/ UR,IQ,NDS	PMAC 12
	DIMENSION UL(1),XL(1),LD(1),P(1),IX(1),ID(1),X(1),F(1), ^ JDIAG(1),DR(1),B(1)	PMAC 13
	DIMENSION WD(9),CT(4,16),LVE(9)	PMAC 14
	DATA WD/4HLOOP,4HNEXT,4HDT ,4HPROP,4HLMAS,4HRODP, 1 4HSTRE,4HDISP,4HCHEC/	PMAC 15
	DATA NWD/9/,ENDM/4HEND /	PMAC 16
C....	INITIALIZATION	PMAC 17
	DT = 0.0	PMAC 18
	PROP = 1.0	PMAC 19
	TIME = 0.0	PMAC 20
	NNEG = NDF*NUMNP	PMAC 21
	NPLD = 0	PMAC 22
	FORCE = 0.	PMAC 23
	ALPHA = 0.	PMAC 24
	WRITE(6,2001) O,HEAD	PMAC 25
	LL = 1	PMAC 26
	LMAX = 16	PMAC 27
	CALL SETMEM(NEND+LMAX*4*IPR)	PMAC 28
	CT(1,1) = WD(1)	PMAC 29
	CT(3,1) = 1.0	PMAC 30
100	LL = LL + 1	PMAC 31
	IF(LL.LT.LMAX) GO TO 110	PMAC 32
	LMAX = LMAX + 16	PMAC 33
	CALL SETMEM(NEND+LMAX*4*IPR)	PMAC 34
110	READ(5,1000) (CT(J,LL),J=1,4)	PMAC 35
	WRITE(6,2000) (CT(J,LL),J=1,4)	PMAC 36
	IF(.NOT.PCOMP(CT(1,LL),ENDM)) GO TO 100	PMAC 37
	CT(1,LL) = WD(2)	PMAC 38
	NEND = NEND +LMAX*4*IPR	PMAC 39
	LX = LL - 1	PMAC 40
	DO 230 L=1,LX	PMAC 41
	IF(.NOT.PCOMP(CT(1,L),WD(1))) GO TO 230	PMAC 42
	J = 1	PMAC 43
	K = L + 1	PMAC 44
	DO 210 I=K,LL	PMAC 45
	IF(PCOMP(CT(1,I),WD(1))) J = J + 1	PMAC 46
	IF(J .GT. 9) GO TO 401	PMAC 47
	IF(PCOMP(CT(1,I),WD(2))) J = J - 1	PMAC 48
210	IF(J.EQ.0) GO TO 220	PMAC 49
	GO TO 400	PMAC 50
220	CT(4,I) = L	PMAC 51
	CT(4,L) = I	PMAC 52
230	CONTINUE	PMAC 53
		PMAC 54
		PMAC 55
		PMAC 56

J = 0	PMAC 57
DO 240 L=1,LL	PMAC 58
IF(PCOMP(CT(1,L),WD(1))) J = J + 1	PMAC 59
240 IF(PCOMP(CT(1,L),WD(2))) J = J - 1	PMAC 60
IF(J.NE.0) GO TO 400	PMAC 61
LU = 0	PMAC 62
L = 1	PMAC 63
299 DO 300 J=1,NWD	PMAC 64
300 IF(PCOMP(CT(1,L),WD(J))) GO TO 310	PMAC 65
GO TO 330	PMAC 66
310 I = L - 1	PMAC 67
GO TO (1,2,3,4,5,6,7,8,9),J	PMAC 68
C.... SET LOOP START INDICATORS	PMAC 69
1 LU = LU + 1	PMAC 70
LX = CT(4,L)	PMAC 71
LVE(LU) = LX	PMAC 72
CT(3,LX) = 1.	PMAC 73
GO TO 330	PMAC 74
C.... LOOP TERMINATOR CONTROL	PMAC 75
2 N = CT(4,L)	PMAC 76
CT(3,L) = CT(3,L) + 1.0	PMAC 77
IF(CT(3,L).GT.CT(3,N)) LU = LU - 1	PMAC 78
IF(CT(3,L).LE.CT(3,N)) L = N	PMAC 79
GO TO 330	PMAC 80
C.... SET TIME INCREMENT	PMAC 81
3 DT = CT(3,L)	PMAC 82
DDT = DT*DT	PMAC 83
GO TO 330	PMAC 84
C.... INPUT PROPORTIONAL LOAD TABLE	PMAC 85
4 NPLD = CT(3,L)	PMAC 86
PROP = PROPLD(0.,NPLD)	PMAC 87
GO TO 330	PMAC 88
C.... FORM LUMPED MASS MATRIX	PMAC 89
5 ISN=3	PMAC 90
CALL KMLIB	PMAC 91
GO TO 330	PMAC 92
C.... IMPACT	PMAC 93
6 NDS=CT(3,L)	PMAC 94
IF(NDS.EQ.0) NDS=1	PMAC 95
CALL RODIPCT	PMAC 96
GO TO 330	PMAC 97
C.... PRINT STRESS/STRAIN VALUE	PMAC 98
7 ISN=4	PMAC 99
LX = LVE(LU)	PMAC100
IF(AMOD(CT(3,LX),AMAX1(CT(3,L),1.))) 330,71,330	PMAC101
71 CALL FSTREA(UL,XL,LD,P,IX,ID,X,F,JDIAG,DR,B,NDF,NDM,NEN,NST,NNEQ)	PMAC102
GO TO 330	PMAC103
C.... PRINT DISPLACEMENTS	PMAC104
8 LX = LVE(LU)	PMAC105
IF(AMOD(CT(3,LX),AMAX1(CT(3,L),1.))) 330,81,330	PMAC106
81 CALL FRDIS(UL,ID,X,B,F,DR,NDM,NDF)	PMAC107
GO TO 330	PMAC108
C.... CHECK	PMAC109
9 WRITE(6,5001) NEND,JDIAG(NEQ)	PMAC110
RETURN	PMAC111
330 L=L+1	PMAC112
IF(L.GT.LL) RETURN	PMAC113
GO TO 299	PMAC114
C.... PRINT ERROR FORMATS	PMAC115
400 WRITE(6,4000)	PMAC116
RETURN	PMAC117
401 WRITE(6,4001)	PMAC118
RETURN	PMAC119
C.... INPUT/OUTPUT FORMATS	PMAC120
1000 FORMAT(A4,1X,A4,1X,2F5.0)	PMAC121
2000 FORMAT(10X,A4,1X,A4,1X,2G15.5)	PMAC122
2001 FORMAT(A1,20A4//,5X,18HMACRO INSTRUCTIONS//5X,15HMACRO STATEMENT	PMAC123
^ ,5X,10HUVARIABLE 1,5X,10HUVARIABLE 2)	PMAC124
4000 FORMAT(5X,46H**PMACR ERROR 01** UNBALANCED LOOP/NEXT MACROS)	PMAC125
4001 FORMAT(5X,45H**PMACR ERROE 02** LOOPS NESTED DEEPER THAN 8)	PMAC126

5001	FORMAT(1H1,////5X,32HCHECK MESH DATA AND MEMORY SPACE//	PMAC127
	^ 10X,12H NEND =,I10//10X,12HJDIAG(NEQ) =,I10)	PMAC128
	END	PMAC129
C		
	SUBROUTINE PZERO(U,NN)	PZER 1
C****	ZERO REAL ARRAY	PZER 2
	DIMENSION U(NN)	PZER 3
	DO 100 N=1,NN	PZER 4
100	U(N) = 0.0	PZER 5
	RETURN	PZER 6
	END	PZER 7
C		
	SUBROUTINE SETMEM(J)	SETM 1
C****	MONITOR AVAIABLE MEMORY IN BLANK COMMON	SETM 2
	COMMON /PRSIZE/ MAX	SETM 3
	K = J	SETM 4
	IF(K.LE.MAX) RETURN	SETM 5
	WRITE(6,1000) K,MAX	SETM 6
	STOP	SETM 7
1000	FORMAT(5X,49H**SETMEM ERROR 01** INSUFFICIENT STORAGE IN BLANK,	SETM 8
	^ 8H COMMON //17X,11HREQUIRED =,I8/17X,11HAVALIABLE =,I8)	SETM 9
	END	SETM 10
C		
	LOGICAL FUNCTION PCOMP(A,B)	PCOM 1
C****	LOGICAL COMPARISON	PCOM 2
	IF(A-B) 10,20,10	PCOM 3
10	PCOMP = .FALSE.	PCOM 4
	RETURN	PCOM 5
20	PCOMP = .TRUE.	PCOM 6
	RETURN	PCOM 7
	END	PCOM 8
C		
	SUBROUTINE ACTCOL(A,B,JDIAG,NEQ,AFAC,BACK,ISS)	ACTC 1
C****	ACTIVE COLUMN PROFILE SYMMETRIC EQUATION SOLVER	ACTC 2
	LOGICAL AFAC,BACK,FLAG	ACTC 3
	DIMENSION A(1),B(1),JDIAG(1)	ACTC 4
C....	FACTOR A TO UT*D*U, REDUCE B	ACTC 5
	FLAG=.FALSE.	ACTC 6
	JR = 0	ACTC 7
	DO 600 J=1,NEQ	ACTC 8
	JD = JDIAG(J)	ACTC 9
	JH = JD - JR	ACTC 10
	IS = J - JH + 2	ACTC 11
	IF(JH-2) 600,300,100	ACTC 12
100	IF(.NOT.AFAC) GO TO 500	ACTC 13
	IE = J - 1	ACTC 14
	K = JR + 2	ACTC 15
	ID = JDIAG(IS-1)	ACTC 16
C....	REDUCE ALL EQUATIONS EXCEPT DIAGONAL	ACTC 17
	DO 200 I=IS,IE	ACTC 18
	IR = ID	ACTC 19
	ID = JDIAG(I)	ACTC 20
	IH = MIN0(ID-IR-1,I-IS+1)	ACTC 21
	IF(IH.GT.0) A(K)=A(K)-DOT(A(K-IH),A(ID-IH),IH)	ACTC 22
200	K = K + 1	ACTC 23
C....	REDUCE DIGONAL TERM	ACTC 24
300	IF(.NOT.AFAC) GO TO 500	ACTC 25
	IR = JR + 1	ACTC 26
	IE = JD - 1	ACTC 27
	K = J - JD	ACTC 28
	DO 400 I=IR,IE	ACTC 29
	ID = JDIAG(K+I)	ACTC 30
	IF(A(ID)) 301,400,301	ACTC 31
301	D = A(I)	ACTC 32
	A(I) = A(I)/A(ID)	ACTC 33
	A(JD) = A(JD) - D*A(I)	ACTC 34
400	CONTINUE	ACTC 35
	IF(A(JD))450,450,500	ACTC 36
450	IF(ISS.NE.0) GO TO 500	ACTC 37
	IF(FLAG) GO TO 465	ACTC 38

	WRITE(6,460)	ACTC 39
460	FORMAT(/50H**ACTCOL ERROR 01** STIFFNESS MATRIX NOT POSITIVE ,	ACTC 40
	1 8HDEFINITE)	ACTC 41
	FLAG=.TRUE.	ACTC 42
465	WRITE(6,466) J,A(JD)	ACTC 43
466	FORMAT(32H NONPOSITIVE PIVOT FOR EQUATION ,I4,5X,7HPOUIT =,	ACTC 44
	^ E20.10)	ACTC 45
C....	REDUCE RHS	ACTC 46
500	IF(BACK) B(J) = B(J) - DOT(A(JR+1),B(IS-1),JH-1)	ACTC 47
600	JR = JD	ACTC 48
	IF(FLAG) STOP	ACTC 49
	IF(.NOT.BACK) RETURN	ACTC 50
C....	DIVIDED BY DIAGONAL PIVOTS	ACTC 51
	DO 700 I=1,NEQ	ACTC 52
	ID = JDIAG(I)	ACTC 53
	IF(A(ID)) 650,700,650	ACTC 54
650	B(I) = B(I)/A(ID)	ACTC 55
700	CONTINUE	ACTC 56
C....	BACK SUBSTITUTE	ACTC 57
	J = NEQ	ACTC 58
	JD = JDIAG(J)	ACTC 59
800	D = B(J)	ACTC 60
	J = J - 1	ACTC 61
	IF(J.LE.0) RETURN	ACTC 62
	JR = JDIAG(J)	ACTC 63
	IF(JD-JR.LE.1) GO TO 1000	ACTC 64
	IS = J - JD + JR + 2	ACTC 65
	K = JR - IS + 1	ACTC 66
	DO 900 I=IS,J	ACTC 67
900	B(I) = B(I) - A(I+K)*D	ACTC 68
1000	JD = JR	ACTC 69
	GO TO 800	ACTC 70
	END	ACTC 71
C		
	SUBROUTINE ADDSTF(A,S,P,JDIAG,LD,NST,NEL,FLG)	ADDS 1
C****	ASSEMBLE GLOBAL ARRAYS	ADDS 2
	LOGICAL FLG	ADDS 3
	DIMENSION A(1),S(NST,1),P(1),JDIAG(1),LD(1)	ADDS 4
	DO 200 J=1,NEL	ADDS 5
	K = LD(J)	ADDS 6
	IF(K.EQ.0) GO TO 200	ADDS 7
	IF(FLG) GO TO 50	ADDS 8
	A(K)=A(K)+P(J)	ADDS 9
	GO TO 200	ADDS 10
50	L = JDIAG(K) - K	ADDS 11
	DO 100 I=1,NEL	ADDS 12
	M = LD(I)	ADDS 13
	IF(M.GT.K .OR. M.EQ.0) GO TO 100	ADDS 14
	M = L + M	ADDS 15
	A(M)=A(M)+S(I,J)	ADDS 16
100	CONTINUE	ADDS 17
200	CONTINUE	ADDS 18
	RETURN	ADDS 19
	END	ADDS 20
C		
	FUNCTION DOT(A,B,N)	DOT 1
C****	VECTOR DOT PRODUCT	DOT 2
	DIMENSION A(1),B(1)	DOT 3
	DOT = 0.0	DOT 4
	DO 100 I=1,N	DOT 5
100	DOT = DOT + A(I)*B(I)	DOT 6
	RETURN	DOT 7
	END	DOT 8
C		
	SUBROUTINE PLOAD(ID,F,B,NN,P)	PLOA 1
C****	FORM LOAD VECTOR IN COMPACT FORM	PLOA 2
	DIMENSION ID(1),F(1),B(1)	PLOA 3
	DO 100 N=1,NN	PLOA 4
	J=ID(N)	PLOA 5
100	IF(J.GT.0) B(J)=F(N)*P	PLOA 6

ORIGINAL PAGE IS
OF POOR QUALITY

134

RETURN	PLOA	7
END	PLOA	8
C		
FUNCTION PROPLD(T,J)	PROP	1
C**** PROPORTIONAL LOAD TABLE (ONE LOAD CARD ONLY)	PROP	2
COMMON /CTDATA/ O,HEAD(20),NUMNP,NUMEL,LAYER,NEQ,IPR	PROP	3
DIMENSION A(5)	PROP	4
IF (J.LE. 0) GO TO 200	PROP	5
C.... INPUT TABLE OF PROPORTIONAL LOADS	PROP	6
I=1	PROP	7
READ(5,1000) K,L,TMIN,TMAX,(A(KKK),KKK=1,5)	PROP	8
WRITE(6,2000) O,HEAD,I,K,L,TMIN,TMAX,(A(KKK),KKK=1,5)	PROP	9
RETURN	PROP	10
C.... COMPUTE VALUE AT TIME T	PROP	11
200 PROPLD = 0.0	PROP	12
IF(T.LT.TMIN .OR. T.GT.TMAX) RETURN	PROP	13
L = MAX0(L,1)	PROP	14
PROPLD = A(1)+A(2)*T+A(3)*(SIN(A(4)*T+A(5)))*#L	PROP	15
RETURN	PROP	16
1000 FORMAT(2I5,7F10.0)	PROP	17
2000 FORMAT(A1,20A4//5X,23HPROPORTIONAL LOAD TABLE//11H NUMBER ,	PROP	18
1 43H TYPE EXP. MINIMUM TIME MAXIMUM TIME,13X,2HA1,13X,	PROP	19
2 2HA2,13X,2HA3,13X,2HA4,13X,2HA5/(3I8,7G15.5))	PROP	20
END	PROP	21
C		
SUBROUTINE PRDIS(UL, ID, X, B, F, T, NDM, NDF)	PRTD	1
C**** OUTPUT NODAL VALUES	PRTD	2
LOGICAL PCOMP	PRTD	3
COMMON /PROLOD/ PROP	PRTD	4
COMMON /CTDATA/ O,HEAD(20),NUMNP,NUMEL,LAYER,NEQ,IPR	PRTD	5
COMMON /LABELS/ PDIS(6),A(6),BC(2),DI(6),CD(3),FD(3)	PRTD	6
COMMON /TMDATA/ TIME,DT,DDT,FORCE,ALPHA	PRTD	7
DIMENSION X(NDM,1),B(1),UL(6),ID(NDF,1),F(NDF,1),T(1)	PRTD	8
DATA BL/4HBLAN/	PRTD	9
DO 102 N=1,NUMNP	PRTD	10
IF(PCOMP(X(1,N),BL)) GO TO 101	PRTD	11
DO 100 I=1,NDF	PRTD	12
UL(I) = F(I,N)*PROP	PRTD	13
K = IABS(ID(I,N))	PRTD	14
100 IF(K.GT.0) UL(I)=B(K)	PRTD	15
T(N)=UL(3)	PRTD	16
101 CONTINUE	PRTD	17
102 CONTINUE	PRTD	18
WRITE(3,2001) (T(I),I=1,NUMNP)	PRTD	19
RETURN	PRTD	20
2001 FORMAT(6E12.4)	PRTD	21
END	PRTD	22
C		
SUBROUTINE FSTREA(UL,XL,LD,P,IX,ID,X,F,JDIAG,DR,B,NDF,NDM,NEN,	FSTR	1
^ NST,NNEQ)	FSTR	2
C**** ELEMENT ROUTINE	FSTR	3
COMMON /CTDATA/ O,HEAD(20),NUMNP,NUMEL,LAYER,NEQ,IPR	FSTR	4
COMMON /ELDATA/ N,NEL,MCT	FSTR	5
COMMON /ISWIDX/ ISW	FSTR	6
COMMON /PROLOD/ PROP	FSTR	7
DIMENSION UL(NDF,1),XL(NDM,1),LD(NDF,1),P(1),IX(NEN,1),	FSTR	8
1 ID(NDF,1),X(NDM,1),F(NDF,1),JDIAG(1),DR(1),B(1),S(1)	FSTR	9
IF(ISW.EQ.5) CALL PLOAD(ID,F,DR,NNEQ,PROP)	FSTR	10
MCT=0	FSTR	11
DO 110 N=1,NUMEL	FSTR	12
CALL PFORM(UL,XL,LD,IX,ID,X,F,B,NDF,NDM,NEN,ISW)	FSTR	13
CALL ELMT01(UL,XL,IX(1,N),P,NDF,NDM,NST,ISW)	FSTR	14
IF(ISW.NE.4) CALL ADDSTF(DR,S,P,JDIAG,LD,1,NEL*NDF,.FALSE.)	FSTR	15
110 CONTINUE	FSTR	16
RETURN	FSTR	17
END	FSTR	18
C		
SUBROUTINE PFORM(UL,XL,LD,IX,ID,X,F,U,NDF,NDM,NEN,ISW)	PFOR	1
C**** FORM LOCAL ARRAYS	PFOR	2
COMMON /ELDATA/ N,NEL,MCT	PFOR	3

	COMMON /PROLOD/ PROP	PFOR 4
	DIMENSION UL(NDF,1),XL(NDM,1),LD(NDF,1),IX(NEN,1),ID(NDF,1),	PFOR 5
	^ X(NDM,1),F(NDF,1),U(1)	PFOR 6
	DO 108 I=1,NEN	PFOR 7
	II = IX(I,N)	PFOR 8
	IF(II .NE. 0) GO TO 105	PFOR 9
	DO 103 J=1,NDM	PFOR 10
103	XL(J,I) = 0.	PFOR 11
	DO 104 J=1,NDF	PFOR 12
	UL(J,I) = 0.	PFOR 13
104	LD(J,I) = 0	PFOR 14
	GO TO 108	PFOR 15
105	IID = II*NDF - NDF	PFOR 16
	NEL = I	PFOR 17
	DO 106 J=1,NDM	PFOR 18
106	XL(J,I) = X(J,II)	PFOR 19
	DO 107 J=1,NDF	PFOR 20
	K = IABS(ID(J,II))	PFOR 21
	UL(J,I) = F(J,II)*PROP	PFOR 22
	IF(K.GT.0) UL(J,I)=U(K)	PFOR 23
	IF(ISW.EQ.6) K=IID+J	PFOR 24
107	LD(J,I) = K	PFOR 25
108	CONTINUE	PFOR 26
	RETURN	PFOR 27
	END	PFOR 28
C		
C****	SUBROUTINE ELMT01(UL,XL,IX,P,NDF,NDM,NST,ISW)	ELMT 1
	LINEAR ELASTIC IN-PLANE ^ BENDING ELEMENT ROUTINE	ELMT 2
	LOGICAL TAN	ELMT 3
	COMMON /ELDATA/ N,NEL,NCT	ELMT 4
	COMMON /MTDATA/ RHO,UU12,E1,E2,G12,G13,G23,THK,WIDTH	ELMT 5
	COMMON /COMPST/ ABD(6,6),DS(2,2),QBR(3,3,25),QBS(2,2,25),	ELMT 6
	^ TH(25),ZK(25)	ELMT 7
	COMMON /DMATIX/ D(10),DB(6,6),LINT	ELMT 8
	COMMON /TMDATA/ TIME,DT,DDT,FORCE,ALPHA	ELMT 9
	COMMON /GAUSSP/ SG(16),TG(16),WG(16)	ELMT 10
	COMMON /EXTRAS/ TAN	ELMT 11
	DIMENSION UL(NDF,1),XL(NDM,1),IX(1),P(1),SHP(3,12),	ELMT 12
1	SIGT(3),SIGB(3),SIGS(2),EPT(3),EPB(3),EPS(2)	ELMT 13
C		ELMT 14
	DO 20 L=1,NST	ELMT 15
20	P(L) = 0.0	ELMT 16
C....	COMPUTE NEUTRAL STRAINS AND STRESS RESULTANTS	ELMT 17
	L = D(1)	ELMT 18
	IF(ISW.EQ.4) L=D(3)	ELMT 19
	CALL PGAUSS(L,LINT)	ELMT 20
	DO 600 L=1,LINT	ELMT 21
C ..	COMPUTE ELEMENT SHAPE FUNCTIONS	ELMT 22
	CALL SHAPE(SG(L),TG(L),XL,SHP,XSJ,NDM,NEL,IX,.FALSE.)	ELMT 23
C ..	COMPUTE STRAINS AND COORDINATES	ELMT 24
	DO 410 I=1,3	ELMT 25
	EPT(I) = 0.0	ELMT 26
410	EPB(I) = 0.0	ELMT 27
	DO 420 I=1,2	ELMT 28
420	EPS(I) = 0.0	ELMT 29
	XX = 0.0	ELMT 30
	YY = 0.0	ELMT 31
	DO 430 J=1,NEL	ELMT 32
	XX = XX + SHP(3,J)*XL(1,J)	ELMT 33
	YY = YY + SHP(3,J)*XL(2,J)	ELMT 34
C ..	IN-PLANE STRAINS	ELMT 35
	EPT(1) = EPT(1) + SHP(1,J)*UL(1,J)	ELMT 36
	EPT(2) = EPT(2) + SHP(2,J)*UL(2,J)	ELMT 37
	EPT(3) = EPT(3) + SHP(1,J)*UL(2,J) + SHP(2,J)*UL(1,J)	ELMT 38
C ..	BENDING CURVATURES	ELMT 39
	EPB(1) = EPB(1) - SHP(1,J)*UL(4,J)	ELMT 40
	EPB(2) = EPB(2) - SHP(2,J)*UL(5,J)	ELMT 41
	EPB(3) = EPB(3) - SHP(1,J)*UL(5,J) - SHP(2,J)*UL(4,J)	ELMT 42
C ..	SHEARING STRAINS	ELMT 43
	EPS(1) = EPS(1) + SHP(1,J)*UL(3,J) - SHP(3,J)*UL(4,J)	ELMT 44

```

430 EPS(2) = EPS(2) + SHP(2,J)*UL(3,J) - SHP(3,J)*UL(5,J)
IF(ISW.EQ.5.AND.TAN)
^ WRITE(9,9001) N,L,(EPB(II),II=1,3),(EPS(II),I=1,2)
9001 FORMAT(2I6,5E12.4)
C .. COMPUTE STRESS RESULTANTS
DO 440 I=1,3
SIGT(I) = 0.
SIGB(I) = 0.
DO 440 J=1,3
SIGT(I) = SIGT(I) + ABD(I,J)*EPT(J) + ABD(I,J+3)*EPB(J)
440 SIGB(I) = SIGB(I) + ABD(I+3,J)*EPT(J) + ABD(I+3,J+3)*EPB(J)
DO 450 I=1,2
SIGS(I) = 0.
DO 450 J=1,2
450 SIGS(I) = SIGS(I) + DS(I,J)*EPS(J)
IF(ISW.GT.4) GO TO 620
C .. OUTPUT STRESS RESULTANTS AND STRAINS
MCT = MCT - 2
IF(MCT.GT.0) GO TO 470
WRITE(6,2001) TIME
MCT = 50
470 WRITE(6,2002) N,XX,YY,EPT,EPB,EPS,SIGT,SIGB,SIGS
GO TO 600
C.... COMPUTE INTERNAL FORCES
620 DU = XSJ*WG(L)
J1 = 1
DO 610 J=1,NEL
P(J1 ) = P(J1 ) - (SHP(1,J)*SIGT(1)+SHP(2,J)*SIGT(3))*DU
P(J1+1) = P(J1+1) - (SHP(2,J)*SIGT(2)+SHP(1,J)*SIGT(3))*DU
P(J1+2) = P(J1+2) - (SHP(1,J)*SIGS(1)+SHP(2,J)*SIGS(2))*DU
P(J1+3) = P(J1+3) + (SHP(1,J)*SIGB(1)+SHP(2,J)*SIGB(3)+SHP(3,J)
^ *SIGS(1))*DU
^ P(J1+4) = P(J1+4) + (SHP(2,J)*SIGB(2)+SHP(1,J)*SIGB(3)+SHP(3,J)
^ *SIGS(2))*DU
610 J1 = J1 + NDF
600 CONTINUE
RETURN
C
2001 FORMAT(1H1//
^ 5X,6HTIME =,E12.3//5X,33HELEMENT STRAINS/STRESS RESULTANTS//
1 8H ELEMENT,3X,7H1-COORD,3X,7H2-COORD,4X,9HXX-STRAIN,4X,
2 9HYY-STRAIN,4X,9HXY-STRAIN,3X,10HKXX-STRAIN,3X,
3 10HKYY-STRAIN,3X,10HKXY-STRAIN,4X,9HSX-STRAIN,4X,
4 9HSY-STRAIN/28X,8(6X,7H-STRESS)//
2002 FORMAT(I8,2F10.4,8E13.4/28X,8E13.4)
END
C
SUBROUTINE PGAUSS(LL,LINT)
C**** GAUSSIAN POINTS AND WEIGHTS FOR TWO DIMENSIONS
COMMON /GAUSSP/ SG(16),TG(16),WG(16)
DIMENSION LR(9),LZ(9),LW(9),WR(2),GR(2),GC(2)
DATA LR/-1,1,1,-1,0,1,0,-1,0/,LZ/-1,-1,1,1,-1,0,1,0,0/
DATA LW/4*25,4*40,64/
DATA GR/0.861136311594053,0.339981043584856/
DATA GC/1.0,0.33333333333/
DATA WR/0.347854845137454,0.652145154862546/
LINT = LL*LL
L=IABS(LL)
GO TO (1,2,3,4),L
C.... 1X1 INTEGRATION
1 SG(1) = 0.
TG(1) = 0.
WG(1) = 4.
RETURN
C.... 2X2 INTEGRATION
2 G = 1./SQRT(3.)
IF(LL.LT.0) G=1.
DO 21 I=1,4
SG(I) = G*LR(I)
TG(I) = G*LZ(I)

```

ELMT 45
ELMT 46
ELMT 47
ELMT 48
ELMT 49
ELMT 50
ELMT 51
ELMT 52
ELMT 53
ELMT 54
ELMT 55
ELMT 56
ELMT 57
ELMT 58
ELMT 59
ELMT 60
ELMT 61
ELMT 62
ELMT 63
ELMT 64
ELMT 65
ELMT 66
ELMT 67
ELMT 68
ELMT 69
ELMT 70
ELMT 71
ELMT 72
ELMT 73
ELMT 74
ELMT 75
ELMT 76
ELMT 77
ELMT 78
ELMT 79
ELMT 80
ELMT 81
ELMT 82
ELMT 83
ELMT 84
ELMT 85
ELMT 86
ELMT 87
ELMT 88
ELMT 89
ELMT 90

PGAU 1
PGAU 2
PGAU 3
PGAU 4
PGAU 5
PGAU 6
PGAU 7
PGAU 8
PGAU 9
PGAU 10
PGAU 11
PGAU 12
PGAU 13
PGAU 14
PGAU 15
PGAU 16
PGAU 17
PGAU 18
PGAU 19
PGAU 20
PGAU 21
PGAU 22
PGAU 23

```

21 WG(I) = 1.
RETURN
C.... 3X3 INTEGRATION
3 G = SORT(0.6)
IF(LL.LT.0) G=1.
H = 1./81.
DO 31 I=1,9
SG(I) = G*LR(I)
TG(I) = G*LZ(I)
31 WG(I) = H*LN(I)
RETURN
C.... 4X4 INTEGRATION
4 DO 41 I=1,4
I1 = 1+MOD(I+1,2)
I2 = 1
IF(I.GT.2) I2 = 2
DO 41 J=1,4
JJ = (I-1)*4+J
SG(JJ) = LR(J)*GR(I1)
IF(LL.LT.0) SG(JJ) = LR(J)*GC(I1)
TG(JJ) = LZ(J)*GR(I2)
IF(LL.LT.0) TG(JJ) = LZ(J)*GC(I2)
41 WG(JJ) = WR(I1)*WR(I2)
RETURN
END
C
SUBROUTINE SHAPE(SS,TT,X,SHP,XSJ,NDM,NEL,IX,FLG)
C**** SHAPE FUNCTION ROUTINE FOR TWO DIMENSIONAL ELEMENTS
LOGICAL FLG
DIMENSION SHP(3,4),X(NDM,1),S(4),T(4),XS(2,2),SX(2,2),IX(9)
DATA S/-0.5,0.5,0.5,-0.5/,T/-0.5,-0.5,0.5,0.5/
C.... FORM 4-NODE QUADRILATERAL SHAPE FUNCTIONS
DO 100 I=1,4
SHP(3,I) = (0.5+S(I)*SS)*(0.5+T(I)*TT)
SHP(1,I) = S(I)*(0.5+T(I)*TT)
100 SHP(2,I) = T(I)*(0.5+S(I)*SS)
IF(NEL.GE.4) GO TO 120
C.... FORM TRIANGLE BY ADDING THIRD AND FOURTH TOGETHER
DO 110 I=1,3
110 SHP(I,3) = SHP(I,3)+SHP(I,4)
C.... ADD QUADRATIC TERMS IF NECESSARY
120 IF(NEL.GT.4 .AND. NEL.LT.10) CALL SHAP2(SS,TT,SHP,IX,NEL)
C.... ADD CUBIC TERMS IF NECESSARY
IF(NEL.GT.9) CALL SHAP3(SS,TT,SHP,IX,NEL)
C.... CONSTRUCT JACOBIAN AND ITS INVERSE
DO 130 I=1,NDM
DO 130 J=1,2
XS(I,J) = 0.0
DO 130 K=1,NEL
130 XS(I,J) = XS(I,J)+ X(J,K)*SHP(I,K)
XSJ = XS(1,1)*XS(2,2)-XS(1,2)*XS(2,1)
IF(XSJ .GT. 0.00000001) GO TO 135
WRITE(6,2000) IX
C
STOP
135 IF(FLG) RETURN
SX(1,1) = XS(2,2)/XSJ
SX(2,2) = XS(1,1)/XSJ
SX(1,2) = -XS(1,2)/XSJ
SX(2,1) = -XS(2,1)/XSJ
C.... FORM GLOBAL DERIVATIVES
DO 140 I=1,NEL
TP = SHP(1,I)*SX(1,1)+SHP(2,I)*SX(2,1)
SHP(2,I) = SHP(1,I)*SX(1,2)+SHP(2,I)*SX(2,2)
140 SHP(1,I) = TP
RETURN
2000 FORMAT(5X,67H***SHAPE ERROR 01** ZERO OR NEGATIVE JACOBIAN DET. FOR
^ELEMENT NODES:/20X,12I4)
END
C
SUBROUTINE SHAP2(S,T,SHP,IX,NEL)

```

PGAU 24
PGAU 25
PGAU 26
PGAU 27
PGAU 28
PGAU 29
PGAU 30
PGAU 31
PGAU 32
PGAU 33
PGAU 34
PGAU 35
PGAU 36
PGAU 37
PGAU 38
PGAU 39
PGAU 40
PGAU 41
PGAU 42
PGAU 43
PGAU 44
PGAU 45
PGAU 46
PGAU 47
PGAU 48

SHAP 1
SHAP 2
SHAP 3
SHAP 4
SHAP 5
SHAP 6
SHAP 7
SHAP 8
SHAP 9
SHAP 10
SHAP 11
SHAP 12
SHAP 13
SHAP 14
SHAP 15
SHAP 16
SHAP 17
SHAP 18
SHAP 19
SHAP 20
SHAP 21
SHAP 22
SHAP 23
SHAP 24
SHAP 25
SHAP 26
SHAP 27
SHAP 28
SHAP 29
SHAP 30
SHAP 31
SHAP 32
SHAP 33
SHAP 34
SHAP 35
SHAP 36
SHAP 37
SHAP 38
SHAP 39
SHAP 40
SHAP 41
SHAP 42

SHAP 1

```

C****      ADD QUADRATIC FUNCTIONS AS NECESSARY
      DIMENSION IX(9),SHP(3,12)
      S2 = (1.-S*S)/2.
      T2 = (1.-T*T)/2.
      DO 100 I=5,NEL
      DO 100 J=1,3
100 SHP(J,I) = 0.0
C....      MIDSIDE NODES (SERENDIPITY)
      IF(IX(5).EQ.0) GO TO 101
      SHP(1,5) = -S*(1.-T)
      SHP(2,5) = -S2
      SHP(3,5) = S2*(1.-T)
101 IF(NEL.LT.6) GO TO 107
      IF(IX(6).EQ.0) GO TO 102
      SHP(1,6) = T2
      SHP(2,6) = -T*(1.+S)
      SHP(3,6) = T2*(1.+S)
102 IF(NEL.LT.7) GO TO 107
      IF(IX(7).EQ.0) GO TO 103
      SHP(1,7) = -S*(1.+T)
      SHP(2,7) = S2
      SHP(3,7) = S2*(1.+T)
103 IF(NEL.LT.8) GO TO 107
      IF(IX(8).EQ.0) GO TO 104
      SHP(1,8) = -T2
      SHP(2,8) = -T*(1.-S)
      SHP(3,8) = T2*(1.-S)
C....      INTERIOR NODE (LAGRANGIAN)
104 IF(NEL.LT.9) GO TO 107
      IF(IX(9).EQ.0) GO TO 107
      SHP(1,9) = -4.*S*T2
      SHP(2,9) = -4.*T*S2
      SHP(3,9) = 4.*S2*T2
C....      CORRECT EDGE NODES FOR INTERIOR NODE(LAGRANGIAN)
      DO 106 J=1,3
      DO 106 I=1,4
105 SHP(J,I) = SHP(J,I) - 0.25*SHP(J,9)
      DO 106 I=5,8
106 IF(IX(I).NE.0) SHP(J,I) = SHP(J,I) - 0.5*SHP(J,9)
C....      CORRECT CORNER NODES FOR PRESENCE OF MIDSIDE NODES
107 K = 8
      DO 109 I=1,4
      L = I + 4
      DO 108 J=1,3
108 SHP(J,I) = SHP(J,I) - 0.5*(SHP(J,K)+SHP(J,L))
109 K = L
      RETURN
      END
C
      SUBROUTINE SHAP3(S,T,SHP,IX,NEL)
C****      ADD CUBIC FUNCTION AS NECESSARY (SERENDIPITY)
      DIMENSION IX(12),SHP(3,12)
      DO 100 I=5,NEL
      DO 100 J=1,3
100 SHP(J,I)=0.0
      IF(IX(5).EQ.0) GO TO 101
      S1=-1./3.
      T1=-1.
      CALL CSHAPE(S,T,S1,T1,SHP,1,5)
101 IF(IX(6).EQ.0) GO TO 102
      S1=1.
      T1=-1./3.
      CALL CSHAPE(S,T,S1,T1,SHP,2,6)
102 IF(IX(7).EQ.0) GO TO 103
      S1=1./3.
      T1=1.
      CALL CSHAPE(S,T,S1,T1,SHP,1,7)
103 IF(IX(8).EQ.0) GO TO 104
      S1=-1.
      T1=1./3.

```

SHAP 2
SHAP 3
SHAP 4
SHAP 5
SHAP 6
SHAP 7
SHAP 8
SHAP 9
SHAP 10
SHAP 11
SHAP 12
SHAP 13
SHAP 14
SHAP 15
SHAP 16
SHAP 17
SHAP 18
SHAP 19
SHAP 20
SHAP 21
SHAP 22
SHAP 23
SHAP 24
SHAP 25
SHAP 26
SHAP 27
SHAP 28
SHAP 29
SHAP 30
SHAP 31
SHAP 32
SHAP 33
SHAP 34
SHAP 35
SHAP 36
SHAP 37
SHAP 38
SHAP 39
SHAP 40
SHAP 41
SHAP 42
SHAP 43
SHAP 44
SHAP 45
SHAP 46
SHAP 47
SHAP 48
SHAP 49

SHAP 1
SHAP 2
SHAP 3
SHAP 4
SHAP 5
SHAP 6
SHAP 7
SHAP 8
SHAP 9
SHAP 10
SHAP 11
SHAP 12
SHAP 13
SHAP 14
SHAP 15
SHAP 16
SHAP 17
SHAP 18
SHAP 19
SHAP 20
SHAP 21

```

CALL CSHAPE(S,T,S1,T1,SHP,2,8)
104 IF(IX(9).EQ.0) GO TO 105
    S1=-1.
    T1=-1./3.
CALL CSHAPE(S,T,S1,T1,SHP,2,9)
105 IF(NEL.LT.10) GO TO 200
    IF(IX(10).EQ.0) GO TO 106
    S1=1./3.
    T1=-1.
CALL CSHAPE(S,T,S1,T1,SHP,1,10)
106 IF(NEL.LT.11) GO TO 200
    IF(IX(11).EQ.0) GO TO 107
    S1=1.
    T1=1./3.
CALL CSHAPE(S,T,S1,T1,SHP,2,11)
107 IF(NEL.LT.12) GO TO 200
    IF(IX(12).EQ.0) GO TO 200
    S1=-1./3.
    T1=1.
CALL CSHAPE(S,T,S1,T1,SHP,1,12)
C.... CORRECT CORNER NODES
200 DO 210 I=1,4
    I1=I+4
    I2=I+8
    IF(I.EQ.1) I3=I+7
    IF(I.GT.1) I3=I+3
    IF(I.LT.4) I4=I+9
    IF(I.EQ.4) I4=I+5
    DO 210 J=1,3
210 SHP(J,I)=SHP(J,I)-2./3.*(SHP(J,I1)+SHP(J,I2))-1./3.*(SHP(J,I3)
    ^ +SHP(J,I4))
    RETURN
    END
C
C***** SUBROUTINE CSHAPE(S,T,S1,T1,SHP,K,L)
        SUPPLEMENTAL ROUTINE FOR THE SHAPE FUNCTIONS
        DIMENSION SHP(3,12)
        C=9./32.
        GO TO (1,2),K
1 SHP(1,L)=C*(1.+T1*T)*(9.*S1-2.*S-27.*S1*S*S)
SHP(2,L)=C*T1*(1.-S*S)*(1.+9.*S1*S)
SHP(3,L)=C*(1.+T1*T)*(1.-S*S)*(1.+9.*S1*S)
RETURN
2 SHP(1,L)=C*S1*(1.-T*T)*(1.+9.*T1*T)
SHP(2,L)=C*(1.+S1*S)*(9.*T1-2.*T-27.*T1*T*T)
SHP(3,L)=C*(1.+S1*S)*(1.-T*T)*(1.+9.*T1*T)
RETURN
END
C
C***** SUBROUTINE PMESH(IDL,XL,IX,ID,X,F,JDIAG,NDF,NDM,NEN,NKM)
        INPUT MESH DATA
        LOGICAL PRT,ERR,PCOMP
        COMMON /CTDATA/ O,HEAD(20),NUMNP,NUMEL,LAYER,NEQ,IPR
        COMMON /MTDATA/ RHO,UU12,E1,E2,G12,G13,G23,THK,WIDTH
        COMMON /LABELS/ PDIS(6),A(6),BC(2),DI(6),CD(3),FD(3)
        COMMON /EXDATA/ QLAW(4)
        COMMON /RODATA/ UR,IG,NDS
        DIMENSION IDL(6),XL(7),IX(NEN,1),ID(NDF,1),X(NDM,1),
    ^ F(NDF,1),DUM(1),WD(13),JDIAG(1)
        DATA WD/4HCOOR,4HELEM,4HMATE,4HBOUN,4HFORC,4HROD ,
    ^ 4HEND ,4HPRIN,4HNOPR,4HPAGE,4HEXPE/
        DATA BL/4HBLAN/,LIST/11/,PRT/.TRUE./
C.... INITIALIZE ARRAYS
ERR = .FALSE.
DO 501 I=1,4
501 QLAW(I)=0.
DO 502 N=1,NUMNP
DO 502 I=1,NDF
ID(I,N)=0
F(I,N)=0.

```

SHAP 22
SHAP 23
SHAP 24
SHAP 25
SHAP 26
SHAP 27
SHAP 28
SHAP 29
SHAP 30
SHAP 31
SHAP 32
SHAP 33
SHAP 34
SHAP 35
SHAP 36
SHAP 37
SHAP 38
SHAP 39
SHAP 40
SHAP 41
SHAP 42
SHAP 43
SHAP 44
SHAP 45
SHAP 46
SHAP 47
SHAP 48
SHAP 49
SHAP 50
SHAP 51
SHAP 52
SHAP 53
SHAP 54

CSHA 1
CSHA 2
CSHA 3
CSHA 4
CSHA 5
CSHA 6
CSHA 7
CSHA 8
CSHA 9
CSHA 10
CSHA 11
CSHA 12
CSHA 13
CSHA 14

PMES 1
PMES 2
PMES 3
PMES 4
PMES 5
PMES 6
PMES 7
PMES 8
PMES 9
PMES 10
PMES 11
PMES 12
PMES 13
PMES 14
PMES 15
PMES 16
PMES 17
PMES 18
PMES 19
PMES 20
PMES 21

502 CONTINUE	PMES 22
C.... READ A CARD AND COMPARE WITH MACRO LIST	PMES 23
10 READ(5,1000) CC	PMES 24
DO 20 I=1,LIST	PMES 25
20 IF(PCOMP(CC,WD(I))) GO TO 30	PMES 26
GO TO 10	PMES 27
30 GO TO (1,2,3,4,5,6,7,8,9,11,12),I	PMES 28
C.... NODAL COORDINATE DATA INPUT	PMES 29
1 DO 102 N=1,NUMNP	PMES 30
102 X(1,N)= BL	PMES 31
CALL GENUVEC(NDM,XL,X,CD,PRT,ERR)	PMES 32
GO TO 10	PMES 33
C.... ELEMENT DATA INPUT	PMES 34
2 L=0	PMES 35
DO 206 I=1,NUMEL,50	PMES 36
IF(PRT) WRITE(6,2001) O,HEAD, (K,K=1,NEN)	PMES 37
J = MINO(NUMEL,I+49)	PMES 38
DO 206 N=1,J	PMES 39
IF(L-N) 200,202,203	PMES 40
200 READ(5,1001) L, (IDL(K),K=1,NEN),LX	PMES 41
IF(L.EQ.0) L=NUMEL+1	PMES 42
IF(LX.EQ.0) LX=1	PMES 43
IF(L-N) 201,202,203	PMES 44
201 WRITE(6,3001) L,N	PMES 45
ERR = .TRUE.	PMES 46
GO TO 206	PMES 47
202 NX = LX	PMES 48
DO 207 K=1,NEN	PMES 49
207 IX(K,L) = IDL(K)	PMES 50
GO TO 205	PMES 51
203 IX(NEN,N) = IX(NEN,N-1)	PMES 52
DO 204 K=1,NEN	PMES 53
IX(K,N) = IX(K,N-1) + NX	PMES 54
IF(IX(K,N-1).EQ.0) IX(K,N) = 0	PMES 55
205 IF(PRT) WRITE(6,2002) N, (IX(K,N),K=1,NEN)	PMES 56
206 CONTINUE	PMES 57
GO TO 10	PMES 58
C.... MATERIAL DATA INPUT	PMES 59
3 WRITE(6,2004) O,HEAD	PMES 60
CALL MATLIB	PMES 61
GO TO 10	PMES 62
C.... READ IN THE RESTRAINT CONDITIONS FOR EACH NODE	PMES 63
4 IF(PRT) WRITE(6,2000) O,HEAD, (I,BC,I=1,NDF)	PMES 64
N = 0	PMES 65
NG = 0	PMES 66
420 L = N	PMES 67
LG = NG	PMES 68
READ(5,1001) N,NG,IDL	PMES 69
IF(N.LE.0 .OR. N.GT.NUMNP) GO TO 50	PMES 70
DO 41 I=1,NDF	PMES 71
ID(I,N) = IDL(I)	PMES 72
41 IF(L.NE.0 .AND. IDL(I).EQ.0 .AND. ID(I,L).LT.0) ID(I,N)=-1	PMES 73
LG = ISIGN(LG,N-L)	PMES 74
42 L = L+LG	PMES 75
IF((N-L)*LG .LE. 0) GO TO 420	PMES 76
DO 43 I=1,NDF	PMES 77
43 IF(ID(I,L-LG) .LT. 0) ID(I,L) = -1	PMES 78
GO TO 42	PMES 79
50 DO 48 N=1,NUMNP	PMES 80
DO 46 I=1,NDF	PMES 81
46 IF(ID(I,N) .NE. 0) GO TO 47	PMES 82
GO TO 48	PMES 83
47 IF(PRT) WRITE(6,2007) N, (ID(I,N),I=1,NDF)	PMES 84
48 CONTINUE	PMES 85
GO TO 10	PMES 86
C.... FORCE/DISPL DATA INPUT	PMES 87
5 CALL GENUVEC(NDF,XL,F,FD,PRT,ERR)	PMES 88
GO TO 10	PMES 89
C.... END OF MESH DATA INPUT	PMES 90
C.... COMPUTE THE PROFILE OF GLOBLE ARRAYS	PMES 91

```

7 IF(ERR) STOP
CALL PROFIL(JDIAG, ID, IX, NDF, NEN, NKM, PRT)
RETURN
C.... PRINT OPTION
8 PRT = .TRUE.
GO TO 10
C.... NOPRINT OPTION
9 PRT = .FALSE.
GO TO 10
C.... READ IN PAPER EJECTION OPTION
11 READ(5,1000) O
GO TO 10
C.... INPUT EXPERIMENTAL INDENTATION LAW
12 READ(5,1007) (QLAW(I), I=1,4)
WRITE(6,2008) O, HEAD, (QLAW(I), I=1,4)
GO TO 10
C.... INPUT INITIAL IMPACT CONDITION
6 WRITE(6,2009) O, HEAD
READ(5,1002) NG, INDF, UR
WRITE(6,2010) NG, INDF, UR
F(INDF, NG)=1.0
IQ=ID(INDF, NG)
GO TO 10
C.... INPUT/OUTPUT FORMATS
1000 FORMAT(A4, 75X, A1)
1001 FORMAT(16I5)
1002 FORMAT(2I5, F10.0)
1007 FORMAT(4F10.0)
2000 FORMAT(A1, 20A4//5X, 10HNODAL B.C., 7X//6X, 5HNODE, 9(I7, A4, A2)/1X)
2001 FORMAT(A1, 20A4//5X, 8HELEMENTS//3X, 7HELEMENT,
^ 14(I3, 5H NODE)//(20X, 14(I3, 5H NODE)))
2002 FORMAT(I10, 14I8/(10X, 14I8))
2004 FORMAT(A1, 20A4//5X, 19HMATERIAL PROPERTIES)
2007 FORMAT(I10, 9I13)
2008 FORMAT(A1, 20A4//5X, #EXPERIMENTAL INDENTATION LAW#//
1 10X, #CONTACT COEFFICIENT: #, E12.4/
2 10X, #CRITICAL INDENTATION: # E12.4/
3 10X, #CONSTANT S: # E12.4/
4 10X, #POWER INDEX OF UNLOADING LAW: # F12.3)
3001 FORMAT(5X, 2GH**PMESH ERROR 01** ELEMENT, I5,
^ 22H APPEARS AFTER ELEMENT, I5)
2009 FORMAT(A1, 20A4//5X, #IMPACT OF LAMINATED PLATE#)
2010 FORMAT(//10X, #IMPACT NODAL POINT: #, I10/
^ 10X, #IMPACT D.O.F.: #, I10/
^ 10X, #INITIAL IMPACT VELOCITY: #, E12.4)
END
C
SUBROUTINE GENUCC(NDM, XL, X, CD, PRT, ERR)
C**** GENERATE REAL DATA ARRAYS BY LINEAR INTERPOLATION
LOGICAL PRT, ERR, PCOMP
COMMON /CTDATA/ O, HEAD(20), NUMNP, NUMEL, LAYER, NEG, IPR
DIMENSION X(NDM, 1), XL(7), CD(3)
DATA BL/4HBLAN/
N=0
NG=0
102 L=N
LG=NG
READ(5,1000) N, NG, XL
IF(N.LE.0 .OR. N.GT.NUMNP) GO TO 108
DO 103 I=1, NDM
103 X(I, N)=XL(I)
IF(LG) 104, 102, 104
104 LG=ISIGN(LG, N-L)
LI=(IABS(N-L+LG)-1)/IABS(LG)
DO 105 I=1, NDM
105 XL(I)=X(I, N)-X(I, L)/LI
106 L=L+LG
IF((N-L)*LG .LE. 0) GO TO 102
IF(L.LE.0 .OR. L.GT.NUMNP) GO TO 110
DO 107 I=1, NDM

```

PMES 92
PMES 93
PMES 94
PMES 95
PMES 96
PMES 97
PMES 98
PMES 99
PMES100
PMES101
PMES102
PMES103
PMES104
PMES105
PMES106
PMES107
PMES108
PMES109
PMES110
PMES111
PMES112
PMES113
PMES114
PMES115
PMES116
PMES117
PMES118
PMES119
PMES120
PMES121
PMES122
PMES123
PMES124
PMES125
PMES126
PMES127
PMES128
PMES129
PMES130
PMES131
PMES132
PMES133
PMES134
PMES135
PMES136
PMES137

GENU 1
GENU 2
GENU 3
GENU 4
GENU 5
GENU 6
GENU 7
GENU 8
GENU 9
GENU 10
GENU 11
GENU 12
GENU 13
GENU 14
GENU 15
GENU 16
GENU 17
GENU 18
GENU 19
GENU 20
GENU 21
GENU 22
GENU 23

107	X(I,L)=X(I,L-LG)+XL(I)	GENU	24
	GO TO 106	GENU	25
110	WRITE(6,3000) L,(CD(I),I=1,3)	GENU	26
	ERR = .TRUE.	GENU	27
	GO TO 102	GENU	28
108	DO 109 I=1,NUMNP,50	GENU	29
	IF(FRT) WRITE(6,2000)O,HEAD,(CD(L),L=1,3),(L,CD(1),CD(2),L=1,NDM)	GENU	30
	N = NINO(NUMNP,I+49)	GENU	31
	DO 109 J=I,N	GENU	32
	IF(PCOMP(X(1,J),BL).AND.PRT) WRITE(6,2008) N	GENU	33
109	IF(.NOT.PCOMP(X(1,J),BL).AND.PRT) WRITE(6,2009) J,(X(L,J),L=1,NDM)	GENU	34
	RETURN	GENU	35
1000	FORMAT(2I5,7F10.0)	GENU	36
2000	FORMAT(A1,20A4//5X,5HNDAL,3A4//6X,4HNODE,9(I7,A4,A2))	GENU	37
2008	FORMAT(5X,21H**GENUEC WARNING 01**,I10,	GENU	38
	^ 32H HAS NOT BEEN INPUT OR GENERATED)	GENU	39
2009	FORMAT(I10,9F13.4)	GENU	40
3000	FORMAT(5X,44H**GENUEC ERROR 01**ATTEMPT TO GENETATE NODE,IS,	GENU	41
	1 3H IN,3A4)	GENU	42
	END	GENU	43
C	SUBROUTINE PROFIL(JDIAG,ID,IX,NDF,NEN,NKM,PRT)	PROF	1
C****	COMPUTE PROFILE OF GLOBAL ARRAYS	PROF	2
	LOGICAL PRT	PROF	3
	COMMON /CTDATA/ O,HEAD(20),NUMNP,NUMEL,LAYER,NEG,IPR	PROF	4
	DIMENSION JDIAG(1),ID(NDF,1),IX(NEN,1),EQ(2)	PROF	5
	DATA EQ/4H DOF,2H. /	PROF	6
C....	SET UP THE EQUATION NUMBERS	PROF	7
	NEG = 0	PROF	8
	DO 50 N=1,NUMNP	PROF	9
	DO 40 I=1,NDF	PROF	10
	J = ID(I,N)	PROF	11
	IF(J) 30,20,30	PROF	12
20	NEG = NEG + 1	PROF	13
	ID(I,N) = NEG	PROF	14
	JDIAG(NEG) = 0	PROF	15
	GO TO 40	PROF	16
30	ID(I,N) = 0	PROF	17
40	CONTINUE	PROF	18
50	CONTINUE	PROF	19
	IF(.NOT.PRT) GO TO 70	PROF	20
	WRITE(6,2000) O,HEAD,(I,EQ,I=1,NDF)	PROF	21
	DO 60 I=1,NUMNP	PROF	22
60	WRITE(6,2001) I,(ID(K,I),K=1,NDF)	PROF	23
C....	COMPUTE COLUMN HEIGHTS	PROF	24
70	DO 500 N=1,NUMEL	PROF	25
	DO 400 I=1,NEN	PROF	26
	II = IX(I,N)	PROF	27
	IF(II.EQ.0) GO TO 400	PROF	28
	DO 300 K=1,NDF	PROF	29
	KK = ID(K,II)	PROF	30
	IF(KK.EQ.0) GO TO 300	PROF	31
	DO 200 J=I,NEN	PROF	32
	JJ = IX(J,N)	PROF	33
	IF(JJ.EQ.0) GO TO 200	PROF	34
	DO 100 L=1,NDF	PROF	35
	LL = ID(L,JJ)	PROF	36
	IF(LL.EQ.0) GO TO 100	PROF	37
	M = MAX0(KK,LL)	PROF	38
	JDIAG(M) = MAX0(JDIAG(M),IABS(KK-LL))	PROF	39
100	CONTINUE	PROF	40
200	CONTINUE	PROF	41
300	CONTINUE	PROF	42
400	CONTINUE	PROF	43
500	CONTINUE	PROF	44
C....	COMPUTE DIAGONAL POINTERS FOR PROFILE	PROF	45
	NKM = 1	PROF	46
	JDIAG(1) = 1	PROF	47
	IF(NEG.EQ.1) RETURN	PROF	48
	DO 600 N=2,NEG	PROF	49

ORIGINAL PAGE IS
OF POOR QUALITY

```

600 JDIAG(N) = JDIAG(N) + JDIAG(N-1) + 1
      NKM = JDIAG(NEQ)
2000 FORMAT(A1,20A4//5X,16HEQUATION NUMBERS//6X,5HNODE ,
      ^ 9(I5,A4,A2)/1X)
2001 FORNAT(I10,9I11)
      RETURN
      END)

C
C**** SUBROUTINE MATLID
      MATERIAL PROPERTIES ROUTINE
      COMMON /CTDATA/ O,HEAD(20),NUMNP,NUMEL,LAYER,NEQ,IPR
      COMMON /MTDATA/ RHO,UU12,E1,E2,G12,G13,G23,THK,WIDTH
      COMMON /COMPST/ ABD(6,6),DS(2,2),QBR(3,3,25),QBS(2,2,25),
      ^ TH(25),ZK(25)
      COMMON /DMATIX/ D(10),DB(6,6),LINT
      DIMENSION WD(5)
      DATA WD/GH ISO-,GH ORTHO,GHTROPIC,GH COMP,GHOSITE /
C.... INPUT MATERIAL PROPERTIES
      READ(5,1000) L1,L2,K,THK,WIDTH
      READ(5,1001) RHO,UU12,E1,E2,G12,G13,G23
      DO 150 J=1,3
      DO 150 I=1,3
      IF(I.EQ.3 .OR. J.EQ.3) GO TO 150
      DS(J,I) = 0.
150 ABD(J,I) = ABD(J+3,I) = ABD(J,I+3) = ABD(J+3,I+3) = 0,
      L1 = MINO(4,MAXO(1,L1))
      D(1) = L1
      L2 = MINO(4,MAXO(1,L2))
      D(2) = L2
      D(3) = K
      LINT=0
      IF(E1-E2) 120,110,120
110 G12=E1/(2.*(1.+UU12))
      J1=1 $ J2=3
      GO TO 200
120 J1=4 $ J2=5
      IF(LAYER.EQ.1) J1=2 $ J2=3
200 WRITE(6,2000) LAYER,WD(J1),WD(J2),THK,E1,E2,G12,G13,G23,UU12,
      ^ RHO,L1,L2,"
      CALL CNPD
      RETURN
C.... FORMAT FOR INPUT-OUTPUT
1000 FORMAT(3I5,2F10.0)
1001 FORMAT(7F10.0)
2000 FORMAT(/5X,12,12H LAYER(S) OF,2AG,21H PLATE WITH THICKNESS,
1 F10.4//10X,15HYOUNG=S MODULUS,10X,#E1=#,E10.4,10X,#E2=#,E10.4/
2 10X,15HSHEAR MODULUS,9X,#G12=#,E10.4,9X,#G13=#,E10.4,9X,
3 #G23=#,E10.4/10X,15HPOISSON RATIO,8X,#UU12=#,F5.3/10X,
4 7HDENSITY,17X,#RHO=#,E10.4/10X,13HGAUSS PTS/DIR,12X,#L1=#,15,
5 5X,#L2=#,15/10X,12HSTRESS POINT,14X,#K=#,15/)
      END)

C
C**** SUBROUTINE CNPD
      COMPUTE #ABD# MATRIX AND #DS# MATRIX
      COMMON /CTDATA/ O,HEAD(20),NUMNP,NUMEL,LAYER,NEQ,IPR
      COMMON /MTDATA/ RHO,UU12,E1,E2,G12,G13,G23,THK,WIDTH
      COMMON /COMPST/ ABD(6,6),DS(2,2),QBR(3,3,25),QBS(2,2,25),
      ^ TH(25),ZK(25)
      DIMENSION Q(3,3),QS(2,2),TK(25)
      LL=LAYER
      NN=LL+1
      READ(5,1000) (L,TH(L),TK(L),I=1,LL)
      ZK(1)=TTK=0.0
      DO 15 I=1,LL
      TTK=TTK+TK(I)
      ZK(I+1)=TK(I)+ZK(I)
15 CONTINUE
      DO 25 I=1,NN
      ZK(I)=ZK(I)-TTK/2.
25 CONTINUE

```

PROF 50
PROF 51
PROF 52
PROF 53
PROF 54
PROF 55
PROF 56

NATL 1
NATL 2
NATL 3
NATL 4
NATL 5
NATL 6
NATL 7
NATL 8
NATL 9
NATL 10
NATL 11
NATL 12
NATL 13
NATL 14
NATL 15
NATL 16
NATL 17
NATL 18
NATL 19
NATL 20
NATL 21
NATL 22
NATL 23
NATL 24
NATL 25
NATL 26
NATL 27
NATL 28
NATL 29
NATL 30
NATL 31
NATL 32
NATL 33
NATL 34
NATL 35
NATL 36
NATL 37
NATL 38
NATL 39
NATL 40
NATL 41
NATL 42
NATL 43

CNPD 1
CNPD 2
CNPD 3
CNPD 4
CNPD 5
CNPD 6
CNPD 7
CNPD 8
CNPD 9
CNPD 10
CNPD 11
CNPD 12
CNPD 13
CNPD 14
CNPD 15
CNPD 16
CNPD 17
CNPD 18

```

DEL=4.*ATAN(1.)/180.
DEN = 1. - E2*UU12**2/E1
Q(1,1) = E1/DEN
Q(2,2) = E2/DEN
Q(1,2) = Q(2,1) = UU12*Q(2,2)
Q(3,3) = G12
Q(1,3) = Q(2,3) = Q(3,1) = Q(3,2) = 0.0
QS(1,1) = G13
QS(2,2) = G23
QS(1,2) = QS(2,1) = 0.0
DO 40 I=1,LL
ANGL=TH(I)*DEL
C=COS(ANGL)
W=SIN(ANGL)
QBR(1,1,I)=Q(1,1)*C**4+2.*(Q(1,2)+2.*Q(3,3))*(C*W)**2+Q(2,2)*W**4
QBR(1,2,I)=QBR(2,1,I)=(Q(1,1)+Q(2,2)-4.*Q(3,3))*(C*W)**2
$ +Q(1,2)*(W**4 +C**4 )
QBR(2,2,I)=Q(1,1)*W**4+2.*(Q(1,2)+2.*Q(3,3))*(C*W)**2+Q(2,2)*C**4
QBR(1,3,I)=QBR(3,1,I)=(Q(1,1)-Q(1,2)-2.*Q(3,3))*W*C**3 +
$ (Q(1,2)-Q(2,2)+2.*Q(3,3))*C*W**3
QBR(2,3,I)=QBR(3,2,I)=(Q(1,1)-Q(1,2)-2.*Q(3,3))*W**3 *C+
$ (Q(1,2)-Q(2,2)+2.*Q(3,3))*W*C**3
QBR(3,3,I)=(Q(1,1)+Q(2,2)-2.*Q(1,2)-2.*Q(3,3))*(W*C)**2+
$ Q(3,3)*(W**4 +C**4 )
QBS(1,1,I) = QS(1,1)*C**2 + QS(2,2)*W**2
QBS(2,2,I) = QS(1,1)*W**2 + QS(2,2)*C**2
QBS(1,2,I) = QBS(2,1,I) = (QS(1,1)-QS(2,2))*C*W
40 CONTINUE
DO 50 J=1,3
DO 50 K=1,3
DO 50 I=1,LL
ABD(J ,K )= ABD(J ,K )+QBR(J,K,I)*(ZK(I+1)-ZK(I))
ABD(J+3,K )= ABD(J ,K+3)= ABD(J+3,K)+QBR(J,K,I)*
$ (ZK(I+1)**2-ZK(I)**2)/2.
ABD(J+3,K+3)= ABD(J+3,K+3)+QBR(J,K,I)*(ZK(I+1)**3-ZK(I)**3)/3.
50 CONTINUE
DO 55 I=1,6
DO 55 J=1,6
IF(I.GE.3 .OR. J.GE.3) GO TO 55
IF(ABS(DS(I,J)) .LT. 1.E-06) DS(I,J)=0.0
55 IF(ABS(ABD(I,J)) .LT. 1.E-06) ABD(I,J)=0.0
WRITE(6,2001) ((ABD(I,J),J=1,6),I=1,6)
DO 60 J=1,2
DO 60 K=1,2
DO 60 I=1,LL
60 DS(J,K) = DS(J,K) + QBS(J,K,I)*(ZK(I+1)-ZK(I))
WRITE(6,2002) ((DS(I,J),J=1,2),I=1,2)
1000 FORMAT(15,F5.0,F10.0)
2001 FORMAT(/,1X,10HABD MATRIX//6(2X,6E13.4/))
2002 FORMAT(/,1X,9HDS MATRIX//2(2X,2E13.4/))
RETURN
END
C
SUBROUTINE KMLIB
C**** ASSEMBLE GLOBLE ARRAY
COMMON G(1)
DIMENSION M(1)
EQUIVALENCE (G(1),M(1))
COMMON /ISWIDX/ ISW
COMMON /CTDATA/ O,HEAD(20),NUMNP,NUMEL,LAYER,NEG,IPR
COMMON /LODATA/ NDF,NDM,NEN,NST,NKM
COMMON /PARATS/ NPAR(14),NEND
N1=NEND
N2=N1+NST*NST*IPR
IF(ISW.LE.2) NE=N2+NKM*IPR
IF(ISW.GT.2) NE=N2+NEG*IPR
CALL SETMEM(NE)
CALL PZERO(G(NEND),NE-NEND)
CALL MASSO1(G(NPAR(1)),G(NPAR(2)),M(NPAR(3)),G(NPAR(4)),
1 M(NPAR(5)),M(NPAR(6)),G(NPAR(7)),G(NPAR(8)),M(NPAR(9)),
KMLI 1
KMLI 2
KMLI 3
KMLI 4
KMLI 5
KMLI 6
KMLI 7
KMLI 8
KMLI 9
KMLI 10
KMLI 11
KMLI 12
KMLI 13
KMLI 14
KMLI 15
KMLI 16
KMLI 17

```

```

2   G(NPAR(11)),G(N1),G(N2),NDF,NDM,NEN,NST,NKM)
RETURN
END
C
SUBROUTINE MASS01(UL,XL,LD,P,IX,ID,X,F,JDIAG,B,S,A,NDF,NDM,NEN,
^ NST,NKM)
C**** FORM MASS MATRIX
COMMON /CTDATA/ O,HEAD(20),NUMNP,NUMEL,LAYER,NEQ,IPR
COMMON /MTDATA/ RHO,UU12,E1,E2,G12,G13,G23,THK,WIDTH
COMMON /DMATIX/ D(10),DB(6,6),LINT
COMMON /ELDATA/ N,NEL,MCT
COMMON /ISWIDX/ ISW
COMMON /GAUSSP/ SG(16),TG(16),WG(16)
DIMENSION UL(1),XL(NDM,1),LD(NDF,1),P(1),IX(NEN,1),ID(NDF,1),
1   X(NDM,1),F(1),JDIAG(1),B(1),S(NST,1),A(1),SHP(3,12)
C.... LOOP ON ELEMENTS
DO 110 N=1,NUMEL
DO 10 I=1,NST
DO 10 J=1,NST
10 S(I,J)=0.
C.... SET UP LOCAL ARRAYS
CALL PFORM(UL,XL,LD,IX,ID,X,F,B,NDF,NDM,NEN,ISW)
C.... COMPUTE CONSISTENT MASS MATRIX
L = D(1)
CALL PGAUSS(L,LINT)
DO 500 L=1,LINT
C .. COMPUTE SHAPE FUNCTIONS
CALL SHAPE(SG(L),TG(L),XL,SHP,XSJ,NDM,NEL,IX,.FALSE.)
DU = WG(L)*XSJ*RHO*THK
C .. FOR EACH NODE J COMPUTE DB=RHO*SHAPE*DU
K1 = 1
DO 500 J=1,NEL
W11 = SHP(3,J)*DU
W33 = W11*THK**2/12.
C .. FOR EACH NODE K COMPUTE MASS MATRIX (UPPER TRIANGULAR PART)
J1 = K1
DO 510 K=J,NEL
S(J1 ,K1 ) = S(J1 ,K1 ) + SHP(3,K)*W11
S(J1+3,K1+3) = S(J1+3,K1+3) + SHP(3,K)*W33
510 J1 = J1 + NDF
500 K1 = K1 + NDF
C .. COMPUTE MISSING PARTS AND LOWER PART BY SYMMETRY
NSL = NEL*NDF
DO 530 K=1,NSL,NDF
DO 520 J=K,NSL,NDF
S(J+2,K+2) = S(J+1,K+1) = S(J ,K )
S(J+4,K+4) = S(J+3,K+3)
S(K ,J ) = S(J ,K )
S(K+3,J+3) = S(J+3,K+3)
S(K+2,J+2) = S(K+1,J+1) = S(J ,K )
520 S(K+4,J+4) = S(J+3,K+3)
530 CONTINUE
IF(ISW.EQ.2) GO TO 100
C.... LUMPED MASS MATRIX
SUM1 = 0.0
SUM2 = 0.0
SUMD1 = 0.0
SUMD2 = 0.0
DO 540 I=1,NSL,NDF
SUMD1 = SUMD1 + S(I,I)
SUMD2 = SUMD2 + S(I+3,I+3)
DO 540 J=1,NSL,NDF
SUM1 = SUM1 + S(I,J)
540 SUM2 = SUM2 + S(I+3,J+3)
DO 550 I=1,NSL,NDF
P(I) = S(I,I)*SUM1/SUMD1
P(I+2) = P(I+1) = P(I)
P(I+3) = S(I+3,I+3)*SUM2/SUMD2
550 P(I+4) = P(I+3)
C.... ADD TO TOTAL ARRAY

```

KMLI 18
KMLI 19
KMLI 20
MASS 1
MASS 2
MASS 3
MASS 4
MASS 5
MASS 6
MASS 7
MASS 8
MASS 9
MASS 10
MASS 11
MASS 12
MASS 13
MASS 14
MASS 15
MASS 16
MASS 17
MASS 18
MASS 19
MASS 20
MASS 21
MASS 22
MASS 23
MASS 24
MASS 25
MASS 26
MASS 27
MASS 28
MASS 29
MASS 30
MASS 31
MASS 32
MASS 33
MASS 34
MASS 35
MASS 36
MASS 37
MASS 38
MASS 39
MASS 40
MASS 41
MASS 42
MASS 43
MASS 44
MASS 45
MASS 46
MASS 47
MASS 48
MASS 49
MASS 50
MASS 51
MASS 52
MASS 53
MASS 54
MASS 55
MASS 56
MASS 57
MASS 58
MASS 59
MASS 60
MASS 61
MASS 62
MASS 63
MASS 64
MASS 65
MASS 66

```

100 CALL ADDSTF(A,S,P,JDIAG,LD,NST,NEL*NDP,.FALSE.)
110 CONTINUE
    REWIND 2
    IF(ISW.EQ.2) WRITE(2) (A(I),I=1,NKM)
    IF(ISW.EQ.3) WRITE(2) (A(I),I=1,NEQ)
    RETURN
    END

```

MASS 67
MASS 68
MASS 69
MASS 70
MASS 71
MASS 72
MASS 73

C

^
C**** SUBROUTINE RODIPCT

```

LOGICAL FLAG
COMMON G(1)
DIMENSION M(1)
EQUIVALENCE (G(1),M(1))
COMMON /CTDATA/ O,HEAD(20),NUMNP,NUMEL,LAYER,NEQ,IPR
COMMON /LODATA/ NDF,NDM,NEN,NST,NKM
COMMON /PARATS/ NPAR(14),NEND
COMMON /RODATA/ UR,IQ,NDS
COMMON /ROELEM/ NER,NEQR,ER
DATA FLAG/.FALSE./,NER/20/,ER/30000000./

```

RODI 1
RODI 2
RODI 3
RODI 4
RODI 5
RODI 6
RODI 7
RODI 8
RODI 9
RODI 10
RODI 11
RODI 12
RODI 13
RODI 14
RODI 15
RODI 16
RODI 17
RODI 18
RODI 19
RODI 20
RODI 21
RODI 22
RODI 23
RODI 24
RODI 25
RODI 26
RODI 27
RODI 28
RODI 29
RODI 30
RODI 31
RODI 32
RODI 33
RODI 34
RODI 35
RODI 36
RODI 37

```

IF(FLAG) GO TO 50
NEQR=2*(NER+1)
NKMR=7*NER+3
N1=NEND
N2=N1+NEQ*IPR
N3=N2+NEQ*IPR
N4=N3+NEQ*IPR
N5=N4+NKMR*IPR
N6=N5+NEQR*IPR
N7=N6+NEQR
N8=N7+NEQR*IPR
N9=N8+NEQR*IPR
N10=N9+NEQR*IPR
N11=N10+NEQR*IPR
NE=N11+NEQR*IPR
CALL SETMEM(NE)
CALL PZERO(G(NEND),NE-NEND)
FLAG=.TRUE.

```

```

50 CALL WIMPCT(G(NPAR(1)),G(NPAR(2)),M(NPAR(3)),G(NPAR(4)),
1      M(NPAR(5)),M(NPAR(6)),G(NPAR(7)),G(NPAR(8)),
2      M(NPAR(9)),G(NPAR(10)),G(NPAR(11)),G(N1),G(N2),
3      G(N3),G(N4),G(N5),M(N6),G(N7),G(N8),G(N9),G(N10),
4      G(N11))
    RETURN
    END

```

C

^
C**** SUBROUTINE WIMPCT(UL,XL,LD,P,IX,ID,X,F,JDIAG,DR,U,B,U,A,RK,RM,
JDR,RU,RV,RA,RB,FR)

```

LOGICAL FLAG,TAN
COMMON G(1)
DIMENSION M(1)
EQUIVALENCE (G(1),M(1))
COMMON /CTDATA/ O,HEAD(20),NUMNP,NUMEL,LAYER,NEQ,IPR
COMMON /TMDATA/ TIME,DT,DDT,FORCE,ALPHA
COMMON /LODATA/ NDF,NDM,NEN,NST,NKM
COMMON /NITERS/ ITR
COMMON /PARATS/ NPAR(14),NEND
COMMON /RODATA/ UR,IQ,NDS
COMMON /ROELEM/ NER,NEQR,ER
COMMON /CONSTS/ A0,A2,A4,A5,A6,A7,A8,AREA
COMMON /PROLOD/ PROP
COMMON /ISWIDX/ ISW
COMMON /EXTRAS/ TAN
DIMENSION UL(1),XL(1),LD(1),P(1),IX(1),ID(1),X(1),F(1),JDIAG(1),
1      DR(1),U(1),B(1),V(1),A(1),RK(1),RM(1),JDR(1),RU(1),
2      RU(1),RA(1),RB(1),FR(1),Q(3),QP(3)
DATA ITR/5/,FLAG/.FALSE./,WIL/1.4/,INTE/24/
IF(FLAG) GO TO 50
DO 1 I=1,3

```

WIMP 1
WIMP 2
WIMP 3
WIMP 4
WIMP 5
WIMP 6
WIMP 7
WIMP 8
WIMP 9
WIMP 10
WIMP 11
WIMP 12
WIMP 13
WIMP 14
WIMP 15
WIMP 16
WIMP 17
WIMP 18
WIMP 19
WIMP 20
WIMP 21
WIMP 22
WIMP 23
WIMP 24

	Q(I)=0.0	WIMP 25
	QP(I)=0.0	WIMP 26
1	CONTINUE	WIMP 27
	IDS=1	WIMP 28
	TAN=.FALSE.	WIMP 29
	REWIND 2	WIMP 30
	READ(2) (B(I), I=1, NEQ)	WIMP 31
	FORCE=0.0	WIMP 32
	ALPHA=0.0	WIMP 33
	PROP=0.0	WIMP 34
	NNEQ=NDF*NUMNP	WIMP 35
	A0=6./(WIL*DT)**2	WIMP 36
	A2=6./(WIL*DT)	WIMP 37
	A4=A0/WIL	WIMP 38
	A5=-A2/WIL	WIMP 39
	A6=1.-3./WIL	WIMP 40
	A7=DT/2.	WIMP 41
	A8=DDT/6.	WIMP 42
	CALL FORMROD(RK, RM, JDR)	WIMP 43
	DO 10 I=1, NEQR	WIMP 44
10	RU(I)=-UR	WIMP 45
	Q(2)=-UR	WIMP 46
	FLAG=.TRUE.	WIMP 47
50	ISW=5	WIMP 48
	IF (IDS.EQ.NDS) TAN=.TRUE.	WIMP 49
	CALL FSTREA(UL, XL, LD, P, IX, ID, X, F, JDIAG, DR, U, NDF, NDM, NEN, NST, NNEQ)	WIMP 50
	DO 20 I=1, NEQ	WIMP 51
	A(I)=DR(I)/B(I)	WIMP 52
	U(I)=U(I)+DT*A(I)	WIMP 53
	U(I)=U(I)+DT*U(I)	WIMP 54
20	CONTINUE	WIMP 55
	QP(1)=U(IQ)	WIMP 56
	QP(2)=U(IQ)	WIMP 57
	QP(3)=A(IQ)	WIMP 58
	DO 30 I=1, NEQR	WIMP 59
	RB(I)=RM(I)*(A0*RU(I)+A2*RU(I)+2.*RA(I))	WIMP 60
30	CONTINUE	WIMP 61
	RBIQ=RU(1)+DT*RU(1)+DDT/3.*RA(1)	WIMP 62
	ROT=0.000001	WIMP 63
	ICOU=0	WIMP 64
	DO 100 IT=1, ITR	WIMP 65
	RUT=RBIQ+Q(3)*DDT/6.	WIMP 66
	AF=-RUT-QP(1)	WIMP 67
	CALL RODLOAD(FIQ, AF)	WIMP 68
	DO 110 I=1, NEQR	WIMP 69
	FR(I)=RB(I)	WIMP 70
110	CONTINUE	WIMP 71
	FR(1)=FR(1)+(1.-WIL)*FORCE+WIL*FIQ	WIMP 72
	CALL ACTCOL(RK, FR, JDR, NEQR, .FALSE., .TRUE., 0)	WIMP 73
	Q(3)=A4*(FR(1)-RU(1))+A5*RU(1)+A6*RA(1)	WIMP 74
	RUTT=RBIQ+Q(3)*DDT/6.	WIMP 75
	ROTR=ABS((RUTT-RUT)/RUTT)	WIMP 76
	IF(ROTR.LT.ROT) ICOU=1	WIMP 77
	IF(ICOU.GT.0) GO TO 200	WIMP 78
100	CONTINUE	WIMP 79
200	DO 210 I=1, NEQR	WIMP 80
	FR(I)=A4*(FR(I)-RU(I))+A5*RU(I)+A6*RA(I)	WIMP 81
	RU(I)=RU(I)+DT*RU(I)+A8*(FR(I)+2.*RA(I))	WIMP 82
	RV(I)=RU(I)+A7*(FR(I)+RA(I))	WIMP 83
	RA(I)=FR(I)	WIMP 84
210	CONTINUE	WIMP 85
	Q(1)=RU(1)	WIMP 86
	Q(2)=RV(1)	WIMP 87
	Q(3)=RA(1)	WIMP 88
	FORCE=FIQ	WIMP 89
	PROP=FORCE	WIMP 90
	ALPHA=-Q(1)-QP(1)	WIMP 91
	RODFR=RU(INTE)*AREA*ER	WIMP 92
	WRITE(8, 8001) FORCE, ALPHA, RODFR, (Q(I), I=1, 3)	WIMP 93
8001	FORMAT(6E12.4)	WIMP 94

ORIGINAL PAGE IS
OF POOR QUALITY

```

IDS=IDS+1
IF (IDS.GT.NDS) IDS=1
TAN=.FALSE.
RETURN
END

C
SUBROUTINE FORMROD(RK, RM, JDR)
C**** FORM STIFFNESS AND MASS MATRICES OF ROD
COMMON /RODATA/ UR, IQ, NDS
COMMON /ROELEM/ NER, NEQR, ER
COMMON /CONSTS/ A0, A2, A4, A5, A6, A7, A8, AREA
DIMENSION RK(1), RM(1), JDR(2), D(6)
DATA RHOR/.0003225/, RL/1.0/
DATA D/.22, .36, .43, .48, .50, .625/
EL=RL/NER
PAI=4.*ATAN(1.)
JDR(1)=1
JDR(2)=3
DO 100 I=1, NER
IF (I.LT.6) A=PAI*(D(I)/2.)*2
IF (I.GE.6) A=PAI*(D(6)/2.)*2
TT=A*ER/30./EL
J1=2*(I+1)-1
J2=J1+1
J1M1=J1-1
J1M2=J1-2
JDR(J1)=JDR(J1M1)+3
JDR(J2)=JDR(J1)+4
K1=JDR(J1M2)
K2=JDR(J1M1)-1
RK(K1 )=RK(K1 )+TT*36.
RK(K2 )=RK(K2 )+TT*3.*EL
RK(K2+1)=RK(K2+1)+TT*4.*EL**2
RK(K2+2)=RK(K2+2)-TT*36.
RK(K2+3)=RK(K2+3)-TT*3.*EL
RK(K2+4)=RK(K2+4)+TT*36.
RK(K2+5)=RK(K2+5)+TT*3.*EL
RK(K2+6)=RK(K2+6)-TT*EL**2
RK(K2+7)=RK(K2+7)-TT*3.*EL
RK(K2+8)=RK(K2+8)+TT*4.*EL**2
TT=RHOR*A*EL
L1=2*I-1
RM(L1 )=RM(L1 )+TT/2.
RM(L1+1)=RM(L1+1)+TT*EL**2/420.
RM(L1+2)=RM(L1+2)+TT/2.
RM(L1+3)=RM(L1+3)+TT*EL**2/420.
100 CONTINUE
AREA=A
DO 20 I=1, NEQR
J=JDR(I)
20 RK(J)=RK(J)+A0*RM(I)
CALL ACTCOL(RK, RM, JDR, NEQR, .TRUE., .FALSE., 0)
RETURN
END

C
SUBROUTINE RODLOAD(F, AF)
C**** COMPUTE CONTACT LOADING
LOGICAL RELD, UNLD, PIL
COMMON /TMDATA/ TIME, DT, DDT, FORCE, ALPHA
COMMON /EXDATA/ Q(4)
DATA UNLD/.FALSE./, PIL/.FALSE./, RELD/.FALSE./
IF (PIL) GO TO 10
AMAX=AMIN=FMAX=0.0
PIL=.TRUE.
10 IF (RELD) GO TO 50
IF (UNLD) GO TO 20
F=Q(1)*AF**1.5
IF (F.GE.FORCE) RETURN
UNLD=.TRUE.
AMAX=ALPHA

```

WIMP 95
WIMP 96
WIMP 97
WIMP 98
WIMP 99

FORM 1
FORM 2
FORM 3
FORM 4
FORM 5
FORM 6
FORM 7
FORM 8
FORM 9
FORM 10
FORM 11
FORM 12
FORM 13
FORM 14
FORM 15
FORM 16
FORM 17
FORM 18
FORM 19
FORM 20
FORM 21
FORM 22
FORM 23
FORM 24
FORM 25
FORM 26
FORM 27
FORM 28
FORM 29
FORM 30
FORM 31
FORM 32
FORM 33
FORM 34
FORM 35
FORM 36
FORM 37
FORM 38
FORM 39
FORM 40
FORM 41
FORM 42
FORM 43
FORM 44
FORM 45
FORM 46
FORM 47
FORM 48

RODL 1
RODL 2
RODL 3
RODL 4
RODL 5
RODL 6
RODL 7
RODL 8
RODL 9
RODL 10
RODL 11
RODL 12
RODL 13
RODL 14
RODL 15

```
FMAX=FORCE
IF (AMAX.GT.Q(2)) UK=FMAX/((1.-Q(3))*AMAX+Q(2)*Q(3))*Q(4)
IF (AMAX.LE.Q(2)) UK=FMAX/AMAX**Q(4)
AMIN=Q(3)*(AMAX-Q(2))
IF (AMIN.LT.0.) AMIN=0.0
20 IF (AF.LE.AMIN) GO TO 30
F=UK*(AF-AMIN)**Q(4)
IF (F.LT.FORCE) RETURN
RELD=,TRUE.
RK=FMAX/(AMAX-AMIN)**1.5
50 IF (AF.LE.AMIN) GO TO 30
F=RK*(AF-AMIN)**1.5
RETURN
30 F=0.0
RETURN
END
```

```
RODL 16
RODL 17
RODL 18
RODL 19
RODL 20
RODL 21
RODL 22
RODL 23
RODL 24
RODL 25
RODL 26
RODL 27
RODL 28
RODL 29
RODL 30
RODL 31
```

NSG 3185

WAVE PROPAGATION IN GRAPHITE/EPOXY LAMINATES DUE TO IMPACT

NASA CR-168057

Advanced Research Projects Agency
Washington DC 20525
Attn: Library

Advanced Technology Center, Inc.
LTV Aerospace Corporation
P.O. Box 6144
Dallas, TX 75222
Attn: D. H. Petersen
W. J. Renton

Air Force Flight Dynamics Laboratory
Wright-Patterson Air Force Base, OH 45433
Attn: E. E. Baily
G. P. Sendecky (FBC)
R. S. Sandhu

Air Force Materials Laboratory
Wright-Patterson Air Force Base, OH 45433
Attn: H. S. Schwartz (LN)
T. J. Reinhart (MBC)
G. P. Peterson (LC)
E. J. Morrissey (LAE)
S. W. Tsai (MBM)
N. J. Pagano
J. M. Whitney (MBM)

Air Force Office of Scientific Research
Washington DC 20333
Attn: J. F. Masi (SREP)

Air Force Office of Scientific Research
1400 Wilson Blvd.
Arlington, VA 22209

AFOSR/NA
Bolling AFB, DC 20332
Attn: A. K. Amos

Air Force Rocket Propulsion Laboratory
Edwards, CA 93523
Attn: Library

Babcock & Wilcox Company
Advanced Composites Department
P.O. Box 419
Alliance, Ohio 44601
Attn: P. M. Leopold

ORIGINAL PAGE IS
OF POOR QUALITY

Bell Helicopter Company
P.O. Box 482
Ft. Worth, TX 76101
Attn: H. Zinberg

The Boeing Company
P. O. Box 3999
Seattle, WA 98124
Attn: J. T. Hoggatt, MS. 88-33
T. R. Porter

The Boeing Company
Vertol Division
Morton, PA 19070
Attn: E. C. Durchlaub

Battelle Memorial Institute
Columbus Laboratories
505 King Avenue
Columbus, OH 43201
Attn: L. E. Hulbert

Bendix Advanced Technology Center
9140 Old Annapolis Rd/Md. 108
Columbia, MD 21045
Attn: O. Hayden Griffin

Brunswick Corporation
Defense Products Division
P. O. Box 4594
43000 Industrial Avenue
Lincoln, NE 68504
Attn: R. Morse

Celanese Research Company
86 Morris Ave.
Summit, NJ 07901
Attn: H. S. Kliger

Commander
Natick Laboratories
U. S. Army
Natick, MA 01762
Attn: Library

ORIGINAL PAGE IS
OF POOR QUALITY

Commander
Naval Air Systems Command
U. S. Navy Department
Washington DC 20360
Attn: M. Stander, AIR-43032D

Commander
Naval Ordnance Systems Command
U.S. Navy Department
Washington DC 20360
Attn: B. Drimmer, ORD-033
M. Kinna, ORD-033A

Cornell University
Dept. Theoretical & Applied Mech.
Thurston Hall
Ithaca, NY 14853
Attn: S. L. Phoenix

Defense Metals Information Center
Battelle Memorial Institute
Columbus Laboratories
505 King Avenue
Columbus, OH 43201

Department of the Army
U.S. Army Aviation Materials Laboratory
Ft. Eustis, VA 23604
Attn: I. E. Figge, Sr.
Library

Department of the Army
U.S. Army Aviation Systems Command
P.O. Box 209
St. Louis, MO 63166
Attn: R. Vollmer, AMSAV-A-UE

Department of the Army
Plastics Technical Evaluation Center
Picatinny Arsenal
Dover, NJ 07801
Attn: H. E. Pebly, Jr.

Department of the Army
Watervliet Arsenal
Watervliet, NY 12189
Attn: G. D'Andrea

Department of the Army
Watertown Arsenal
Watertown, MA 02172
Attn: A. Thomas

ORIGINAL PAGE IS
OF POOR QUALITY

Department of the Army
Redstone Arsenal
Huntsville, AL 35809
Attn: R. J. Thompson, AMSMI-RSS

Department of the Navy
Naval Ordnance Laboratory
White Oak
Silver Spring, MD 20910
Attn: R. Simon

Department of the Navy
U.S. Naval Ship R&D Laboratory
Annapolis, MD 21402
Attn: C. Hersner, Code 2724

Director
Deep Submergence Systems Project
6900 Wisconsin Avenue
Washington DC 20015
Attn: H. Bernstein, DSSP-221

Director
Naval Research Laboratory
Washington DC 20390
Attn: Code 8430
I. Wolock, Code 8433

Drexel University
32nd and Chestnut Streets
Philadelphia, PA 19104
Attn: P. C. Chou

E. I. DuPont DeNemours & Co.
DuPont Experimental Station
Wilmington, DE 19898
Attn: D. L. G. Sturgeon

Fiber Science, Inc.
245 East 157 Street
Gardena, CA 90248
Attn: E. Dunahoo

General Dynamics
P.O. Box 748
Ft. Worth, TX 76100
Attn: D. J. Wilkins
Library

General Dynamics/Convair
P.O. Box 1128
San Diego, CA 92112
Attn: J. L. Christian
R. Adsit

ORIGINAL PAGE IS
OF POOR QUALITY

General Electric Co.
Evendale, OH 45215
Attn: C. Stotler
R. Ravenhall

General Motors Corporation
Detroit Diesel-Allison Division
Indianapolis, IN 46244
Attn: M. Herman

Georgia Institute of Technology
School of Aerospace Engineering
Atlanta, GA 30332
Attn: L. W. Rehfield

Grumman Aerospace Corporation
Bethpage, Long Island, NY 11714
Attn: S. Dastin
J. B. Whiteside

Hamilton Standard Division
United Aircraft Corporation
Windsor Locks, CT 06096
Attn: W. A. Percival

Hercules, Inc.
Allegheny Ballistics Laboratory
P. O. Box 210
Cumberland, MD 21053
Attn: A. A. Vicario

Hughes Aircraft Company
Culver City, CA 90230
Attn: A. Knoell

Illinois Institute of Technology
10 West 32 Street
Chicago, IL 60616
Attn: L. J. Broutman
I. M. Daniel

Dr. Joseph Wolf, Engineering Mechanics Dept.
General Motors Research Labs.
256 Research Drive
Warren, MI 48090

Jet Propulsion Laboratory
4800 Oak Grove Drive
Pasadena, CA 91103
Attn: Library

Lawrence Livermore Laboratory
P.O. Box 808, L-421
Livermore, CA 94550
Attn: T. T. Chiao
E. M. Wu

ORIGINAL PAGE IS
OF POOR QUALITY

Lehigh University
Institute of Fracture &
Solid Mechanics
Bethlehem, PA 18015
Attn: G. C. Sih

Lockheed Georgia Co.
Advanced Composites Information Center
Dept. 72-14, Zone 402
Marietta, GA 30060
Attn: T. M. Hsu

Lockheed Missiles and Space Co.
P.O. Box 504
Sunnyvale, CA 94087
Attn: R. W. Fenn

Lockheed-California
Burbank, CA 91503
Attn: J. T. Ryder
K. N. Lauraitis
J. C. Ekvall

McDonnell Douglas Aircraft Corporation
P.O. Box 516
Lambert Field, MS 63166
Attn: J. C. Watson

McDonnell Douglas Aircraft Corporation
3855 Lakewood Blvd.
Long Beach, CA 90810
Attn: L. B. Greszczuk

Material Sciences Corporation
1777 Walton Road
Blue Bell, PA 19422
Attn: B. W. Rosen

Massachusetts Institute of Technology
Cambridge, MA 02139
Attn: F. J. McGarry
J. F. Mandell
J. W. Mar

NASA-Ames Research Center
Moffett Field, CA 94035
Attn: Dr. J. Parker
Library

NASA-Flight Research Center
 P.O. Box 273
 Edwards, CA 93523
 Attn: Library

ORIGINAL FILED IN
 OF POOR QUALITY

NASA-George C. Marshall Space Flight Center
 Huntsville, AL 35812
 Attn: C. E. Cataldo, S&E-ASTN-MX
 Library

NASA-Goddard Space Flight Center
 Greenbelt, MD 20771
 Attn: Library

NASA-Langley Research Center
 Hampton, VA 23365
 Attn: J. H. Starnes

J. G. Davis, Jr.
 M. C. Card

J. R. Davidson

NASA-Lewis Research Center
 21000 Brookpark Road, Cleveland, OH 44135

Attn: Contracting Officer, MS 501-11
 Tech. Report Control, MS 5-5
 Tech. Utilization, MS 3-16
 AFSC Liaison, MS 501-3
 S&MTD Contract Files, MS 49-6
 L. Berke, MS 49-6
 N. T. Saunders, MS 49-1
 R. F. Lark, MS 49-6
 J. A. Ziemianski, MS 49-6
 R. H. Johns, MS 49-6
 C. C. Chamis, MS 49-6 (4 copies)
 R. L. Thompson, MS 49-6
 T. T. Serafini, MS 49-1
 Library, MS 60-3 (2 copies)

NASA-Lyndon B. Johnson Space Center
 Houston, TX 77001
 Attn: S. Glorioso, SMD-ES52
 Library

NASA Scientific and Tech. Information Facility
 P.O. Box 8757
 Balt/Wash: International Airport, MD 21240
 Attn: Acquisitions Branch (10 copies)

National Aeronautics & Space Administration
 Office of Advanced Research & Technology
 Washington DC 20546

Attn: L. Harris, Code RTM-6
 M. Greenfield, Code RTM-6
 C. Bersch, Code RTM-6

National Aeronautics & Space Administration
Office of Technology Utilization
Washington DC 20546

ORIGINAL PAGE IS
OF POOR QUALITY

National Bureau of Standards
Eng. Mech. Section
Washington DC 20234
Attn: R. Mitchell

National Science Foundation
Engineering Division
1800 G. Street, NW
Washington DC 20540
Attn: Library

Northrop Corporation Aircraft Group
3901 West Broadway
Hawthorne, CA 90250
Attn: R. M. Verette
G. C. Grimes

Pratt & Whitney Aircraft
East Hartford, CT 06108
Attn: J. M. Woodward

Raytheon Co., Missile System Division
Mechanical Systems Laboratory
Bedford, MA
Attn: P. R. Digiovanni

Rensselaer Polytechnic Institute
Troy, NY 12181
Attn: R. Loewy

Rockwell International
Los Angeles Division
International Airport
Los Angeles, CA 90009
Attn: L. M. Lackman
D. Y. Konishi

Sikorsky Aircraft Division
United Aircraft Corporation
Stratford, CT 06602
Attn: Library

Southern Methodist University
Dallas, TX 75275
Attn: R. M. Jones

Space & Missile Systems Organization
Air Force Unit Post Office
Los Angeles, CA 90045
Attn: Technical Data Center

Structural Composites Industries, Inc.
6344 N. Irwindale Avenue
Azusa, CA 91702
Attn: R. Gordon

ORIGINAL PAGE IS
OF POOR QUALITY

Texas A&M
Mechanics & Materials Research Center
College Station, TX 77843
Attn: R. A. Schapery
Y. Weitsman

TRW, Inc.
23555 Euclid Avenue
Cleveland, OH 44117
Attn: I. J. Toth

Union Carbide Corporation
P. O. Box 6116
Cleveland, OH 44101
Attn: J. C. Bowman

United Technologies Research Center
East Hartford, CT 06108
Attn: R. C. Novak
Dr. A. Dennis

University of Dayton Research Institute
Dayton, OH 45409
Attn: R. W. Kim

University of Delaware
Mechanical & Aerospace Engineering
Newark, DE 19711
Attn: B. R. Pipes

University of Illinois
Department of Theoretical & Applied Mechanics
Urbana, IL 61801
Attn: S. S. Wang

University of Oklahoma
School of Aerospace Mechanical & Nuclear Engineering
Norman, OK 73069
Attn: C. W. Bert

University of Wyoming
College of Engineering
University Station Box 3295
Laramie, WY 82071
Attn: D. F. Adams

U. S. Army Materials & Mechanics Research Center
Watertown Arsenal
Watertown, MA 02172
Attn: E. M. Lence
D. W. Oplinger

V.P. I. and S. U.
Dept. of Eng. Mech.
Blacksburg, VA 24061
Attn: R. H. Heller
H. J. Brinson
C. T. Herakovich
K. L. Reifsnider

ORIGINAL PAGE IS
OF POOR QUALITY